THESIS FOR THE DEGREE OF DOCTOR OF PHILOSOPHY

# Creating Ultrafast Biosensors for Neuroscience

YUANMO WANG


CHALMERS
UNIVERSITY OF TECHNOLOGY

Department of Chemistry and Chemical Engineering
CHALMERS UNIVERSITY OF TECHNOLOGY
GÖTEBORG, SWEDEN 2019

**Creating Ultrafast Biosensors for Neuroscience**

YUANMO WANG

ISBN: 978-91-7905-150-1



Doktorsavhandlingar vid Chalmers Tekniska Högskola

Ny series nr: 4617

ISSN: 0346-718X

Department of Chemistry and Chemical Engineering

Chalmers University of Technology

SE-412 96 Göteborg

Sweden

Telephone +46 (0) 31-772 1000

Cover image:
A graphical illustration of amperometric measurements from vesicular glutamate release at exocytosis activity in rodent brain and from quantification of glutamate in isolated single synaptic vesicles using our ultrafast enzyme-based electrochemical glutamate sensor.

Printed by Chalmers Reproservice

Göteborg, Sweden 2019

# Creating Ultrafast Biosensors for Neuroscience

YUANMO WANG

Department of Chemistry and Chemical Engineering
Chalmers University of Technology

## ABSTRACT

Neuronal communication is the basis for all our brain function and relies on regulated exocytosis, a cell function that involves release of quantal amounts of neurotransmitters into the gap space between interconnected neurons to serve as chemical signals. To study exocytosis, which is a fast process that occurs on the timescale of sub-milliseconds to milliseconds, a toolbox of analytical methods has been developed where the electrochemical based techniques offer quantitative and sufficient high temporal recording speed. However, neuronal activity involving non-electroactive neurotransmitters such as acetylcholine and glutamate have long time suffered from a limited detection speed about 3 orders of magnitude slow for capturing the rapid transients from exocytosis release by these non-electroactive compounds. In this work, we have focused on a new approach for the development of amperometric enzyme-nanoparticle-based sensors that significantly improve recording speed of important non-electroactive brain analytes and are suitable for ultrafast recording in neuroscience research.

In **Paper I**, an acetylcholine sensor was designed and fabricated by modifying the sensor surface with gold nanoparticles (AuNPs) and two sequential enzymes, where the enzyme coating was limited to a monolayer in thickness to minimize enzyme product diffusion distance to be detected by the electrode surface. This novel sensor provided the first proof of concept to improving enzyme-based sensors speed by 2 orders of magnitude compared to existing technology and was fast enough to temporally resolve single millisecond vesicle release events of acetylcholine from an artificial cell model that mimics exocytosis.

In **Paper II**, a new and analytical method was introduced that provided a significantly faster and a non-toxic way to quantify AuNP immobilized enzymes during sensor surface characterization in comparison to the previous method used in **Paper I** that involved using toxic cyanide solutions. This method was based on electrochemical stripping of AuNPs from the electrode surface after enzymes were attached, followed by quantifying the number of enzymes released, to determine the average number of enzymes attached to each single nanoparticle.

In **Paper III**, an ultrafast glutamate sensor was developed by careful characterization of the conditions for controlling the enzyme coverage on a AuNP decorated electrode surface to a monolayer. By placing this novel sensor in the Nucleus Accumbens of rodent brain slice, recording of spontaneous glutamate activity and various isolated dynamic current transients from single exocytotic events on the sub-millisecond timescale were captured.

In **Paper IV**, the conjugation of enzyme glucose oxidase (GOx) to AuNP surfaces was used to study how physical crowding affects enzyme stability and activity when immobilized at a highly curved nanoparticle surface. This work showed that by crowding a gold nanoparticle surface with its maximum number of enzymes that can theoretically fit, while maintaining a monolayer coverage, the retained enzymatic activity of immobilized enzyme improved 300% compared to GOx free in solution. Implementing these findings to a nanostructured electrochemical biosensor for glucose confirmed a recording speed for glucose on the millisecond timescale

In **Paper V**, using our novel ultrafast glutamate sensor, a novel method was developed for quantification of the quantal glutamate content in single synaptic vesicles, and quantification of the quantal amount glutamate released from single exocytosis events in rodent brain tissue.

**Keywords**: Biosensor, amperometry, acetylcholine, glutamate, glucose, acetylcholine esterase, choline oxidase, glutamate oxidase, glucose oxidase, gold nanoparticles, artificial cell, exocytosis, enzyme monolayer, brain slice, adsorption, quantification, deformation, enzymatic activity, enzyme stability

## LIST OF PUBLICATIONS

This thesis is written based on the following publications and manuscripts:

I. **Amperometric Detection of Single Vesicle Acetylcholine Release Events from an Artificial Cell**
Jacqueline D. Keighron, Joakim Wigström, Michael E. Kurczy, Jenny Bergman, Yuanmo Wang and Ann-Sofie Cans*
*ACS Chemical Neuroscience*, 2015, 6:181-88.

II. **Counting the Number of Enzymes Immobilized onto a Nanoparticle Coated Electrode**
Jenny Bergman, Yuanmo Wang, Joakim Wigström and Ann-Sofie Cans*
*Analytical and Bioanalytical Chemistry.* 2018, 410(6): 1775-83.

III. **Ultrafast Glutamate Biosensor Recordings in Brain Slices Reveal Complex Single Exocytosis Transients**
Yuanmo Wang, Devesh Mishra, Jenny Bergman, Jacqueline D. Keighron, Karolina P. Skibicka and Ann-Sofie Cans*
*ACS Chemical Neuroscience*, 2019, 10(3): 1744-1752

IV. **Molecular Crowding and a Minimal Footprint at a Gold Nanoparticle Support Stabilize Glucose Oxidase and Boost its Activity**
Yuanmo Wang, Rima Jonkute, Hampus Lindmark, Jacqueline D. Keighron and Ann-Sofie Cans*
*Submitted manuscript.*

V. **Counting the Number of Glutamate Molecules in Single Synaptic Vesicles**
Yuanmo Wang, Hoda Fathali, Devesh Mishra, Thomas Olsson, Jacqueline D. Keighron, Karolina P. Skibicka, and Ann-Sofie Cans*
*Submitted manuscript.*

# CONTRIBUTION REPORT

**Pager I.** I performed the experiments for determining the acetylcholine sensor response time together with Joakim Wigström and Jenny Bergman.

**Paper II.** I assisted with enzyme labelling for the quantitative fluorescence measurements. I performed the imaging of AuNP coated electrodes using scanning electron microscopy and assisted with the image analysis.

**Paper III.** I conceived the project together with all my co-authors. I characterized the interaction of glutamate oxidase (GluOx) and AuNP by performing a flocculation assays using spectrophotometry, and measured the resulting size of GluOx-AuNP conjugates from the assays using dynamic light scattering (DLS) and nanoparticle tracking analysis (NTA). I performed sensor selectivity experiments using cyclic voltammetry. I carried out the *ex vivo* amperometric glutamate recordings in mouse and rat brain slices together with Devesh Mishra. I analysed all the data. I prepared all the figures for the manuscript. I wrote the manuscript with input from all co-authors.

**Paper IV.** I conceived the project together with Ann-Sofie Cans. I performed all the experiments for this project. I analysed all the data and prepared all the figures for the manuscript. I wrote the manuscript together with Ann-Sofie Cans and Jacqueline D. Keighron.

**Paper V.** I conceived the project together with Hoda Fathali and Ann-Sofie Cans. I characterized this new quantitative method and performed all the amperometric measurement of glutamate vesicle release from glutamate-filled LUVs and isolated synaptic vesicles. I performed all the data analysis and prepared all the figures for the manuscript. I wrote the manuscript together with Ann-Sofie Cans.

## RELATED PUBLICATION NOT INCLUDED IN THIS THESIS

I. **Co-Detection of Dopamine and Glucose with High Temporal Resolution.**
Jenny Bergman, Lisa Mellander, Yuanmo Wang and Ann-Sofie Cans*
*Catalysts.* 2018, 8(1): 34.

# TABLE OF CONTENTS

## LIST OF ABBREVIATIONS

| | |
|---|---|
| NAc | Nucleus accumbens |
| CNS | Central nervous system |
| PNS | Peripheral nervous system |
| ATP | Adenosine triphosphate |
| SNARE | Soluble N-ethylmaleimide-sensitive fusion protein attachment protein receptors |
| SM | Sec1/Munc18-like |
| NSF | N-ethylmaleimide-sensitive fusion protein |
| EM | Electron microscopy |
| HRP | Horseradish peroxidase |
| PC | Phosphatidylcholine |
| PE | Phosphatidylethanolamine |
| PS | Phosphatidylserine |
| PI | Phosphatidylinositol |
| VNT | Vesicular neurotransmitter transporters |
| $H^+$ | Proton |
| ADP | Adenosine diphosphate |
| VMAT | Vesicular monoamine transporter |
| VAChT | Vesicular acetylcholine transporter |
| VGAT | Vesicular GABA and glycine transporter |
| VGLUT | Vesicular glutamate transporter |
| L-DOPA | 3,4-Dihydroxy-**l**-phenylalanine |
| ANS | Autonomic nervous system |
| PNMT | Phenylethanolamine *N*-methyltransferase |
| GABA | *gamma*-Aminobutyric acid |
| TCA | Tricarboxylic acid |
| AMP | Adenosine monophosphate |
| SEM | Scanning electron microscope |
| TEM | Transmission electron microscope |

| | |
|---|---|
| STEM | Scanning transmission electron microscope |
| GFP | Green fluorescent protein |
| iGluSnFR | Intensity-based glutamate-sensing fluorescent reporter |
| GluBP | Glutamate binding protein |
| Qdots | Quantum dots |
| FFNs | Fluorescent false neurotransmitters |
| TIRFM | Total internal reflection fluorescence microscope |
| CV | Cyclic voltammetry |
| FSCV | Fast scanning cyclic voltammetry |
| AuNP | Gold nanoparticle |
| IHP | Inner Helmholtz plane |
| OHP | Outer Helmholtz plane |
| NHE | Normal hydrogen electrode |
| GOx | Glucose oxidase |
| FAD | Flavin adenine dinucleotide |
| NPs | Nanoparticles |
| CNT | Carbon nanotube |
| SWCNT | Single-walled carbon nanotube |
| MWCNT | Multi-walled carbon nanotube |
| DLS | Dynamic light scattering |
| NTA | Nanoparticle tracking analysis |
| UV-Vis | Ultraviolet-visible |

*The difficult is what takes a little time;*
*the impossible is what takes a little longer.*

*- Fridtjof Nansen*

To my Mom
&
my dear families

# 1. The Human Brain

The human brain with its connected nervous system is the most complex organ in the human body, and it is probably the most complex neuronal network that provides the highest precision and efficiency to current knowledge of humankind. The brain receives its information from various sensory organs. The signal transportation is processed by integration and coordination that result in decision making and final instructions for the whole body's various activities, which are controlled by the brain. The human brain is estimated to consist of approximately 100 billion neurons and 10 times more glial cells (nonneuronal cells),[1] or a rather equal number of neurons (about 86.1 billion) and glial cells (approximate 84.6 billion).[2]

The brain as an organ is made up of three major parts: the brainstem, the cerebellum and the cerebrum (Figure 1). Cerebellum is an area at the back of brain and is placed under the cerebrum. It is mainly involved in motor control, for instance by regulating the balance. The brainstem lies at the base of the brain, connecting cerebellum and cerebrum and continues as the spinal cord. Cerebrum is the largest among these three brain regions. It is formed by two (left and right) cerebral hemispheres that are similar in shape and separated by a deep groove called longitudinal fissure. Both of these two hemispheres are commonly composed by four major regions: 1) frontal lobe, which is the largest part and positioned at the front of both hemispheres, is involved in voluntary movement such as finger tapping and walking. It also controls other executive functions such as abstract thinking, planning, and self-control; 2) occipital lobe, which is located at the back of the brain, is mainly responsible for vision; 3) temporal lobe locating at the bottom middle part of the brain plays an important role in organizing sensory input such as auditory and visual stimuli, to process and interpret received information into meaningful formats like speech and memory; 4) parietal lobe, which is an area behind the frontal lobe and above the temporal lobe. One of its main

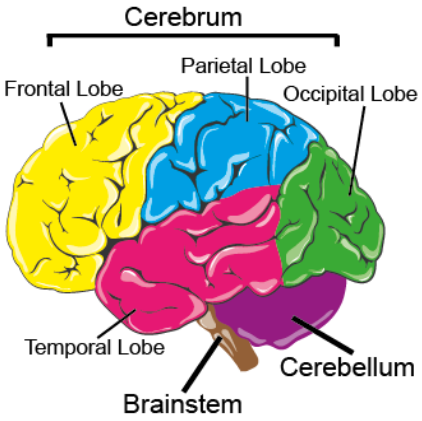


**Figure 1.** General illustration of the human brain structure.

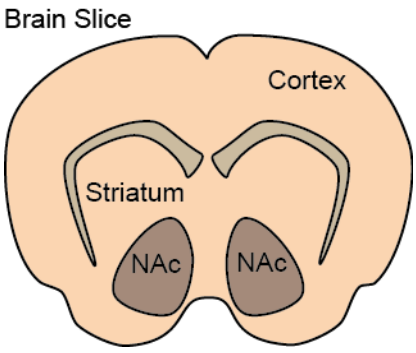


**Figure 2.** Illustration of the location for nucleus accumbens in mouse brain slice.

functions is integration of sensory information from the body like sensation through skin in response to, for example, temperature and pain. This brain region is also involved in processing spatial and oriental information sensed from vision or touch.

Nucleus accumbens (NAc) is a small brain region located in the basal forebrain below striatum as illustrated in Figure 2. It is divided into two sub-regions: the outer shell and the inner core. NAc plays an important role in reward-related motor action, learning and regulation of slow-wave sleep.[3] It is also involved in addiction and depression.[4] This brain region was used in our experiments for sensing of spontaneous neuronal activity in **Paper III** and **Paper V**.

### 1.1 The Central Nervous System

The nervous system is a complex organ system, which consists of a network of neurons that transmits signals to coordinate different functions in the body. The nerve system (Figure 3) is divided into two main subdivisions: the central nervous system (CNS) and the peripheral nervous system (PNS). CNS is further made up by two major parts, the brain and the spinal cord, which are located in and protected by the skull and the vertebral column.[5–7] Its main role is to receive information and give instructions for body actions in the whole body. PNS is mainly made up of all nerves that link CNS to other parts of the body. The CNS is composed by white and gray matter that is easy to distinguish by the color difference in fresh tissue.[6,7] The gray matter is mainly composed of bodies of nerve cells with their support structures, and white matter is primarily constituted by nerve fibers (i.e. axons).[5–7] Glial cells exist in both of these two tissues, although there are more of them in the white matter.

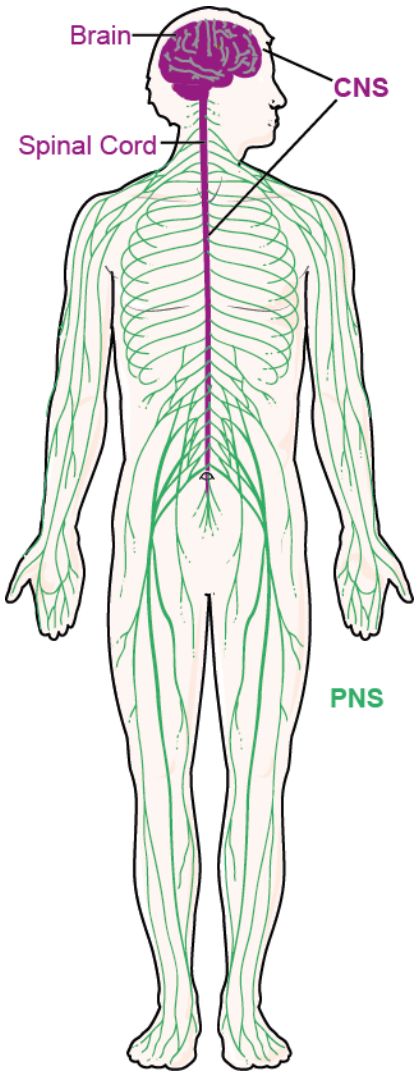


**Figure 3.** Illustration of the central nervous system (CNS) and the peripheral nervous system (PNS) in the human body.

#### 1.1.1 Neurons

Nervous tissue contains mainly two cell types, neurons and glia cells, which are responsible for supporting and protecting neurons.[7] Neurons (or nerve cells, Figure 4) are the fundamental units of the nervous system. They are highly specialized cells for receiving, processing and

transmitting information via electric and chemical signals. Neurons display large variation in size and shape. Their size varies greatly compared to cells in other biological tissue. For instance, sensory neurons with axons can be over 1.5 meters long in human adults when measured from the toes to the spinal cord. Single axons in giraffes can therefore be several meters long as they span through the entire length of their necks. In the human body, the cell body of neurons can range from anything from 5 μm to more than 100 μm (about 120 μm) in diameter,[8] and the volume of the cell body can vary from 300 $\mu m^3$ to 200000 $\mu m^3$.[9] Although there is a difference in the morphology among various types of neurons, the structural components of a neuron include four common main regions: cell body (soma), dendrites, axon and axon terminals (Figure 4). The cell body of neuron possesses typical eukaryotic cell components (or organelles) such as nucleus that contains most of the genetic materials,[10] mitochondria for generating the essential cell energy, Golgi apparatus for providing a station for protein or lipids synthesis and endoplasmic reticulum, which is an interconnected network of membranous tubules that serve to fold protein molecules correctly and transport proteins to the Golgi apparatus. Meanwhile the cell body is compact, the dendrites and axon are elongated extrusions and prolongations that extend from the cell body. Dendrites are usually short and extend from a neuron with many branches, so called 'dendritic tree'. The dendrites main function is to propagate electrical input received by surrounding neurons and transfer the information to the cell body, where this information is processed. The number of dendrite (branches) that extend from a neuron vary from 1 or 2 to more than 1000, and the role of dendrites are to assist the cell body to receive input signals from other neurons. Different from dendrites, the axon is typically long and maintains a constant diameter during extension or along its length. The axon serves to transport electrical signals from the cell body to the axon terminal for signal delivery to other neurons, muscles or glands. A

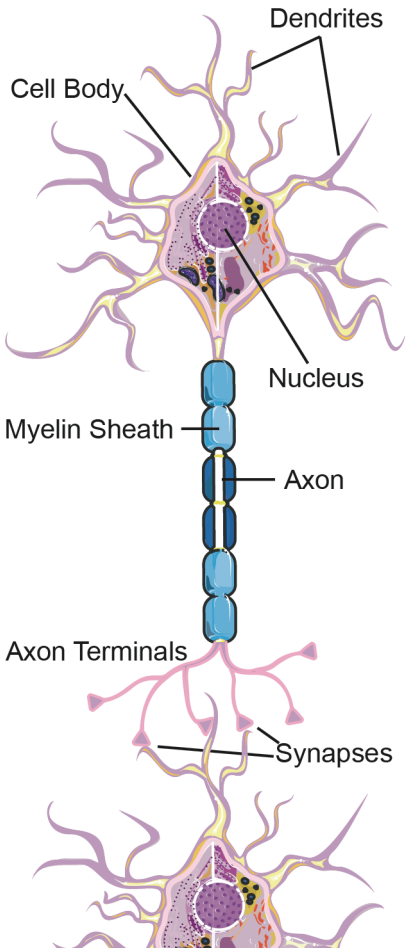


**Figure 4.** Schematic of a neuron and its interconnection with a neighboring neuron.

neuron usually has no more than one axon, and in some cases neuron does not have any axon or dendrites.

Based on structural polarity, neurons can be classified into four main types (Figure 5): *Unipolar neurons, Bipolar neurons, Multipolar neurons* and *pseudounipolar*. Unipolar neurons contain only one extension from cell body structurally. Bipolar neutrons have two prolongations from the cell body, one dendrite and one axon. Multipolar neurons have one axon and many dendrites (two or more) extending from the cell body. Pseudounipolar neurons contain one axon extended from the cell body and this axon is later split into two distinct branches.

Based on functions, neurons are categorized into three major classes: sensory neuron (afferent neurons), motor neuron (efferent neurons) and interneurons.[5] Sensory neurons collect information of stimulus, for instance, light, sound and touch, and bring this information towards the CNS. Motor neurons receive signals from the CNS, carry these signals away from the CNS to command muscles, organs and glands. Interneurons only exist in the CNS and link neurons to other neurons (from sensory neuron to motor neurons). Depending on the distance that signal has to travel, interneurons can be divided into two types: local interneurons and relay interneurons. Local interneurons contain short axons and process small pieces of information from nearby neurons to form neural circuits. Relay interneurons link neural circuits in one region to other region through its long axons.[11]

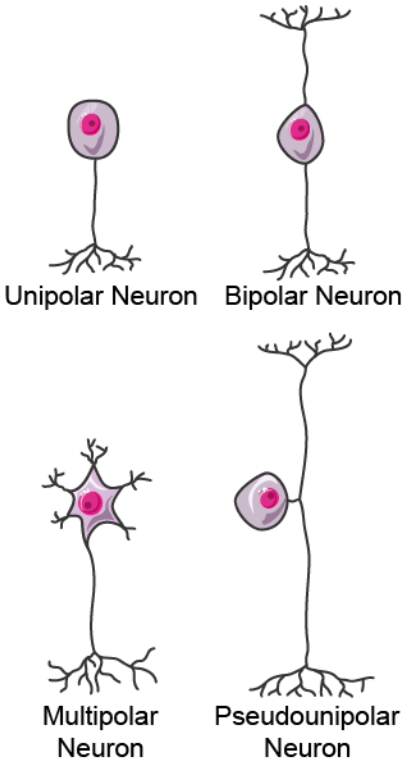


**Figure 5.** Schematic of different classified types of neurons.

### 1.1.2 Glial Cells

Glial cells (also called Glia or neuroglia) surround neurons and offer their support and protection by structuring a framework for neurons by supplying them with oxygen ($O_2$) and nutrients. They also provide insulation to neurons and to each other. Similarly to neurons, glial cells also contain basic organelles of eukaryotic cells such as mitochondria, endoplasmic reticulum and Golgi apparatus.[5] But, different from neurons, glial cells are not conductive for signaling using electric impulses[5] and their size are smaller than neurons in general. The type of glial cells that are present

in the CNS includes oligodendrocytes, astrocytes, ependymal cells and microglia, as well as Schwann cells and satellite cells, which are another two types of glial cells in the PNS. Glial cells also have complex extended structures from their cell bodies, but they do not function in the same way as dendrites and neuronal axons.[5] Many studies have suggested that the release of neurotransmitters from presynaptic terminals activates receptors of glial cells, and thereby evoke glial cells to dynamically regulate synaptic transmission by releasing adenosine triphosphate (ATP) and neurotransmitters like glutamate and hence take an active role during neuronal communication.[12,13]

#### 1.1.2.1 Astrocytes

Astrocytes (also called *astroglia* or *astrocytic glial cells*, Figure 6, "star shape") are an abundant type of star-shaped macroglial cells that are restricted to the CNS. Depending on counting technique used, the proportion of astrocytes in the brain has been estimated to constitute from 20% to 40% of all glia in various brain regions.[14] Astrocytes have many functions, and one of them is to maintain a nutritive environment. They play a key role in maintaining the brain metabolism and providing the nervous tissue with the energy needed for neuronal signaling. They do this by taking part in building up a barrier that separates the brain from the blood stream, and often is referred to as "the blood-brain barrier'', which function to separate metabolites from the blood and supply to the neurons that need the energy to keep up their activity in neurotransmission.[15] In addition, astrocytes can maintain the ion balance in the extracellular space and are involved in the scarring and repairing processes of brain tissue and spinal cord after getting injuries. Astrocytes also communicate through signals to each other and to presynaptic neurons by releasing ATP. They help recycle (i.e. uptake and release) neurotransmitters such as glutamate after activation of neurotransmitter release from presynaptic terminals, thereby involving in the regulation of synaptic transmission as part of controlling inhibitory or excitatory pathways.[12,13]

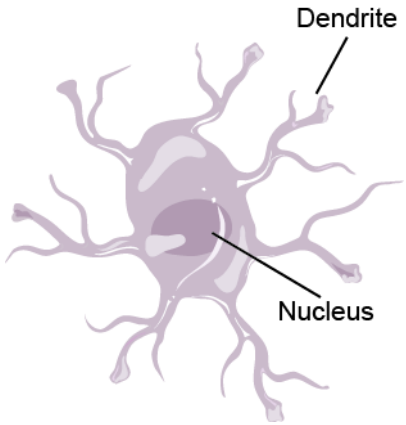


**Figure 6.** Schematic of a star-shape astrocyte.

### 1.2 Neuronal Communication

To properly function, the nervous system crucially relies on neuronal communication. In the neuronal system, each single neuron communicates with many other neurons to share information by forming networks or circuits. In neuronal communication, a neuron responsible for sending a signal into the neuronal network is often referred to as a presynaptic neuron, while a neuron receiving a signal from a neighboring neuron is called a postsynaptic neuron. Specifically, neurons communicate both chemically and electronically with each other via tiny gap junctions, called synapses, which is a connection structure between two neighboring neurons. Most commonly a synapse is located between a presynaptic terminal and postsynaptic terminal. The presynaptic terminal can place its connection to a postsynaptic site in connection to a dendrite or a cell body or a non-neuronal cell. In general, neurons receive signals via dendrites and send down signals outwards to axon terminals via axon, and eventually signals are passed to the other neurons through transmission of neurochemical signals.

#### 1.2.1 Electrical Signals of Neurons

Neurons can generate electrical signals based on ions flux across their cell membrane and unevenly distributed ion concentrations between the outside and inside of the membrane. Almost all cell membranes have an electric potential difference between the inside (negative) and outside (positive) of the membrane.[16] There are three main types (Figure 7) of membrane potential: resting membrane potential, graded potential and action potential.

Resting membrane potential is conventionally defined as the membrane potential that lasts without significant changes over a long time period, and is relatively stable when a neuron is not active, similar to a battery. In most cases, the resting membrane potential in neurons varies approximately from -60 mV to -70 mV.[17] The resting membrane potential can be estimated by the Goldman equation that is an extension from the Nernst equation and considers the factors of ion charges, concentration

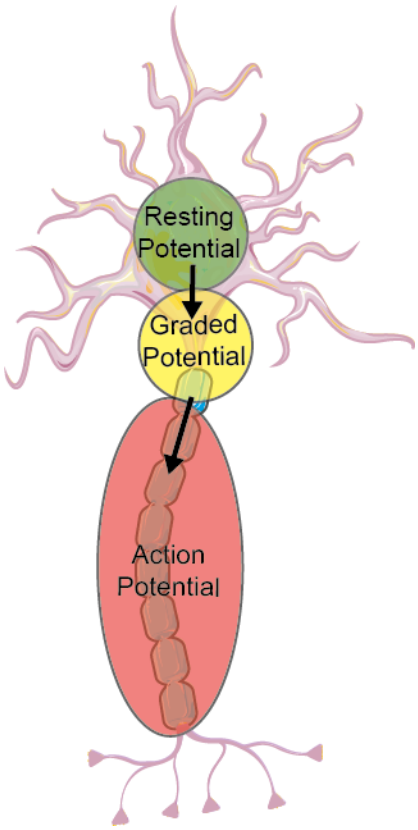


**Figure 7.** Schematic presentation of the different classified types of membrane potentials in neurons.

differences of ions between two sides of a cell membrane and the selective membrane permeability to ions. Normally it is assumed that only chloride ($Cl^-$), sodium ($Na^+$) and potassium ($K^+$) play important roles for resting membrane potential, according to:

$$E_m = \frac{RT}{F} \ln \left( \frac{P_K[K^+]_{out} + P_{Na}[Na^+]_{out} + P_{Cl}[Cl^-]_{in}}{P_K[K^+]_{in} + P_{Na}[Na^+]_{in} + P_{Cl}[Cl^-]_{out}} \right) \quad (1)$$

where $R$ is the universal gas constant, $T$ is the absolute temperature, $F$ is the Faraday constant, $P_i$ is the relative permeability of ion $i$, $[i^+]_{out}$ and $[i^+]_{in}$ stand for the concentration of ion $i^+$ in the extracellular solution and intracellular solution, respectively. The concentration of intracellular $K^+$ is about 20 times higher than the concentration of extracellular $K^+$ in a neuron, while the extracellular concentration of $Na^+$ is roughly 9 times larger than the concentration of $Na^+$ in the intracellular space.[18,19] Other ions like calcium ($Ca^{2+}$) and magnesium ($Mg^{2+}$) can be brought into this equation when they play important roles in different cell functions.[19] The negative inner resting membrane potential is mainly caused by the higher permeability of $K^+$ than that of other ions across the cell membrane and result in a higher concentration of intracellular $K^+$ than that of extracellular $K^+$ of a neuron.[5]

The potential of plasma membrane is not always static. Graded potentials (Figure 7) are also generated by local depolarization of membranes and occur for instance at the postsynaptic membrane in response to binding of neurotransmitters released from presynaptic terminals. When neurotransmitters function in an excitatory way, they can affect the graded potential to be more positive after binding to the postsynaptic receptors and to increase the possibility of producing an action potential. In contrast, when neurotransmitters act in an inhibitory way, they can influence the graded potential to be more negative, thus reducing the possibility of having an action potential.

The details of generating an action potential are described in the following processes (Figure 8 and 9). Once the graded potential hits the threshold potential at around

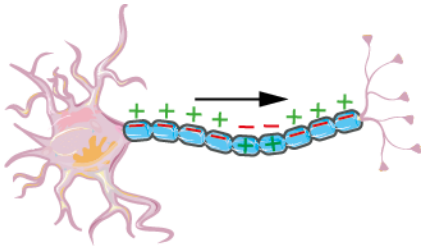

**Figure 8.** Illustration of an action potential travelling from the cell body down an axon of neuron and towards the axon terminals.

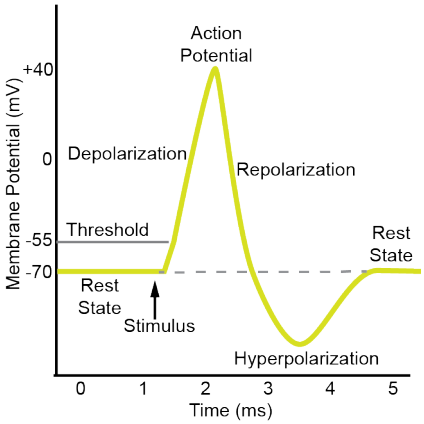


**Figure 9.** An approximate diagram displaying the phases of a typical depolarizing action potential across the cell plasma membrane over time.

-55 mV, the voltage-gated $Na^+$-ion channels are widely opened (depolarization) and this allows a large amount of $Na^+$ ions to flow into the cell, which depolarizes the membrane potential (less negative). This, in turns, triggers more voltage-gated $Na^+$ ion channels to open and to explosively produce a potential increase by the influx of the $Na^+$ ions, which eventually reverses the polarity of the cell membrane (negative interior and positive exterior). Meanwhile, voltage-gated $Na^+$ ion channels become inactive, voltage-gated $K^+$ ion channels get activated (repolarization), which allows the efflux of $K^+$ to lower the membrane potential (hyperpolarization) to a more negative potential shift (afterhyperpolarization) before it finally returns back to the original resting potential. After being generated, the action potential travels along the axon and down to the axon terminals via reversing the membrane potential alternately from negative to positive by the altered membrane permeability to $Na^+$ and $K^+$.[5]

### 1.2.2 Synapse

It is estimated that there are approximate 100 to 500 trillion synapses in an adult human brain.[20] The synapse is a key site in neurotransmission where information from one neuron gets transferred to another, and thus is an essential part of all our brain functions. Synapses can be fundamentally divided into two general types: electrical synapses and chemical synapse.

At the electrical synapse (Figure 10), an intercellular narrow gap called gap junction, about 3.8 nm,[11] is formed to link a presynaptic neuron with postsynaptic neurons. Electrical synapses are electrically conductive. Each gap junction contains numerous channels with about 1.2 nm to 2.0 nm inner diameter and that connect two neighboring neurons.[21,22] When an action potential arrives to an axon terminal of a presynaptic neuron, the membrane potential in that region changes, which leads to a flux of ions from the presynaptic neuron to the postsynaptic neuron through the gap junction. The signal transmission in electric synapse can be bidirectional. This means that the ions can propagate in either direction between the two-coupled

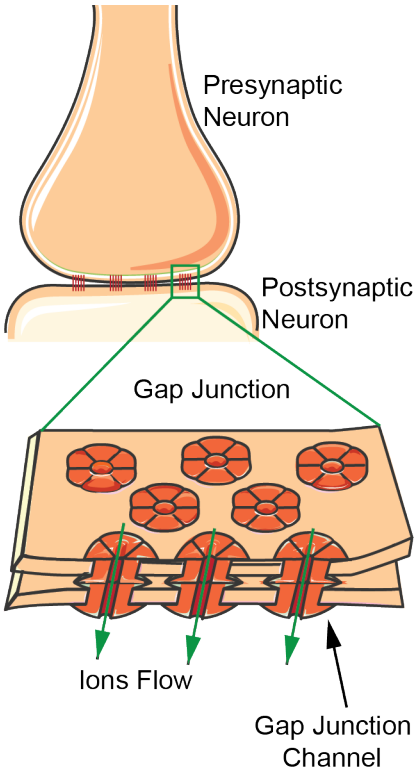


**Figure 10.** Schematic of an electrical synapse.

neurons, depending on the side at which the action potential is triggered. The received signal by postsynaptic neurons is normally smaller than or maintains the same magnitude as the original signal.[5] Besides, electrical synapses conduct signals across the synapse faster than chemical synapses.[5]

In chemical synapses (Figure 11), the change of membrane potential caused by the arrival of an action potential to the axon terminal of a presynaptic neuron, triggers the opening of voltage-gated calcium channels in the presynaptic membrane. This leads to a rapid influx of $Ca^{2+}$ ions from the extracellular space into the presynaptic terminals because of the steep $Ca^{2+}$ concentration gradient between the two sides of the presynaptic membrane.[5] The rapid local increase of $Ca^{2+}$ concentration inside of the presynaptic terminals triggers neurotransmitter-filled synaptic vesicles to fuse with the cell plasma membrane and release the vesicle content of neurotransmitters into the synaptic cleft,[5,23] which is an approximately 20 nm small space between the presynaptic neuron and the postsynaptic neuron and is a much wider space than at an electrical synapse. The process of fusion of synaptic vesicles to the plasma membrane, which results in vesicle content release into the extracellular space, is called exocytosis and is a fast process that occurs in less than a millisecond.[24] The neurotransmitters released then diffuse across the synaptic cleft where they can bind to specific receptors on the postsynaptic membrane of adjacent cells to complete the delivery process of chemical messengers. The binding of neurotransmitters may then lead to triggering of a nerve signal to be further transmitted into the neuronal network.

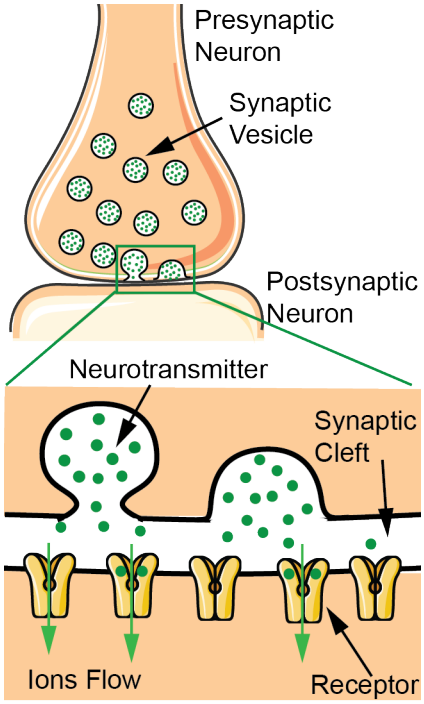


**Figure 11.** Schematic of a chemical synapse.

### 1.2.3 Exocytosis in Chemical Synapses

There are mainly two common types of exocytosis and are based on the mechanisms for how the process is triggered. The main pathway of exocytosis in neuronal chemical synapses is called regulated exocytosis that commonly exists in secretory cells but not in all types of cells. Regulated exocytosis occurs in response to an external

stimulation, for example, by a nerve signal that triggers the influx of $Ca^{2+}$ ions into the cytoplasm, as described in the Section 1.2.2 of chemical synapse. Unlike regulated (non-constitutive) exocytosis, constitutive (i.e. non-regulated) exocytosis takes place in all cells. Here, vesicles either release their cargo of internal components to the extracellular space or supply the cell plasma membrane with newly synthesized membrane proteins that are carried in the membrane of transport vesicles and are delivered to cell plasma membranes after vesicle fusion.[16] As the topic for this thesis is neurochemistry, the focus here will be on regulated exocytosis in chemical synapses.

### 1.2.3.1 Pre-steps Involved in Regulated Exocytosis

In neurons, the synaptic vesicle function as a storage compartment for a quantal amount of neurotransmitters until these molecules are needed for neurochemical signaling. This vesicle compartment filled with the chemical information is then triggered to release its content into the extracellular space. This process needs to be spatially controlled and as neuronal signals need to be fast, this process also needs to be efficient. Hence the machinery for regulated exocytosis has evolved to involve four major pre-steps (Figure 12). These involve vesicle 1) loading 2) docking 3) priming and 4) fusion. Neurotransmitters are loaded into synaptic vesicles with the assistance of transport proteins in the vesicular membrane, where the main transport proteins that drive the neurotransmitter transport are chemically selective transporter proteins and a proton pump ATPase.[25,26] Synaptic vesicles that have been loaded are transported to the area near the exocytosis release site, the so called “active zone”. Here the vesicles dock followed by prime to the cell plasma membrane through interactions with SNARE- (soluble N-ethylmaleimide-sensitive fusion protein attachment protein receptors) proteins and are ready to on command to fuse with the plasma membrane. In response to triggered $Ca^{2+}$ influx through voltage-gated calcium channels located by the active zone, the formation of SNARE-protein complexes drives the synaptic vesicle to

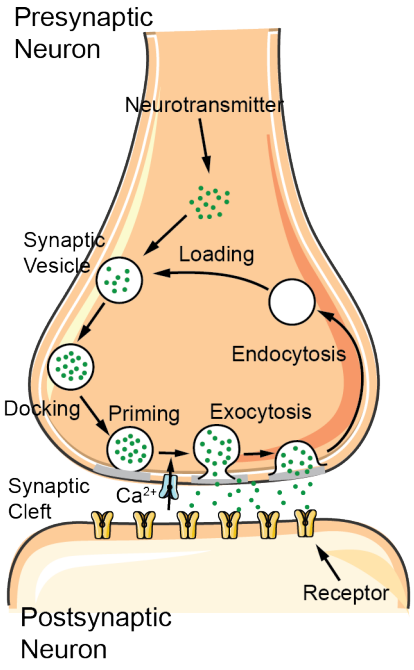


**Figure 12.** Illustration of the pre-processes involved in the regulated exocytotic events during neuronal communication.

come in close enough contact with the plasma membrane for the two membranes to fuse.[5] This creates initially a few nanometer sized fusion pore that spans from the synaptic vesicle compartment to the plasma membrane, which then dilates to a larger size and allows for the synaptic vesicle neurotransmitter content to be released through the pore and into the extracellular space (i.e. synaptic cleft).

### 1.2.3.2 Molecular Mechanism of Neurotransmitter Release

To date, the whole precise picture of molecular mechanisms for regulated neurotransmitter release caused by intracellular membrane fusion of vesicles in axon terminals is still not completed. However, several proteins involved in this process and their important roles have been studied and deduced. Currently, one well-accepted model (Figure 13) hypothesizes that the intracellular fusion of vesicle membrane with plasma membrane is a protein-mediated process that is driven by the mechanical force generated from the formation of the SNARE-complex.[27] This driving force offers enough energy to overcome the tendency of separation within protein helices themselves[28,29] and to overcome the electrostatic repulsion between the membranes that need to fuse.[30,31] The main SNARE-proteins involved in complex formation are syntaxin and SNAP-25, which are found on the presynaptic plasma membrane, and synaptobrevin that is a vesicle membrane protein. These SNARE-proteins spontaneously assemble together and form a four-helix bundle (partial trans-SNARE complex assembly) that is the core SNARE-complex containing a syntaxin, synaptobrevin and 2 helices of SNAP-25, which dramatically stabilizes the connection between the two membranes.[32,33] The partial assembly of *trans*-SNARE-complex during the priming step links the two membranes and forces them to come close together when the SNAREs zippers up and the membrane fuses. Synaptotagmin is a protein found in the vesicular membrane and is thought to serve as a $Ca^{2+}$-sensor in this process.[5,34,35] When $Ca^{2+}$-channels open causing a flux of $Ca^{2+}$-ions into the cytoplasm at the active zone, the

(1) Vesicle docks onto the membrane of presynaptic terminal

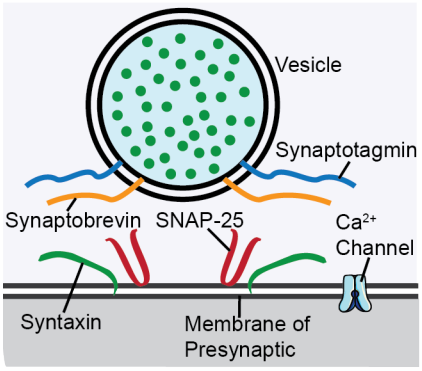


(2) Vesicle is pulled closer to the presynaptic terminal membrane by the formation of SNARE complex.

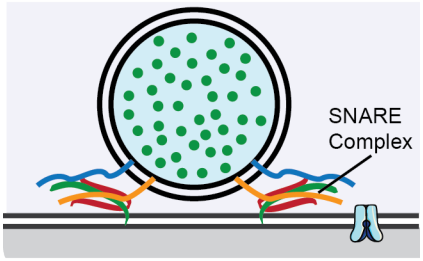


(3) $Ca^{2+}$ enters into presynapse and binds to synaptotagmin

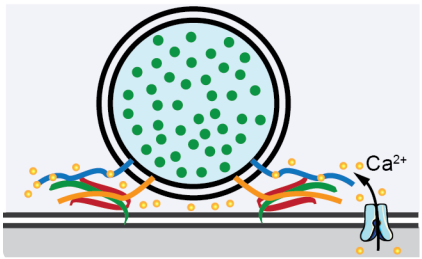


(4) Synaptotagmin bound with $Ca^{2+}$ catalyzes membrane fusion and fusion pore opening

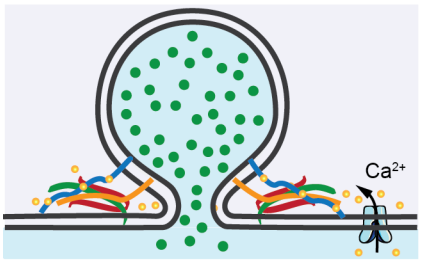


**Figure 13.** Illustration of molecular mechanism of exocytotic event during vesicular release.

conformation of synaptotagmin changes upon binding of $Ca^{2+}$, which triggers membrane fusion and fusion pore formation between the vesicle and cell plasma membrane upon full *trans*-SNARE complex assembly.[5,34] The fusion pore is then thought to continue expanding with formation of *cis*-SNARE complex converted from *trans*-SNARE complex.[27] In addition to the proteins mentioned above, more proteins like SM (Sec1/Munc18-like) proteins, complexins, and NSF (N-ethylmaleimide-sensitive fusion protein) have been identified to play important roles for associating the fusion of synaptic vesicle with presynaptic plasma membrane.[34,36,37]

#### 1.2.3.3 Different Modes of Exocytosis and Vesicle Recycling

The amount of neurotransmitters stored within synaptic vesicles is often referred to as quanta. The hypothesis of quantal neurotransmitter release via axon terminals was proposed in 1950s via measuring acetylcholine release from neuromuscular junction by Jose del Castillo and Bernard Katz who became a Nobel Prize winner for his findings.[38–40] The dynamics of exocytosis via quantal release has been roughly divided into two main categorizes: *full release* that involves the release of entire vesicle content after vesicle fusion, and *partial release* where only a fraction of the vesicle content is released before the vesicle compartment is recaptured. From early 1970s, the research of both Heuser and Reese, as well as Ceccarelli with colleagues, suggested that synaptic vesicles fuse with, and are rapidly retrieved from, the presynaptic plasma membrane to release quantal neurotransmitters.[41–43]

However, they proposed two different pathways of synaptic vesicle recycling, which are associated with two different dynamic aspects of exocytosis process. In the research of Heuser, Reese and their colleagues, synaptic vesicle recycling was suggested to reply on a relatively slow process, with time scales of within one minute (endocytosis) via formation of coated vesicles from clathrin coated membrane pits that occur at a site distance away from the neurotransmitter release site (i.e. the active

zone),[43–46] and those coated vesicles then go through endosomes before new vesicles bud off and are reloaded with neurotransmitters for another round of exocytosis.[43] The pathway of exocytosis assumed here is mainly full release via a complete vesicular collapse of the synaptic vesicle that incorporates all its vesicular components with the membrane of the presynaptic active site.[47]

In contrast, the research of Ceccarelli and his colleagues with their continuously systematical studies suggested that the synaptic vesicle recycling occurs in a much faster rate and directly at the site of the active zone. They suggested a mechanism without a complete vesicle membrane fusion (or complete exocytosis) and without the need of coated vesicle formation after a transient reversible exocytosis to rapidly reuse vesicles.[41,42,48–54] This model of exocytosis was officially named 'kiss-and-run', which describes the transient partial exocytotic process by Ceccarelli's colleagues, Fesce *et al.* in 1994.[55]

In 1992, Chow *et al.* demonstrated the regulated neurotransmitter release where the neurotransmitter content (i.e. catecholamines) from vesicles of bovine adrenal chromaffin cells slightly leak before a larger amount neurotransmitters is release via full exocytosis. This was concluded from monitoring vesicle content release via examining amperometric pre-spike features of current spikes called a "foot" indicating a small amount of neurotransmitter is released through the initial fusion pore before detecting the main exocytosis event denoted by the current spike.[56] This hypothesis of pre-leakage before the exocytosis event was confirmed by De Toledo *et al.* in 1993, in which amperometric current spikes with similar shape from mouse mast cells were obtained. This work also suggested the existence of transient secretory vesicle fusion, meaning that it indicated rapid partial release of the exocytosis mode so called 'kiss-and-run'.[57]

Besides, a longer exocytotic process but not full release model was suggested by Sulzer's group in 2004.[58] This model can be regarded as an extended version of 'kiss-and-run' partial release, which results in larger fraction of vesicular content release that is released a little-by-little

from a flickering fusion pore. The retrieved vesicles through this mode of exocytosis also allow a rapid re-usage of the vesicle compartment and more rapid neurotransmitter loading and fusion-ready vesicles. Compared to the direct 'kiss-and-run' exocytosis model that rapidly opens and closes a narrow fusion pore, this longer flickering model is more complicated involving a fusion pore opening and closing (flickering) or enlarging and constricting (fluctuating) while preventing a final complete vesicular membrane collapse into presynaptic membrane.

Full exocytotic release is thought to be correlated with a slow cathrin-mediated endocytosis (vesicle retrieval) process, while transient partial exocytotic release (i.e. kiss-and-run) corresponds to a route for the synaptic vesicle to go through a rapid vesicle retrieval. More pathways of vesicle retrieval have also been suggested.[59,60] Although there is still a controversial debate which mode predominates the synaptic vesicle recycling process,[61,62] it has been well accepted that the two modes associated with full and partial exocytotic release may co-exits together with other potential pathways in the vesicle recycling cycles.

As part of the work of this thesis, we developed a novel ultrafast enzyme-based amperometric microelectrode sensor for the detection of the neurotransmitter glutamate, and this sensor was used for monitoring single exocytosis events during neuronal activity in the nucleus accumbens of mouse and rat brain tissue. In this work[63] we were able to capture rapid sub-millisecond complex exocytosis transients that we believe were examples of a mixture of partial and full exocytosis events, but more work is needed to fully characterize and confirm the mechanisms behind these complex amperometric transients.[64] However interestingly, similar amperometric current shape spikes and frequencies of complex exocytosis events were detected in both mouse and rat measurements, and previously also observed from octopamine release in nerve terminals of *Drosophila melanogaster* larvae.[65] Hence this

suggests a release pattern that is conserved in several species although needs to be better understood.

### 1.2.4 The Synaptic Vesicles

Synaptic vesicles (or neurotransmitter vesicles, Figure 14) are small organelles (about 40 - 50 nm in diameter) loaded with neurotransmitters and localized in the presynaptic terminals of neuron.[66,67] The membrane of synaptic vesicle is confined by a phospholipid bilayer and vesicular membrane proteins that occupy one-fourth of the space of the inner membrane surface of vesicle.[66] The lipid bilayer composition was previously estimated to be made up by roughly 40% phosphatidylcholine (PC), 32% phosphatidylethanolamine (PE), 12% phosphatidylserine (PS), 5% phosphatidylinositol (PI) lipids and 10% cholesterol as measured in weight percentage of purified synaptic vesicle from rat neocortex.[68] However, in a later study by Takamori *et. al* suggest a membrane composition with a larger cholesterol content of 30% - 40% content and a lower concentration of PI lipids of 1 %.[66] Synaptic vesicles are also composed of approximately 410 different proteins in total (Figure 14).[66] These membrane proteins are usually categorized based on their function, and where one group of essential proteins for the synaptic vesicle function is the vesicular neurotransmitter transporter proteins. These proteins span across the synaptic vesicle membrane and are responsible for the uptake of neurotransmitters from the cell cytoplasm into the synaptic vesicle compartment for storage. The neurotransmitter transport protein shuttle the neurotransmitters molecules against the neurotransmitter concentration gradient and is supported by the presence of a proton ($H^+$) gradient across the vesicular membrane. Here, in exchange of protons, the direction of neurotransmitters uptake is opposite to that of the proton flow.[69] The proton gradient is created by v-ATPase that is an enzyme crossing vesicular membrane and catalyzes the hydrolysis of adenosine triphosphate (ATP) to adenosine diphosphate (ADP) to power the continuously pump of protons into the vesicle.[70] This results in a synaptic vesicle with an acid internal pH of between 5.2 to

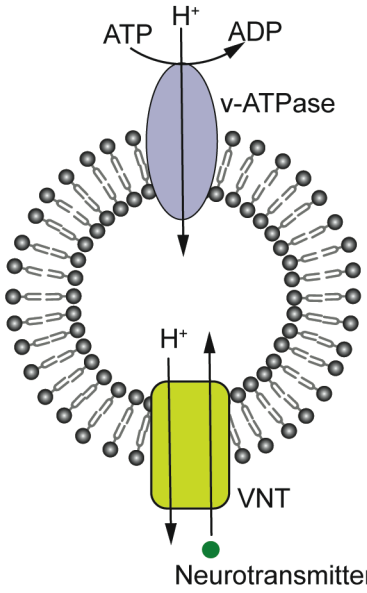


**Figure 14.** Schematic of synaptic vesicle with proton pump and neurotransmitter transporter.

5.5,[71,72] and creates a proton gradient across the vesicle membrane to the cytoplasm where a neutral pH environment (about pH 7.25).[73] There is a majority of four types of vesicular neurotransmitter transport proteins,[74] including vesicular monoamine transporters (VMATs),[75] vesicular acetylcholine transporter (VAChT),[75] vesicular GABA and glycine transporter (VGAT),[76] and vesicular glutamate transporters (VGLUTs).[77] Another important group of vesicular membrane proteins are those that take part in the SNARE-mediated machinery for vesicle docking and fusion of synaptic vesicles, like synaptobrevin, which was previously mentioned, are thus in the category of the vesicle trafficking proteins.

In many studies related to synaptic vesicle function, simplified models are often used. A common model has been to use small or large unilamellar vesicles (LUVs) that are created from synthetic lipids, often referred to as liposomes (Figure 15). These are often synthesized using similar lipid composition to that of the native vesicles as mentioned previously, and are used for instance, in utilization of biosensors and exocytosis studies.[78,79] In this thesis, a combination of both isolated native synaptic vesicles and synthesized liposomes were used for developing a new analytical method for quantification of glutamate content in synaptic vesicles and quantification of glutamate release at exocytosis (**Paper V**).

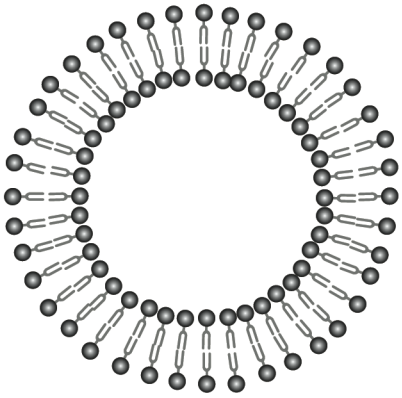

**Figure 15.** Schematic of a liposome with a lipid bilayer consisting of phospholipids.

### 1.2.5 Neurotransmitters

In neuronal communication, more than 100 different neurotransmitters have been identified and that function as chemical messengers,[5] although the exact numbers still remains unknown. There are different ways to classify neurotransmitters based on, for example, their size, functions and chemical structure. If based on size, neurotransmitters can be generally separated into two broad groups:[5] 1) large molecule neuropeptides consisting of 3 to 36 amino acids such as somatostatin and endorphins; 2) small molecule neurotransmitters like amino acids (e.g. glutamate and GABA and histamine), quarterly amines (like acetylcholine) and biogenic amines

such as dopamine, serotonin, epinephrine and norepinephrine and histamine. However, under the category of small molecule neurotransmitters, biogenic amines are frequently discussed separately since they share similar chemical properties and have similar effects on postsynaptic actions. Neurotransmitters function in the nervous system through binding to their specialized receptors to proceed through selective and precise communication. Although the design of the neurotransmitter release machinery is common for all kinds of neurotransmitter system, the specific synthesis, synaptic vesicle loading and release of particular neurotransmitters can differ from each other.

### 1.2.5.1 Catecholamines

Catecholamines are biogenic amine neurotransmitters and/or hormones and include neurotransmitters such as dopamine, epinephrine (adrenaline) and norepinephrine (noradrenaline). The chemical structure of these neurotransmitters all share the catechol moiety,[5,80] and tyrosin, which is an amino acid, is the common precursor in synthesis for all catecholamines. The biosynthesis pathway of catecholamines is an enzymatic process illustrated in Figure 16.

Dopamine ($C_8H_{11}NO_2$, 153.2 g/mol) is produced in different type of cells in different areas of the mammalian body, including neurons in the brain, and endocrine cells in the adrenal medulla and kidney.[81,82] It is synthesized from its precursor 3,4-dihydroxy-**l**-phenylalanine (L-DOPA), which in turn is synthesized from tyrosin in the presence of oxygen ($O_2$), which functions as a co-substrate and biopterin as a cofactor. In the brain, dopamine serves as a neurotransmitter and neuromodulator, where its signaling pathways involve, for example, reward-motivated behavior and control of body movements.[5] Outside of CNS, dopamine has an important physiological role in the kidneys to regulate blood pressure.[82]

Norepinephrine ($C_8H_{11}NO_3$, 169.2 g/mol), also referred to as noradrenaline, is synthesized from dopamine and is also the precursor of epinephrine. Norepinephrine serves as a

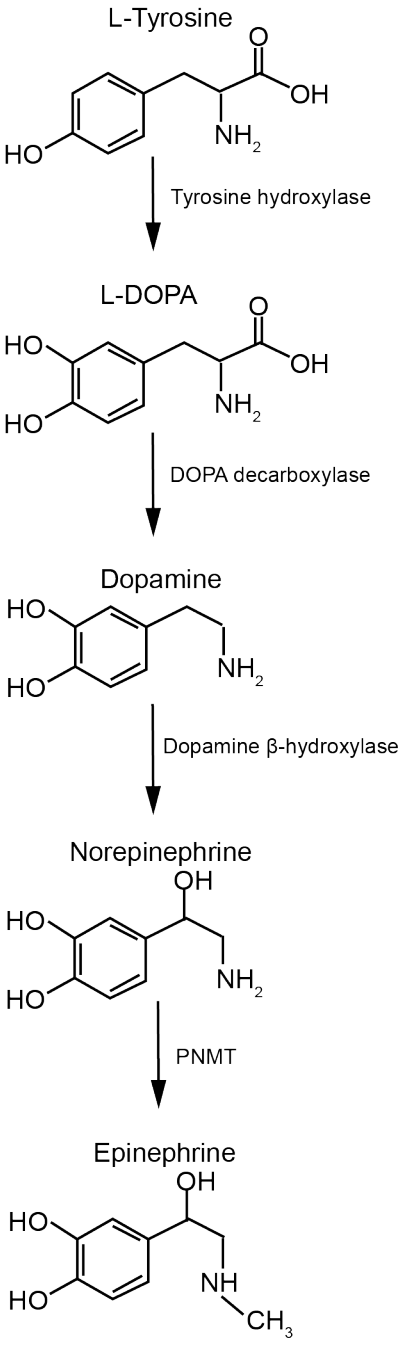


**Figure 16.** The enzyme-catalyzed biosynthesis of catecholamines.

hormone and neurotransmitter in the brain and in the body. In the brain, the most important source of norepinephrine is in the locus coeruleus, which is a brainstem nucleus. Norepinephrine affects brain functions, such as alertness, restlessness and anxiety,[5] and also modulates cognitive functions.[83,84] Outside of the brain, norepinephrine is also found in chromaffin cells of adrenal medulla and postganglionic neurons of the sympathetic nervous system, which is a division of the autonomic nervous system (ANS) in PNS. Here, in these regions norepinephrine takes part to regulate the blood flow, blood pressure and heart rate, especially in the fight-or-flight response under danger or stress. Norepinephrine also plays an important role in other aspects, for example, by affecting behavior including aggression, depression, agitation, and on pathophysiology, like depressive disorder and schizophrenia.[85–87]

Epinephrine ($C_9H_{13}NO_3$, 183.2 g/mol), also named adrenaline, is synthesized from the catalytic methylation of norepinephrine via the enzyme phenylethanolamine *N*-methyltransferase (PNMT). It is mainly produced in adrenal glands, although neurons in the CNS also produce a small amount of epinephrine.[80] Epinephrine serves as a neurotransmitter in the nervous system and as hormones in almost all tissues in the body through binding to several types of adrenergic receptors.[80] Together with norepinephrine, epinephrine also plays an important role in the fight-or-flight response by increasing like heart rate, cardiac output and blood pressure,[88] which was initially suggested by Walter Bradford Cannon in the early 1900s.[89] Epinephrine has also been directly used in medication for conditions like cardiac arrest,[90] anaphylaxis (an allergic reaction)[91] and asthma[92].

#### 1.2.5.2 Acetylcholine

Acetylcholine ($C_7H_{16}NO_2^+$, 146.2 g/mol) is an organic compound regarded as the first identified neurotransmitter.[5] Its chemical structure (Figure 17) is composed of an ester of acetic acid and choline. In the

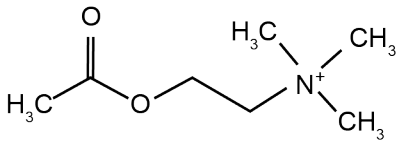


**Figure 17.** Chemical structure of acetylcholine.

presynaptic nerve terminal, the synthesis of acetylcholine is catalyzed by choline acetyltransferase from acetyl coenzyme A and choline.[5] Acetylcholine function in both of the CNS and PNS by binding to two main classes of receptors (cholinergic receptors): nicotinic acetylcholine receptor and muscarinic acetylcholine receptor.[93,94] When released by motor neurons, acetylcholine can activate muscle contraction at the neuromuscular junction.[95] It also functions in ANS to regulate the unconsciously body processes like rate of breath and heartbeat, blood pressure, digestion and certain reflex action such as coughing and sneezing.[96] In contrast to norepinephrine, acetylcholine plays a role on the cognitive functions such as memory and learning.[96,97]

In addition, when released via exocytosis into the synaptic cleft, acetylcholine can also be broken down via the enzyme acetylcholinesterase into acetate and choline, where choline can further be recycled back to the presynaptic terminal via specific membrane transporters to participate in the synthesis of acetylcholine. The same recycling cycle for acetylcholine also occurs intracellularly inside of the presynaptic neuron via the synthesis and decomposition reactions of acetylcholine.

### 1.2.5.3 Glutamate

Glutamate ($C_5H_8NO_4^-$, 146.1 g/mol) is an anion of glutamic acid and a non-essential amino acid that is synthesized in neurons.[5,98] Its chemical structure is illustrated in Figure 18. Glutamate serves as a principal excitatory neurotransmitter and is one of the most abundant amino acids in the vertebrate nervous system and entire human body,[99,100] with more than half of synapses in the brain releasing glutamate.[5]

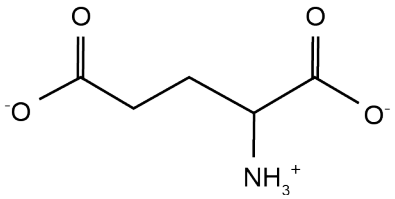


**Figure 18.** Chemical structure of glutamate.

Glutamate can be produced from different pathways. Firstly, it is synthesized from $\alpha$-ketoglutaric acid that is an intermediate of a key metabolic pathway containing series of chemical reactions in the citric acid cycle.[5,101] It can also be synthesized from its main precursor glutamine catalyzed by mitochondrial enzyme glutaminase found in presynaptic

terminals of the CNS.[3,101] After being released to the extracellular space through exocytosis, glutamate in the synaptic cleft can be rapidly removed via binding to glutamate receptors on the membrane of postsynaptic neuron, or via re-uptake mainly by neighboring glial cells or in part by presynaptic neurons.[101] Glutamate that is recaptured into glial cells is then metabolized to glutamine, which is latter released back to the presynaptic neurons.[5,101] This recycling process is known as the glutamate-glutamine cycle that works to maintain a sufficient supply of glutamate in the CNS.[5,101]

Glutamate as a neurotransmitter plays important roles in the nerve system and is involved with most of the major brain functions. Glutamate is also important for the neuronal survival in the developing brain.[99,102] When glutamate uptake by glial cells does not function efficiently, the accumulated glutamate in extracellular space can be neurotoxic and cause chronic and acute neurodegeneration, which may eventually lead to cell death[99,103] and associate with diseases like Alzheimer's disease,[104] cognitive functions (e.g. memory and leaning) especially in the elderly [100] and autism[105].

#### 1.2.5.4 GABA

GABA (*gamma*-aminobutyric acid) is an amino acid, with a chemical formula of $C_4H_9NO_2$ and a molecular weight of 103.1 g/mol. GABA (Figure 19) is primarily synthesized from glutamate. And there is a similar GABA uptake mechanism to that for glutamate.[3]

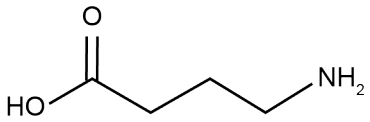


**Figure 19.** Chemical structure of *gamma*-aminobutyric acid.

GABA has been identified in the brain since the 1950s.[106,107] It is the principle inhibitory neurotransmitter that counterbalances the excitability of neurons in the CNS of adult mammalian.[3] After released via exocytosis from presynaptic neuron, the inhibitory function of GABA works by binding to receptors embedded in the membrane of both post- and presynaptic neurons to reduce the membrane potential (i.e. hyperpolarization) via changing the membrane permeability to specific ions, thereby inhibiting the occurrence of an action potential in a neuron. Once the balance between neuronal excitation and

inhibition is disturbed by abnormal GABAergic functions, seizures, anxiety disorders, depression and other diseases in elderly like Parkinson's disease and Alzheimer's disease may occur with a high probability.[108–110] GABA also plays an important role in the development of neurons in many region of the brain as an excitatory elemenet.[111]

### 1.3 Metabolism of the Brain

The human brain is a metabolically expensive organ, it consumes approximate 20 % of whole resting metabolic energy to maintain its brain functions, even though it only accounts for about 2 % of the entire body weight.[112–114] Among the energy consumed in the brain, roughly 75 % is involved in neurotransmission, for instance, to maintain the resting potential of the neuron membrane and the ion gradients between two sides of a neuronal membrane, and to generate action potential.[113,114] The remaining 25 %, which is a small proportion of energy fueled for the brain's function, is utilized to maintain the basic cellular activities, for example, for synthesis, degradation and turnover of proteins, and for axonal transport.[114] The metabolic rate measured in the gray matter is much higher than that in the white matter, and the metabolic rate is also influenced by the local neuronal activities in the brain, which indicates a strong link between the brain function and the energy metabolism.

#### 1.3.1 Glucose Metabolism

The energy metabolism in the brain, as well as body, relies on its major substrate glucose, which is the most important energy source in all organisms, and with a molecular formula of $C_6H_{12}O_6$. Glucose metabolism fuels the brain function by generating ATP from pyruvate via TCA (*tricarboxylic acid* or citric acid) cycle in the present of $O_2$, where pyruvate is converted from glucose via glycolysis. Through these metabolic reactions, 32 ATP are estimated to be produced from one glucose molecule.[113]

In addition to its function as an energy substrate, glucose also serves as a substrate for formation of glycogen that is the main storage form of glucose, and serves as substrate

for synthesis of inositol, which is involved in cellular signal transduction. Besides, its carbon skeleton, as an intermediate of the TCA cycle, can serve as a precursor for neurotransmitters. For example, acetyl-CoA is the precursor of acetylcholine, and α-Ketoglutarate is precursor of both glutamate and GABA.[5,113]

### 1.3.2 ATP and Neuronal Activity

ATP ($C_{10}H_{16}N_5O_{13}P_3$) is a compound that is usually referred to as the currency of energy in the cell. It is estimated that the energy consumed during neuronal transmission in the brain is approximately 21 μmol ATP per gram human brain tissue per minute.[114] The energy stored in ATP is majorly released by the hydrolysis of ATP to produce adenosine diphosphate (ADP) and an inorganic phosphate ($P_i$). This reaction is estimated to release about 28 to 34 kJ/mol of Gibbs free energy at the standard state when the concentrations of ATP, ADP and $P_i$ are 1 M. [115] ATP and ADP can be further converted to AMP (adenosine monophosphate) with a Pi or pyrophosphate ($PP_i$) via hydrolysis to release additional energy.[116] ATP has also been considered as an excitatory neurotransmitter in the category of purines in the nervous system.[5]

# 2. Tools to Monitor Exocytosis

### 2.1 Microscopy

Since the hypothesis of quantal neurotransmitter release was brought up via experiments performed by electrophysiology using microelectrodes in 1950s,[38–40] the visual evidence to support the correctness of this theory was required. Fortunately, it was achieved gradually by the development of imaging techniques like electron microscopy and optical fluorescence microscopy. They contributed tremendously to allow obtaining unique insights of the exocytosis details related to quantal neurotransmitter release.

#### 2.1.1 Electron Microscopy

Electron microcopy (EM) is a powerful imaging method providing a spatial resolution on the sub-nanometer level. However it requires fixation of samples and hence it is an imaging method that can offer snap shot images of cells but is restricted from imaging at live tissue. An electron microscope illuminates the sample using a beam of accelerated electrons produced from an electron gun. The electron microscope is different from optical microscopes (or light microscopes), which usually utilize photons of visible light as the source to illuminate samples. Compared to optical microscope, electron microscope can assist to visualize smaller details of samples such as resolving the structure of the 50 nm synaptic vesicles and their location inside the presynaptic terminal. This is because electrons have shorter wavelength than photons, and the ultrathin sections of cell samples can provide a 2D image of the intracellular environment. When an electron beam shoots a sample, some of the electrons are absorbed into the sample, some are transmitted through the sample and some are scattered out. In details, when the electron interacts with a sample, the energy of the incident electron in turn emits a smaller amount energy, such as in the form of secondary electrons, backscattered electrons, Auger

electrons or X-rays. As described below there are several types of EM techniques that exploit these different types of electrons. To image biological sample, an important EM imaging method is to utilize the absorption of electrons. This method creates the contrast that images are built on.

The first electron micrograph of visualizing synaptic vesicle exocytosis in frog neuromuscular junctions was obtained by Couteaux and Pécot-Dechavassine in around 1970 using tissue samples with chemical fixation.[117] The Ω-shape of synaptic vesicles during vesicle fusion with the presynaptic membrane (i.e. exocytosis) after stimulation in chemically fixed frog neuromuscular junctions was also clearly unveiled using EM by Ceccarelli in 1972.[41] However, stimulated rapid exocytosis events could not be captured by EM since the samples prepared using chemical fixation that is a slow sample preparation process. Until a quick-freezing technique was established as a physical fixation method, snap shot images of triggered exocytosis events in response to a 2-5 ms stimulation were finally obtained in circa 1980,[118,119] which strongly demonstrated that the neurotransmitters were released from quantal vesicles during exocytosis.

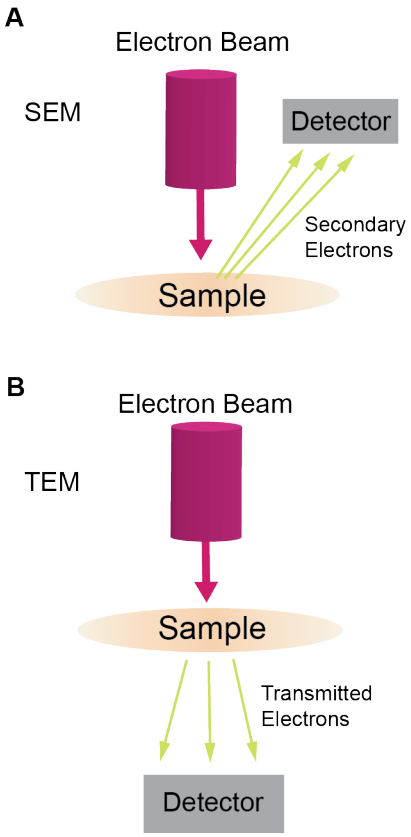


**Figure 20.** A simple illustration of a basic SEM and TEM microscope with different detection modules.

#### 2.1.1.1 Scanning Electron Microscope

The scanning electron microscope (SEM, Figure 20A) is one type of electron microscope. This method images sample by scanning the sample surface with a focused electron beam. Atoms in the sample then interact with the incoming beamed electron. Among various signals, the signals detected by SEM are mainly the emitted secondary electrons that contain information like the sample composition and surface topography, which can be used to produce images of sample topography. Since the samples used in SEM are usually imaged in a high vacuum environment, it is required that the sample is prepared to be extremely dry. It is also required that the sample or at least at its surface, is conductive. Otherwise, non-conductive samples need to be coated with a conductive material like gold or platinum.[120] To obtain a clear image

and prevent charge accumulation that brings noise to the image, the sample must be electrically grounded using, for example, conductive adhesive to connect to the metal specimen holder. The spatial resolution of an SEM image is smaller than 1 nm and was pushed down to a 0.4 nm resolution using a secondary detector in 2009 from Hitachi High-Technology.[121] Due to the high spatial resolution of the topology of conductive surfaces, the SEM method was used in the work of this thesis to characterize the surface of the sensor electrodes used in the development of an enzyme-based for detection of acetylcholine and glucose (**Paper I** and **II**).

#### 2.1.1.2 Transmission Electron Microscope

Transmission electron microscope (TEM) is an imaging technique that allows transmitted electrons to pass through the sample and requires the chemically fixed samples to be stained to achieve imaging contrast and that samples are cut into extremely thin sample slices to allow electron transmission (Figure 20B). The thickness of samples for TEM is typically less than 100 nm. Tissue samples for TEM imaging are also required to be coated with an ultrathin conductive layer to avoid the built-up electrostatic charge at sample surface. The operation of standard TEM imaging system is carried out in a low-pressure environment from $10^{-4}$ Pa to $10^{-9}$ Pa. In general, the spatial resolution of a TEM image is higher than that of an SEM image. A super high resolution of less than 50 pm in Ge crystal using scanning transmission electron microscope (STEM) with an annular dark field detector was reported in 2009.[122] A difference from TEM where the electron beam is focused below the sample, the electron beam from the electron gun in STEM is focused on a sample via a scanning coils positioned before sample.

### 2.1.2 Fluorescence Microscopy

Fluorescence microscope is an optical microscope that illuminates the sample by incident light and images the sample using fluorescence and phosphorescence. Specifically, excitation light is firstly selected with respect

to specific wavelengths using an excitation filter and then is directed at the specimen that often needs a fluorophore labeled for visualization and via a dichroic mirror. In fluorescence imaging, the excitation light illuminating the specimen is absorbed by the fluorophores in the sample and the emitted light with a weaker intensity and longer wavelength (e.g. fluorescence) is collected. The fluorescence emission is filtered with certain wavelengths and finally collected for imaging sample using a detector, which provides a spatial image of where the fluorophores are located in a sample. The structure of a basic fluorescence microscope is illustrated in Figure 21.

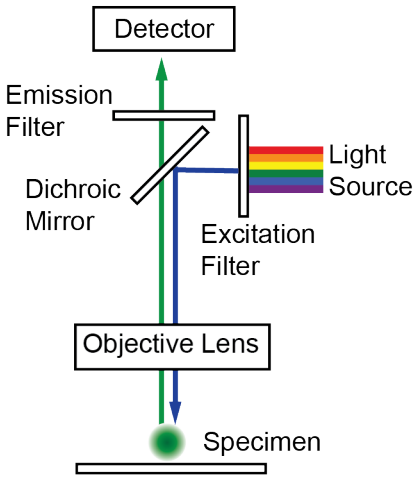


**Figure 21.** Schematic of a basic fluorescence microscope.

### 2.1.2.1 Labeling Schemes

As very few fluorescent molecules naturally exist in biological samples and in order for fluorescence microscopy to be used as an imaging method for cell imaging, the sample most often needs to be stained with fluorophores via various labeling strategies. For using fluorescence microscopy to image secretory cells, several important fluorescent molecules (i.e. fluorophores) have been developed to stain the secretory vesicles, and their implementation in studies on vesicular dynamics at exocytosis is discussed below.

#### 2.1.2.1.1 FM Dyes

The FM-type of dyes are widely used for visualizing lipid bilayers including the secretory vesicle in live cells and have been used in many studies related to the vesicle cycling that include the processes of fast exocytosis and the subsequent slower endocytosis. FM dyes are named using the initials of its inventor's name, Fei Mao who firstly synthesized FM1-43 that was used to visualize and show that the whole vesicle recycling process at the frog neuromuscular terminals takes about 1 minute.[123,124] Later, using the same dye, the time course of endocytosis was determined to about 20 s – 30 s,[125,126] and that a full vesicle cycle was measured to approximately 40s in rat hippocampal nerve terminals.[126]

FM1-43 is a derivative of the styryl dye RH414 and contains a lipophilic group and a divalent cation (Figure 22). FM dyes (also other trityl dyes) stain biological samples by incubation of cells in a solution containing dyes for a short time (e.g. few minutes) as the dye quickly incorporates into membranes by inserting the lipophilic tail into the outer leaflet of a lipid bilayer. Therefore by stimulating cells to exocytosis in the presence of the dye, secretory vesicles fusing with the plasma membrane can incorporate the dye into the vesicle lumen and fluorescently stain the vesicle compartment when the vesicles are recaptured from the cell plasma membrane by endocytosis. Figure 23 illustrates the whole process of the vesicle labeling with FM dyes. With the assistance of lipophilic group, FM dyes inserts into the outer membrane, facing extracellular space, of presynaptic terminals. By nature, the FM dyes are barely fluorescent in aqueous solution and become highly fluorescent when incorporated into the hydrophobic environment of a lipid bilayer. Hence, the intensity of its fluorescence increases significantly when dissolving in the membrane compared to that of the dye in free solution environment. However FM dyes cannot pass through the membrane to the inner side since it carries a cation group. Therefore via the vesicles recapture by endocytosis, FM dyes are encapsulated into synaptic vesicles and result in vesicles that can be visualized as bright spots and tracked by at their location in the cytoplasm of cells. This allows monitoring the vesicles by their movement through the vesicle cycle until the vesicles are stimulated for another round of exocytosis and the encapsulated dye is released. Thus, the process of exocytosis and endocytosis can be timed by observing the fluorescence with fluorescence microscopy. Other FM dyes[127] like FM2-10[128] and FM4-64[129,130] were also synthesized and used to, for instance, observe the mechanism of vesicle recycle and dynamics of exocytosis like 'kiss and run' model.

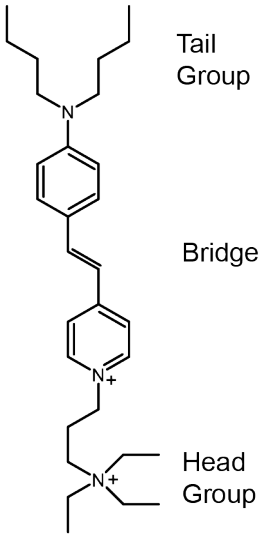


**Figure 22.** Chemical structure of a FM1-43 dye.

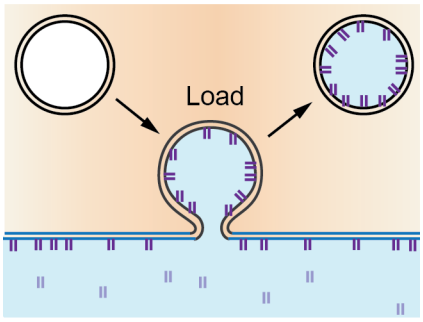


**Figure 23.** The process of FM dyes labeling of synaptic vesicles by stimulating exocytosis and via endocysosis .

**2.1.2.1.2 Green fluorescent protein**

Green fluorescent protein (GFP) is a protein that displays bright green fluorescence by excitation using light with

wavelengths from ultraviolet to blue. The intensity of fluorescence emitted from GFP often changes in different environmental condition such as by a shift in pH, thereby GFP can be used to help track and spatially visualize dynamic processes in living cells where cell function and biochemical reactions for instance lead to alterations in pH. Therefore, GFP has been widely used as a reporting molecule in cell and molecular biology. The wild-type GFP was firstly purified from *Aequorea* by Osamu Shimomura and his colleagues.[131] The achievement of GFP expression in many other species containing yeasts, bacteria, fungi and mammals has been fulfilled using genetic engineering. This technique firstly isolates the DNA coding for the GFP using DNA modification if needed. After copying and multiplying to produce a larger amount of targeted DNA, these DNA replicates are inserted into the host organism as materials for DNA synthesis and recombination. This whole process is called transfection. A pH-sensitive GFP called pHluorin is a mutant of wild type GFP. When pHluorin is fused to synaptobrevin and located on the inner side of vesicle it is called synapto-pHluorin (Figure 24). Synaptobrevin, which was mentioned in Section 1.2.3.2, is one of the SNARE proteins that generate force to drive membrane fusion between synaptic vesicles and the presynaptic plasma membrane during exocytosis. The fluorescent signal of synapto-pHluorin vanishes inside of the synaptic vesicle due to the acidic environment (pH ~ 5.7),[132] but appears rapidly by the initiation of a fusion pore at exocytosis, which creates a vesicle solution exchange with the extracellular space where the physiological environment maintains a neutral pH (pH ~ 7.4). After vesicles fusion and vesicle re-capture, vesicles that are newly endocytosed remain highly fluorescent until re-acidification of the vesicles by the membrane transporters occurs. Therefore, synapto-pHluorin with the assistance of fluorescence microscopy can be used to track vesicular exocytosis events and monitor the vesicle recycling and vesicle re-acidification process using this fluorescent reporter labeling the vesicular membrane.[133,134]

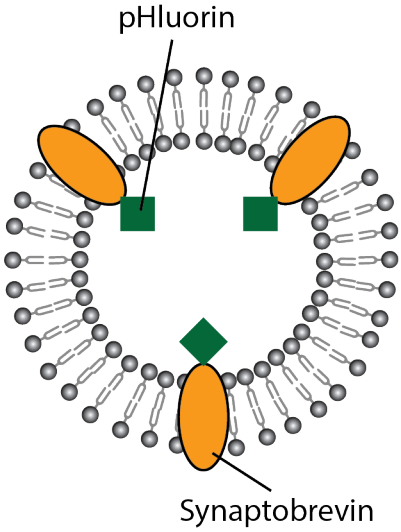


**Figure 24.** Illustration of vesicle loaded with pH-sensitive green fluorescent protein, pHluorin.

Instead of the strategy that fluorescence reporters tag the vesicular membrane and observing the fluorophore response to changes in different environments as described above, fluorescence reporters that respond upon binding to neurotransmitter were employed for detection of synaptic release of neurotransmitters. For example, intensity-based glutamate-sensing fluorescent reporter (iGluSnFR) was developed by Marvin and his colleagues in 2013,[135,136] where the fluorescence of iGluSnFR changes quickly on the millisecond timescale upon binding to glutamate. The iGluSnFR consists of an enhanced GFP fused to a glutamate binding protein (GluBP), the binding of GluBP to glutamate cause change of its molecular shape, which results in an increase in fluorescence intensity with the fluorescent readout using mostly one- or two-photon microscopy.

Two-photon microscopy is a specialized technique for fluorescence imaging that allows imaging of biological tissue with penetration depth up to approximately one millimeter. It is different from the ordinary fluorescence microscopy, which excites samples using one photon that carries shorter wavelength than that of the resulting emission light (Figure 25A), while the wavelengths of the two exiting photons used in two-photon microscopy are longer than that of the resulting emission light (Figure 25B), but where the two photons collectively correspond to the same excitation energy as of a one photon microscope. Two-photon microscopy typically excites samples by absorption of two near-infrared photons that minimize scattering in tissue, while also strongly suppresses the background signal. These two effects result in an increase in imaging penetration depth. It can also result in that the two photons hit fluorescent dyes in samples at the focal point with a bright point of light (Figure 25B), but without the typical cone of light below and above the focal plane in one-photon microscopy (Figure 25A).

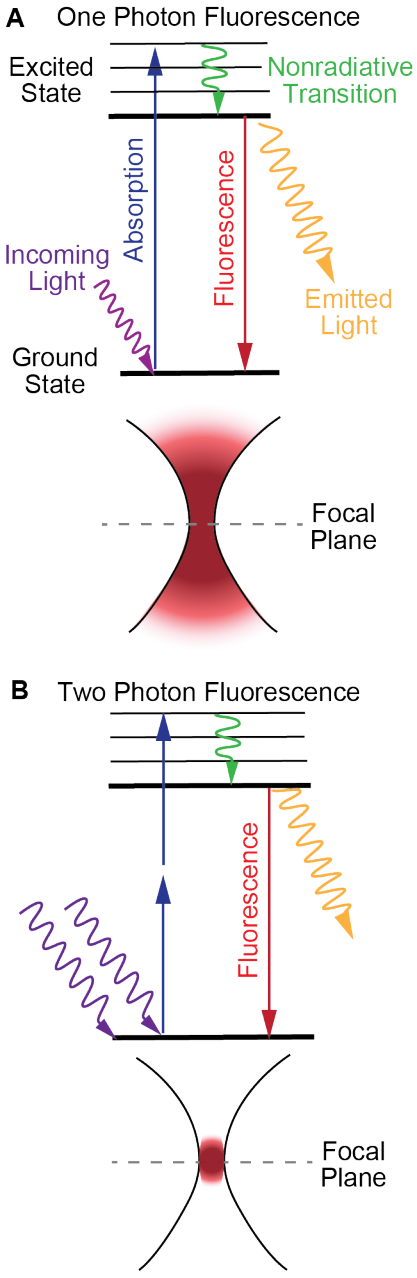


**Figure 25.** Schematic of the one-photon and two-phone microscopy and their excitation mechanisms displayed in a Jablonski diagram and an illustration of the emission light focal plane for illuminating fluorescent dye in a sample.

#### 2.1.2.1.3 Quantum Dots and Fluorescent False Neurotransmitters

In addition to labeling dyes which are inserted into the vesicle membrane, fluorophores like photoluminescent quantum dots (Qdots) and fluorescent false neurotransmitters that can mimic neurotransmitters can be used by loading the internal solution of vesicles.[137–141]

Qdots are colloidal semiconducting particles with a few nanometers in diameter. Because of their optical properties, luminescent Qdots coupled with optical microscopy, can be used to visualize exocytosis processes by their incorporation and release from the synaptic vesicles. Qdots with a size that is smaller than that of synaptic vesicles can be encapsulated into the internal solution of vesicles by triggering neurons to exocytosis in the presence of a Qdot solution. This allows Qdots to then be up-taken via the following process of endocytosis, where vesicles are re-captured with encapsulation of solution from the extracellular space and the random uptake of Qdots into single synaptic vesicles occurs. In the study from Zhang *et al.*,[137] Qdots with 15 nm in diameter were loaded into single synaptic vesicles (40 nm – 50 nm) in rat hippocampal neurons (Figure 26). This work demonstrated that Qdots did not always escape from vesicles during following exocytosis events even though amperometric measurements still noted neurotransmitters were released from the vesicle compartment. This is probably due to the Qdot size, which if larger than that of fusion pore (1 nm - 5 nm) results in that neurotransmitters are released from a fusing vesicle, but Qdot is entrapped inside of the vesicle.[138,139] From their observations they proposed that full release in exocytotic events account for about 50 % or less of the whole fusion events, and the rest are partial release fusion (kiss-and-run) pathway. Chiu and his colleagues could isolate synaptic vesicles encapsulating single 15 nm Qdots from synaptosomes, which offered a new model to study the dynamics of vesicular transporters.[140]

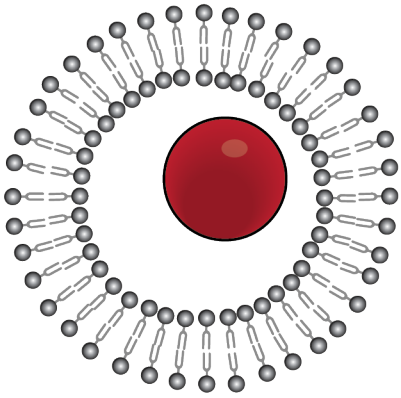

**Figure 26.** Illustration of a Qdot (red ball) loaded inside of a synaptic vesicle.

Unlike dyes binding to the membrane, fluorescent false neurotransmitters (FFNs) were designed as fluorescent

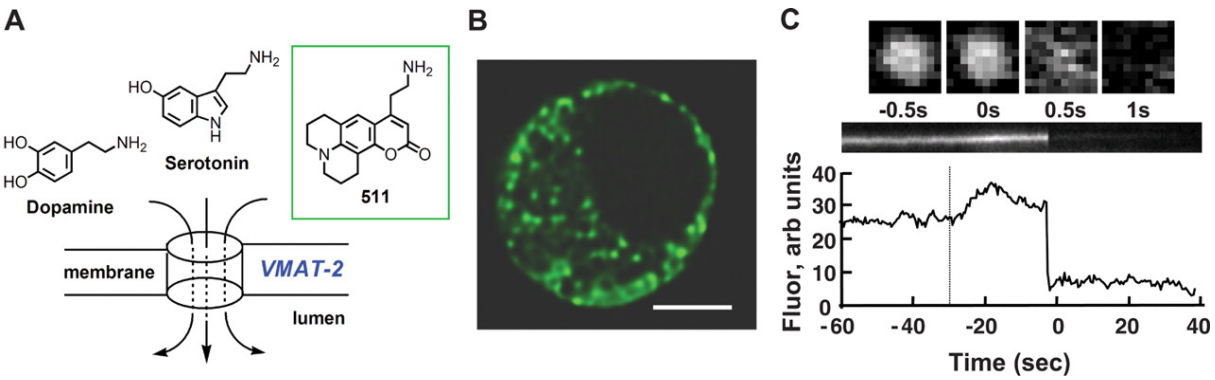


**Figure 27.** Fluorescent false neurotransmitter accumulated in secretory vesicles of a mouse chromaffin cell. (A) The loading of FFN511 into the vesicular lumen via transporter VMAT with illustration of chemical structure of FFN511. (B) Image of a chromaffin cell where vesicles are loaded with FFN511 using multiple fluorescence microscopy. (C) Measurement of exocytotic event of FFN511 loaded vesicle with assistance of fluorescent microscopy. Reprinted with permission from Reference 141.

analogs to the catecholamine neurotransmitter molecules to be used for visualizing the dynamics of neuronal activity and the synaptic vesicle cycle processes. The first FFNs named FFN511 were synthesized via incorporating a fluorophore into the chemical structure of monoamine neurotransmitters like dopamine and serotonin.[141] Because of the similarity in chemical structure with monoamine neurotransmitters carrying the aminoethyl group (Figure 27A), FFN511 could be recognized and transported into synaptic vesicle from cytoplasm via the neuronal vesicular monoamine transporter 2 (VMAT-2). Using this labeling strategy, dopamine release in mouse brain was visualized using FFN511 with the assistance of multi-photon microscopy. A year later, a pH-responsive FFN called Mini202, mimicking monoamine neurotransmitter, was created by the same groups of researchers.[142] The acidity inside of catecholamine secretory vesicles was measured as approximately pH 5.9 by two-photon microscopy imaging of fluorescence intensity emitted from Mini202 that were encapsulated inside of vesicles.

### 2.1.2.2 Total Internal Reflection Fluorescence Microscopy

A special technique of fluorescence microscopy developed by Daniel Axelrod, is called total internal reflection fluorescence microscope (TIRFM). The basic principle of

TIRFM is illustrated in Figure 28. It uses the evanescent wave that is generated during formation of a total internal reflection at the boundary between sample and the microscope slide, to selectively excite fluorophores in a sample that is in close proximity to the surface. Total internal reflection occurs at the glass-water interface when incident light hits the sample at the angle (θ) that is bigger than the critical angle. However, rather than illuminating fluorophores distributed inside the whole sample and its surrounding medium, TIRFM provides an imaging region that is limited to the area near the interface of the sample and the surface of the glass cover slip, since the depth penetrated by evanescent wave reaches about 100 nm from the glass surface and into the sample solution. Therefore, when performing live cell imaging using TIRFM, visualization allows for the cell region where the cell attaches to the glass support. Hence this technique offers great opportunity to selectively monitor cell dynamics that occur close to the basal plasma membrane (that is approximately 7.5 nm thick) of cells[143] such as tracking the movement of individual stained secretory vesicles that approach to the plasma membrane before, during and after docking, priming and exocytosis.[144–146]

TIRFM also enables to monitor single molecules on nanometer scale like integral proteins at vesicular membrane. Research from Dr. Chiu's group brought up the possibility of answering the question of how the quantitative aspects of protein expression in vesicle affect vesicular function by sorting out the copy numbers for several integral vesicular membrane proteins (e.g. proton ATPase, synaptotagmin 1, synaptophysin and synaptogyrin) and their distributions.[147]

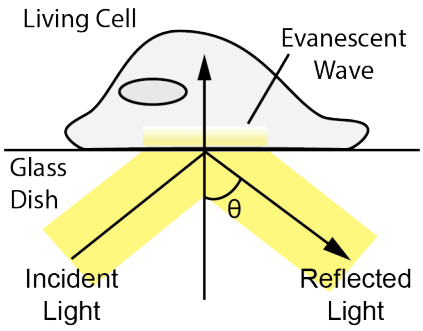


**Figure 28.** Illustration of the basic principle of total internal reflection fluorescence microscopy.

### 2.2 Electrophysiology

Electrophysiology belongs to a branch of technologies aimed to study physiology at cells and that measures electric signals such as voltage or current generated from ions that flow in biological tissues. In neuroscience, electrophysiology is an important tool for being able to measure neuronal action potentials, changes of voltage or

current by single ion channel in neurons and monitor exocytosis events by the capacitive changes at cells from vesicle fusion.

### 2.2.1 Patch Clamp

Patch clamp is an electrophysiological technique that is used for recording of intracellular electric signals derived from ion flow across the cell plasma membrane. The main components (Figure 29) of a patch clamp recording include a glass micropipette that is filled with electrolyte solution and used for placement in tight connection to the cell membrane with an electrode that is placed inside of the micropipette and connects to an amplifier. The set-up is coupled to a reference electrode and the bath containing biological tissues and cells is carefully grounded before recordings.

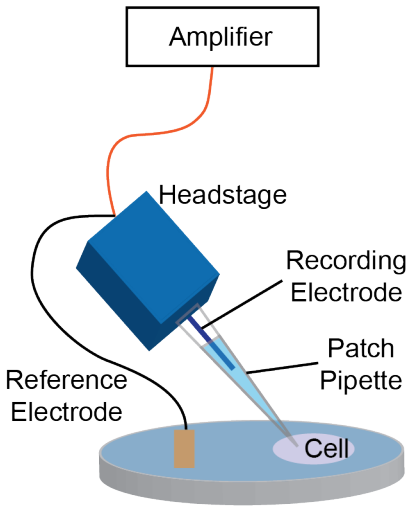


**Figure 29.** The main parts of a patch-clamp setup.

There are several variations of patching cells, where cell-attached (Figure 30A) and whole-cell (Figure 30B) configurations are two mostly common methods. In the cell-attached mode, the micropipette is tightly sealed with the intact cell membrane via gentle aspiration and is used to record ion channels activity through one or few integrated membrane channels in the small region of the patched membrane. Current signals from individual ion channels on cell membrane via cell-attached method were firstly recorded by Erwin Neher and Bert Sakmann, which awarded them the Nobel prize in Physiology 1976 for inventing the patch clamp methodology.[148,149] In the whole-cell method, the region of cell membrane that is tightly sealed with micropipette tip suddenly is ruptured either by applying a stronger suction pressure at the micropipette or by applying of large current pulse through the micropipette. The membrane rupture can also be achieved by simultaneously applying these mechanical and electrical forces to the cell membrane. A successful patch is achieved when the membrane rupture results in a tight seal with the glass pipette and the cell plasma membrane and that the interior of pipette becomes continuous with the cell cytoplasm. Thus, whole-cell method allows recording of electric signals through many ion channels

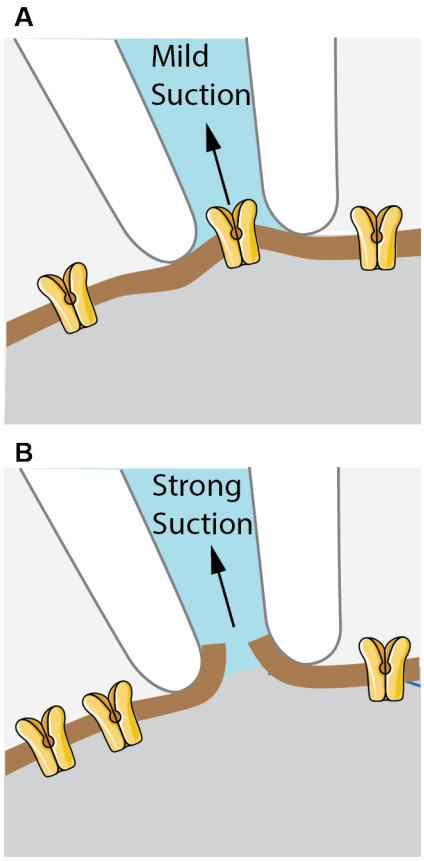


**Figure 30.** Different recording methods of patch-clamp technique. (A) Cell-attached method and (B) Whole-cell recording.

across the entire cell plasma membrane, instead of the small region that has been patched in the cell-attached method.

Patch clamp technique can be performed via two main measuring approaches: voltage clamp and current clamp. In the case of voltage clamp, the membrane potential of cells is clamped (or held) to a set value (or command value). To achieve and maintain the commanded potential, the current generated through the recording electrode that is connected to the amplifier is measured. In the case of current clamp, the current is clamped (or commanded) while the change of potential is recorded.

#### 2.2.1.1 Patch Clamp Capacitance

In the whole-cell patching method, modifying amplifier from voltage-clamp mode allows the output signal to be proportional to capacitance of cell membrane, but independent of its electric conductance (Figure 31). Since the surface area of the cell membrane is proportional to its capacitance, the changes of cell membrane surface area caused by events of exocytosis and endocytosis could be recorded by patch clamp capacitance measurements.[150] Exocytosis event increases the cell plasma membrane surface area by merging vesicles with plasma membrane, whereas endocytosis decreases the membrane surface area by forming vesicles retrieved from the plasma membrane. The time resolution of monitoring exo- and endo-cytosis using this technique can be achieved within hundred-millisecond timescale.[151]

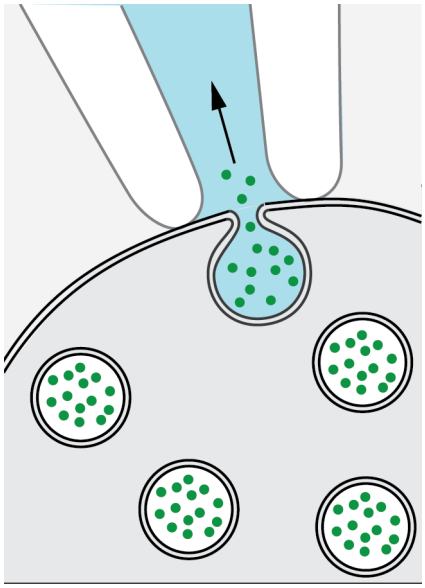

**Figure 31.** Detection of vesicular release via measuring the cell membrane capacitance using patch clamp.

### 2.3 Electrochemical Methods

The development of electrochemical technique during the last 30 years contributed enormously to the investigation and characterization of the details of exocytosis process and the released molecular content. Cyclic voltammetry and amperometry are the two most common electrochemical techniques utilizing carbon fiber microelectrodes to identify and quantify the released vesicular chemical content during exocytosis, and to monitor the dynamic regulatory aspects of exocytosis at

the single cell level with high temporal and spatial resolution and high sensitivity.

### 2.3.1 Cyclic Voltammetry

Cyclic voltammetry (CV) is a type of voltammetry that belongs to electroanalytical methods. It analyzes a substance by measuring the current generated by analyte as a function of potential applied on the working electrode. As detailed in Figure 32A, CV is performed by linearly ramping the potential applied at the working electrode versus time from $E_1$ to $E_2$ ($t_1$ to $t_2$), and then reversing back from $E_2$ to $E_1$ ($t_2$ to $t_1$) to complete a cycle, with the possibility to continuously repeat this process. Meanwhile, the current generated on working electrode from the redox reaction of analyte is measured and plotted versus applied potential as a cyclic voltammogram in Figure 32B and Figure 32C. The speed at which the potential applied is varied, is called the scan rate, which is defined by dividing the potential difference ($\Delta E$) over the duration of time ($\Delta t$) for scanning the potential.

The applied potential usually starts from a value (e.g. $E_1$) in the low range where no redox reaction of the analyte occurs. In fast scan cyclic voltammetry (FSCV, Figure 32B), the rapidly increased potential from low ($E_1$) to high ($E_2$) results in an increasing oxidation current ($i_a$) when the applied potential passes the oxidation potential for the analyte. This is followed by a current decrease after the potential has reached beyond the anodic peak potential ($E_{pa}$) where depletion of the analyte by the oxidation reaction at the surface of the electrode occurs (Section 3.3.2.4.3, Figure 43A). If the redox couple that contains the electron donor for oxidation and electron acceptor for reduction behaves reversible, a reduction current ($i_c$) can be generated when a backward scan of the potential is applied from high ($E_2$) back to low ($E_1$). This marks a current decrease by the reduction current that is initiated by lowering the applied potential below the redox current for the analyte until reaching the cathodic peak potential ($E_{pc}$) where there is a depletion of the oxidized analytes at the

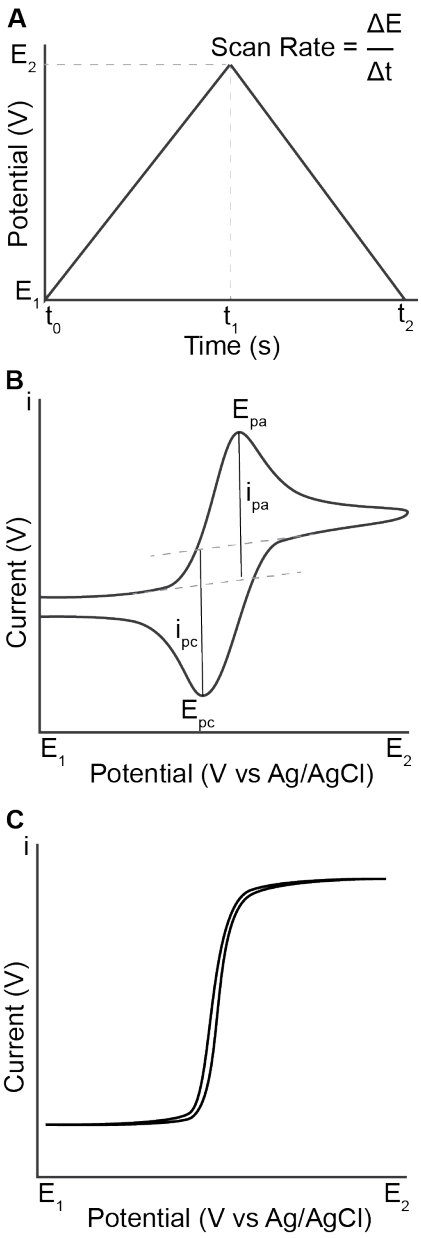


**Figure 32.** Cyclic voltammetry. (A) A potential waveform for a single cycle voltammogram. (B) Plot of current versus potential using fast scan cyclic voltammetry. (C) Plot of current-potential of a slow scan in cyclic voltammetry.

electrode surface. When instead slowly scanning the applied potential, a constant steady-state current appears after reaching the redox potential peaks since the radial diffusion (Section 3.3.2.4.3, Figure 43B) occurs and offers a stable concentration of analyte at the electrode surface as shown in Figure 32C.

The time resolution of data sampling in CV is related to the scan rate and the waiting time between cycles, but cannot be compared to the recording speed of amperometry where by contrast the potential is held constantly during measurement (Section 2.3.2). FSCV is usually applied to identify analytes and therefore function as a complementary method for amperometry, which mainly is a method to quantify molecules released from exocytosis and its recordings are fast enough to monitor the dynamics of exocytosis events that take place on sub-millisecond to millisecond timescale.[152,153]

### 2.3.2 Amperometry

Amperometry is one of the most widely used electrochemical technique in the analytical chemistry field. This method offers high sensitivity, high temporal resolution at sub-millisecond timescale and high spatial resolution. Amperometry measures the electric current or current changes generated from either oxidation or reduction reactions of molecules of interest when a constant potential is applied to the working electrode (Figure 33). In this technique, working electrodes are most commonly placed adjacent to the plasma membrane of a cell. To capture the total signal of vesicular content released from exocytotic events and provide valuable temporal information on the regulation of neurotransmitter release at exocytosis, the distance between the electrode and plasma membrane is minimized by placing the electrode as close as possible to the electrode surface. In 1988, the study of Engstrom *et al.* showed that the amplitude of electric signal derived from exocytosis was decreased when the distance between electrode and cell membrane was increased from 5 μm to

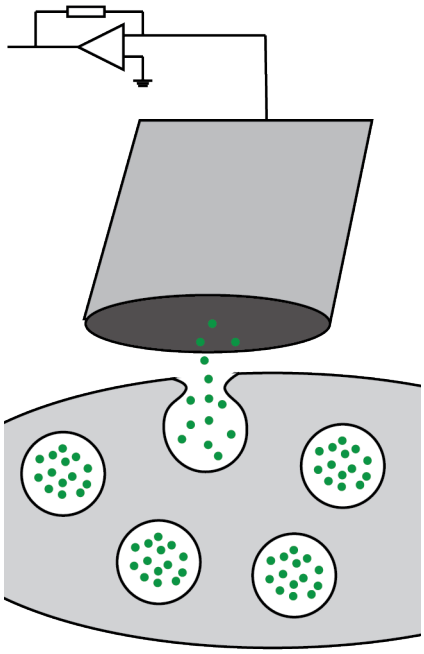

**Figure 33.** Amperometry measurements of exocytosis by placing a microelectrode in close proximity to a cell.

25 μm.[154] This implies that the released vesicular content rapidly diffuses away to other space when the sensing electrode is placed distant to the cell membrane. The high temporal resolution of amperometry allows monitoring the dynamics of single exocytotic events from secretory cells that occur on sub-millisecond to millisecond time scale and result in release of neurotransmitters. The first detection of catecholamine released from single exocytotic events in individual chromaffin cells using amperometry was performed by Wightman and his colleagues in 1991.[155] In that study, current signal generated from the oxidation of catecholamine was captured as a current peak (or spike) (Figure 34) when a 650 mV constant potential was applied onto the carbon fiber working electrode (10 μm in diameter) versus a sodium-saturated calomel reference electrode.

Because amperometry is capable to capture the rapid transients of exocytotic events, the shape of current signal (i.e. spike) can contain many details and can be characterized into several parameters that are likely to be correlated to the dynamics of vesicle fusion process during exocytosis (Figure 34). When analyzing single current spikes, the parameters $T_{rise}$ and $T_{fall}$ are obtained by measuring the time it takes for the current to rise from 25% to 75% of current maximum amplitude ($I_{max}$) and followed by the fall from 75% down to 25%, respectively. These factors extracted from the detected and isolated current spikes are thought to correlate with the opening and closing of the vesicle fusion pore formed during exocytosis. Sometimes a current spike is preceded by a slight rise before a sharp taller current spike is detected and is often referred to as a "foot". This pre-spike foot is thought to represent the initial stage of fusion pore formation where a small amount of neurotransmitter leaks through this narrow pore before it dilates, and this current spike feature was first reported by Chow and his colleagues.[56,156] In addition, a post-spike foot characteristic was identified in amperometric exocytosis recordings and is believed to unveil the stability and rigidity of pore structure at the final

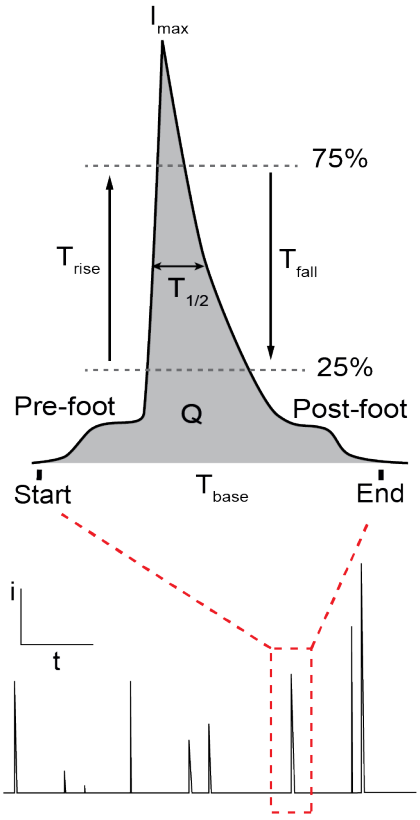


**Figure 34.** Amperometric trace of single exocytotic events. Upper picture is magnification of a single amperometric spike with different dynamic parameters.

stage at exocytosis events that are due to partial exocytosis release.[157] $T_{1/2}$ is the time duration at the half of $I_{max}$ and $T_{base}$ stands for the time spent on the whole exocytotic event. Information from $T_{base}$ together with the spike shape can exhibit the modes of exocytosis that either represents full or partial exocytosis release including the fast exocytosis mode 'kiss-and-run' or longer fusion pore flickering.[64,65]

Usually the neurotransmitters detected by electrochemical techniques are electroactive like monoamines including catecholamines that are easily oxidase at a certain positive potential. However, by the introduction of enzyme-coating at the surface, an electrode allows capturing signals originated from conversion of non-electroactive neurotransmitters like acetylcholine and glutamate to electroactive species via a catalysis reaction by the enzyme. However, these enzyme-based electrochemical sensors for a long time suffered from a slow recording speed with temporal resolution on second time scale, which is orders of magnitude too slow to monitor neuronal activity by the detection of single exocytosis events that occur on sub-millisecond time scale. This is a challenge where the work of this thesis has tried to contribute to the field of neurochemistry. The detection of non-electroactive neurotransmitters released from ultrafast single exocytotic events by amperometry was not achieved until a glutamate carbon fiber sensor constructed with nanoparticles and a novel enzyme coating concept was invented in our lab. This work as firstly published with preliminary data in the thesis of a Cans' PhD student in January of 2018[158] showing the detection of glutamate release from single synaptic glutamate was temporally resolved in rodent brain tissue, and the full paper was later published in January of 2019.[64] In this work, a monolayer of enzyme was coated onto the gold nanoparticle (AuNP) modified sensor surface to minimize the distance between the electrochemical reporting molecule $H_2O_2$, and the working electrode of the sensor. Via detailed studies of enzyme-AuNP conjugates in bulk solution, the conditions needed to obtain an optimal ratio of enzyme-to-AuNP

needed to fully coat the sensor surfaces, while still limiting the enzyme coating to a monolayer. The concept of increasing temporal resolution of enzyme-based sensors by minimizing the thickness of enzyme coating was developed for detection of fast single vesicular release of acetylcholine in Cans group in 2015.[63]

Amperometry also allows quantifying the amount neurotransmitters released through exocytosis from different secretory cells by using the charge (Q) integrated from individual spikes and *Faraday's law*,

$$N = \frac{Q}{nF} \qquad (2)$$

where $N$ is the amount of neurotransmitter molecules in moles, $n$ is the number of electrons released or absorbed in the redox reaction for the analyte, $F$ stands for the Faraday constant (F = 96485 C $mol^{-1}$). Equation (2) can be rewritten as

$$Number\ of\ molecule = \frac{Q}{nFN_A} \qquad (3)$$

where $N_A$ is the Avogadro´s number ($6.02 \times 10^{23}$ $mol^{-1}$). This equation shows that the number of molecule released is proportional to the charge collected from each current spike.

Despite of high temporal resolution, amperometry lacks the ability to identify substrate and distinguish different compounds compared to FSCV.[159] In FSCV measurements, the redox current, which varies depending on different thermodynamic properties of the analyte substance, is plotted with respect to the applied potential in voltammogram (see Figure 32). In amperometry, the redox current measured when applying a constant potential is plotted versus time to monitor the changes of substrate concentration at the surface of the working electrode.

### 2.3.3 Patch Amperometry

It has been described in previous sections that exocytotic events can be detected by electrophysiology techniques such as cell attached configuration in patch-clamp, which can be used for measuring capacitive changes when the surface area of the cell plasma membrane increases from incorporation of vesicular membrane material into the cell plasma membrane by exocytosis. By combining patch-clamp with amperometry and placing a carbon fiber amperometric electrode on the inside of a patch clamp micropipette, a new method was introduced by Albillos *et al.* in 1997.[160] Patch amperometry combines capacitive measurements via patch clamp and by inserting an amperometric carbon fiber electrode inside of the patch pipette. This method showed that simultaneously monitoring of the initial formation of membrane fusion pore by the patch clamp can be correlated in time to the dynamics of regulated neurotransmitter release from single vesicles during exocytotic events by the amperometric carbon fiber microelectrode.

# 3. Electrochemistry

Electrochemistry belongs to the field of physical chemistry. It focuses on observing the interrelation between movements of electrons as part of chemical reactions. Certain chemical reactions can produce electricity in terms of released electrons; and on the contrary, electricity can drive certain chemical reactions that would not occur spontaneously. Electricity is associated with the movement of electric charges, and the rate of a net flow of electric charge passing a region or point is called electric current ($i$). In neuroscience, electrochemical techniques such as cyclic voltammetry and amperometry allow measuring the electron movements generated from the oxidation-reduction (or redox) reaction of released neurotransmitters as detected by the surface of a working electrode when applying a dynamic or constant driving force (i.e. electric potential).

### 3.1 Basics of Electrochemistry

To perform electrochemical experiments at the single cell level, the basic instrument requirements are two electrodes (i.e. a working electrode and a reference electrode) placed in the same electrolyte solution, a potentiostat serving as a power source to apply voltage between two electrodes while also serving as a picoammeter to measure the charge transfer as current at the surface of the working electrode versus a reference electrode.

### 3.2 Microelectrodes

To decrease the damage when implanting electrode into the biological models for *in vivo* electrochemical measurements, and to improve the accuracy of electrode positioning to the defined areas where neuronal activities occur, high spatial resolution of the electrodes is demanded. Therefore, electrodes of micro-size are more popular than larger ones and are frequently utilized in

studies performed on biological samples like single cells and brain slices.

Theoretically, any conductive materials, which are not taking part in the examined reactions, can be used for constructing a working electrode. In practice, metals like platinum, gold and silver and carbon including graphite are materials that are often used. Among them, micro-sized carbon fiber is the most common one to construct for electrochemical measurements of exocytotic events.

To achieve a low-noise and stable baseline for amperometric measurements, the microelectrode is usually insulated in material such as glass, polymers like polypropylene or polyethylene, or vapor deposited silicon oxide, and only a limited area at the tip is used for electrochemical sensing.[159] The microelectrodes used in detection of exocytosis activity in this thesis are made of 30 μm (in diameter) carbon fibers, which are insulated with glass capillaries and sealed using epoxy glue. The tip surface of the electrodes was cut using a scalpel and polished with a 45° angle before use. This type of electrode is called a disc-type microelectrode as referring to the shape of the active electrode surface. Cylinder-shaped microelectrodes have another surface geometry, where a certain length of a bare carbon fiber is allowed to stick out at the tip of the electrode from the surrounding glass insulation, to increase the electroactive surface area and to maintain a small diameter, which can fulfill the high demand on sensitivity of electrode in certain *in vivo* applications. The protruded carbon fiber beyond carbon-glass junction is cut with a scalpel and the remaining length of conductive carbon region is often approximated from 50 to 500 μm.

### 3.3 Processes at Electrode Surfaces

The electrochemical processes taking place at the electrode surface are associated with the kinetics and thermodynamics that describe the chemical reactions in the electrochemical system. The faradaic current generated at the working electrode from oxidation or reduction reactions of chemical species is affected by two

main factors: the rate of mass transport and the rate of electron transfer during chemical reactions. This process is schematically illustrated in Figure 35 for a case where the reduced species are oxidized at the electrode surface. Mass transport is the movement of analytes from bulk solution to the working electrode surface. Once the molecule is brought up to the electrode, which contains a double layer nearest to the surface (Figure 39) and a potential gradient is created at the electrode-solution interface, the electron transfer associated with the electrochemical reaction takes place.

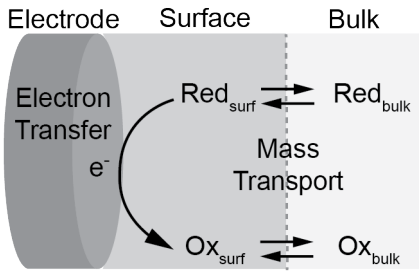


**Figure 35.** Pathway of a general electrochemical reaction at an electrode surface. It basically includes processes of mass transport and electron transfer.

### 3.3.1 Mass Transport

Mass transport describes the dynamic process when chemical species in solution move from one location to another. When solution is unstirred, the movement of mass transport mainly occurs by diffusion, and electrophoretic migration in the case of charged analytes. In stirred solution, fluid flows in the mode of convection.

#### 3.3.1.1 Diffusion

Diffusion (Figure 36) is the random movement of molecules that is mainly driven by a concentration difference (or concentration gradient) between two regions in the solution. The flux spontaneously moves from region of high concentration to region of low concentration, which can be described by the Fick's first and second laws. Fick's first law ( $Equation\ 4$ ) considers diffusion in one-dimension as follows:

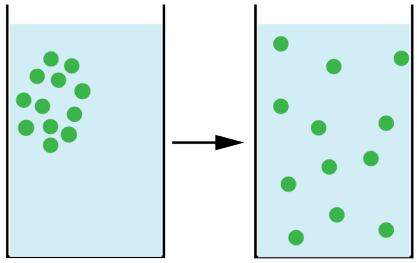

**Figure 36.** Diffusional movement of analyte by a concentration gradient in mass transport.

$$J = -D\,\frac{d\varphi}{dx} \qquad (4)$$

where $J$ is the diffusive flux, $D$ is the diffusion coefficient for a specific chemical species at a certain temperatures, $\varphi$ is the concentration and $x$ is the length or position, and $\frac{d\varphi}{dx}$ indicates the concentration gradient. The magnitude of flux ($J$) is proportional to the concentration gradient ($\frac{d\varphi}{dx}$). Fick's

second law brings the consideration of concentration change caused by diffusion over time.

#### 3.3.1.2 Migration

The potential applied on the working electrode (versus a reference electrode) can generate a local electric field that drives analytes carrying a charge to move in a certain direction, resulting in their migration movement. For example, when a more positive potential is applied on the working electrode, ions carrying negative charge will move towards to working electrode in response to the potential change. Figure 37 describes the migration process when applying the potential from zero to a negative potential at the electrode surface.

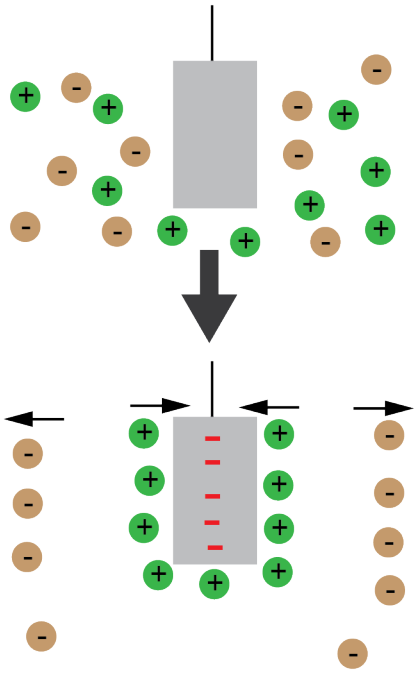

**Figure 37.** Migration movement when a negative potential is applied to the working electrode in an unstirred solution.

#### 3.3.1.3 Convection

Convection is a hydrodynamic movement (or transport) that occurs naturally or is induced by mechanical means like stirring. In a stirred solution, forced convection contributes to mass transport and the stirring speed can be controlled. Figure 38 illustrates the effect of stirring a solution on the mass transport surrounding the electrode.

#### 3.3.1.4 Nernst-Planck Equation

The total mass transport of an analyte from surrounding solution to an electrode surface in one dimension is the sum of contributions from diffusion (concentration gradient), migration (electric field) and convection (hydrodynamic velocity), which can be mathematically described by the *Nernst-Planck equation* as follows:

$$J_i(x) = -D_i \frac{\partial C_i(x)}{\partial x} - \frac{z_i F}{RT} D_i C_i \frac{\partial \varphi(x)}{\partial x} + C_i v(x) \quad (5)$$

where $J_i(x)$ is the flux of chemical species $i$ at a location that is at a distance $x$ from the electrode surface. $D_i$ is the diffusion coefficient of chemical species, $\frac{\partial C_i(x)}{\partial x}$ and $\frac{\partial \varphi(x)}{\partial x}$ are the concentration gradient and electrostatic potential gradient, respectively. $z_i$ and $C_i$ are the charge and

concentration of $i$, respectively. $F$ is the Faraday constant (96485 $C \cdot mol^{-1}$), $v(x)$ is the hydrodynamic velocity of species $i$ in the convection mode.

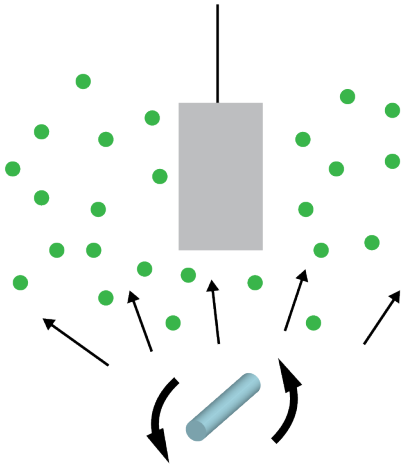

**Figure 38.** Convection movement of mass transport in a stirred solution.

### 3.3.2 Electron Transfer

In electrochemistry, electron transfer occurs at the working electrode surface after the molecule of interest move from bulk solution to the region of the electric double layer by the mass transport process. Electron transfer is an important process that takes place when an electron migrates from a molecule or atom to another molecule or atom during chemical reactions, a process that have both thermodynamic and kinetic aspects. Kinetic aspects are about the rate of reactions, specifically the rate constant ($k$) that is related with the activation energy ($\Delta G^{\ddagger}$) needed to proceed a reaction. While thermodynamics concerns about the stability of chemical species in one state compared to others (or equilibrium), and the state of chemical species relates to the free energy ($\Delta G$) released from spontaneous reaction. In electrochemistry, electrode potential ($E$) is the linking parameter between kinetics and thermodynamics, and it is a powerful tool that can shift the equilibrium and changes the rate of reactions.[161]

#### 3.3.2.1 Electric Double Layer

When placing a charged (Figure 39) electrode (with respect to reference electrode) into the solution containing ions, a region called the electrical double layer is formed at the electrode-solution interface to neutralize the charged surface of electrode. It means that co-ions in solution are repelled by the charged electrode while the counter-ions are attracted to the electrode surface. Electron transfer of chemical species associated with an electrochemical reaction will not occur until they physically arrive and form this electric double layer.

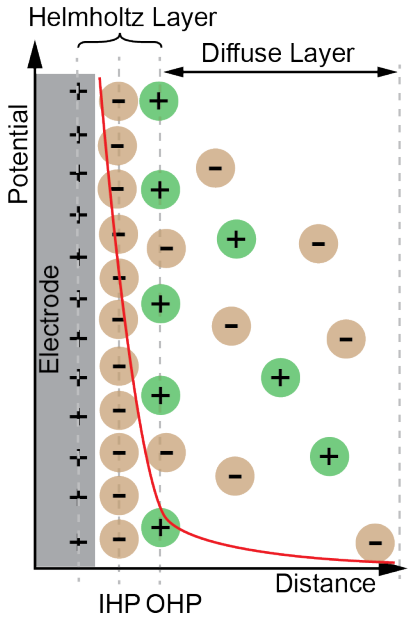


**Figure 39.** Helmholtz double layer represents the solution interface at the surface of a positively charged electrode.

The solution side of double layer actually contains several layers. The closest layer to the electrode surface is densely packed with specifically adsorbed solvent molecules and other non-fully solvated ions and molecules carrying

opposite charges, this layer is called the *inner layer*. The center of the inner layer is defined as the *inner Helmholtz plane* (IHP*)*. The second layer containing loosely adsorbed solvated ions that electrically screen the inner layer and loosely interacts with the electrode surface only at a long range via Coulomb force. The center of the nearest solvated ions in second layers is called the *outer Helmholtz plane* (OHP). The region containing excess ions that extends from OHP to bulk solution at a distance within approximately a hundred Angstroms is called the *diffuse layer*.[162] The potential applied to a working electrode leads to an electric field that decays over the diffuse layer. The thickness of diffuse layer varies with the total concentration of ions in solution at a given potential applied. Here, the thickness of the double layer decreases with the ionic concentration in solution.

Since the electrode-solution interface separates the charge into two layers that look like plates, the double layer has been experimentally shown to perform like a capacitor. When applying a certain potential to the working electrode versus a reference electrode, the total charge ($q^E$) accumulated on working electrode is the same as the total charge ($q^S$) in solution that contains the excess of ions in near the electrode surface, as $q^E = -q^S$ . The capacitance (C) of this electrode-solution interface is defined as the held charge (Q) per applied voltage (U) (i.e. C = Q/U). Under the electrolyte's decomposition voltage, the held charge Q is linearly or may be non-linearly proportional to the applied potential U. In the Gouy-Chapman model of double layer that introduced factors like diffusion or mixing of ions in the diffusive solution, capacitance C is not constant, and is dependent on the potential applied onto the working electrode, the concentration of ions and the composition of ions in solution, which greatly affect the electron transfer processes.

### 3.3.2.2 Redox Reactions

A redox (reduction-oxidation) reaction is a chemical reaction where electrons move between atoms in different molecules, thus the oxidation (or reduction) state of one or more elements of substrate changes with the electron transfer. A one-step reversible reaction at equilibrium is described in $Equation\,6$, where a reduced compound ($Red$) is oxidized to an oxidized form ($Ox$) when losing a certain number ($n$) of electrons ($e$), its oxidation number is increased, and this process is an oxidation reaction. On the contrary, $Ox$ is reduced to its reduced form ($Red$) when gaining electrons and its oxidation number decreases, this process is caused by a reduction potential. The energy stored in reduced compounds is generally higher than that in their oxidized form.

$$Ox + ne \underset{k_b}{\overset{k_f}{\rightleftharpoons}} Red \qquad (6)$$

where $k_f$ and $k_b$ are rate constants of the forward reaction and the backward reaction, respectively. The rate of the forward process (reduction), $v_f$, and the rate of backward process (oxidation), $v_b$, are described as the following equations:

$$v_f = k_f C_{Ox}(0,t) \qquad (7)$$

$$v_b = k_b C_{Red}\,(0,t) \qquad (8)$$

$C_{Ox}(0,t)$ and $C_{Red}\,(0,t)$ are concentrations of chemical species $Ox$ and $Red$ at electrode surface and at time $t$, respectively. The net of conversion rate ($v_{net}$) of oxidized species ($Ox$) to reduced species ($Red$) is

$$v_{net} = k_f C_{Ox}(0,t) - k_b C_{Red}\,(0,t) \qquad (9)$$

Because of the proportional relationship between current ($i$) and its corresponding rate of a reaction ($v$), according to

Faradays law $i = nFAv$, the current of a redox reaction occurring on the surface of an electrode is

$$i = nFAv_{net} = nFA\left[k_f C_{Ox}(0,t) - k_b C_{Red}(0,t)\right] \quad (10)$$

where $A$ is the area of the electrode surface, $n$ is the number of electrons transferred in the redox reaction.

**3.3.2.3 Nernst Equation**

In physiology, Nernst equation has been mentioned in previous section and used for determination of the resting membrane potential of biological cells. In electrochemistry, Nernst equation ($Equation\ 15$) is frequently utilized to describe the relation of an actual potential for an electrochemical reaction (oxidation or reduction) with standard electrode potential, activities (usually concentrations) of chemical species involved in the reaction and temperature. Butler-Volmer equation is a fundamental equation in electrochemical kinetics that describes the strong dependence of the electrode current generated from the potential applied to the electrode surface.

**3.3.2.3.1 Derivation of Nernst Equation**

The standard changes of Gibbs free energy that is related to an electrochemical transformation lead to the Nernst equation. In a galvanic cell, spontaneously reversible electrochemical reaction ($Equation\ 6$) occurs at a constant temperature and pressure, the actual reaction Gibbs free energy change ($\Delta G$) is related to the change of Gibbs free energy ($\Delta G^0$) for a reaction at the standard condition described as follows:

$$\Delta G = \Delta G^0 + RT\ ln\frac{C_{Red}}{C_{Ox}} \quad (11)$$

where $R$ is the gas constant (8.314 $J{\cdot}mol^{-1}{\cdot}K^{-1}$), $T$ is the temperature, $C_{Ox}$ and $C_{Red}$ are concentrations of $Ox$ and $Red$ in solutions, respectively, at equilibrium. The potential

energy ($E$) is related to Gibbs free energy ($\Delta G$) via the following equations:

$$\Delta G = -nFE \quad (12)$$

$$\Delta G^0 = -nFE^0 \quad (13)$$

Since a spontaneous reaction releases free energy (or has a negative change in free energy) to generate an electric potential, there is a negative sign. Inserting $Equation\ 12$ and $Equation\ 13$ into $Equation\ 11$ with rearrangment gives the Nernst equation as follow:

$$E = E^0 - \frac{RT}{nF} ln \frac{C_{Red}}{C_{Ox}} = E^0 + \frac{RT}{nF} ln \frac{C_{Ox}}{C_{Red}} \quad (14)$$

where $E^0$ stands for the standard reduction potential of a chemical species couple (i.e. Ox/Red couple) measured versus normal hydrogen electrode (NHE) at the standard states (25 ℃ or 298 K, $10^5$ Pa) with 1M concentration of all reaction participants. NHE is more difficult to use as a reference electrode in practice, other types of electrodes (e.g. Ag/AgCl, $E^0$= 0.197 V versus NHE) are more commonly chosen to use in electrochemical measurements. $E^0$ of many chemical compounds have been measured and can readily be found in standard potential tables. For reducible compounds, it is harder to reduce molecules having more negative $E^0$ than molecules having less negative $E^0$. For oxidizable compounds, it is more difficult to oxidize molecules having higher positive $E^0$ than molecules having lower positive $E^0$. Usually, the formal potential $E^{0\prime}$ is used to replace the standard potential $E^0$, and Nernst equation can be re-written as:

$$E = E^{0\prime} + \frac{RT}{nF} ln \frac{C_{Ox}}{C_{Red}} \quad (15)$$

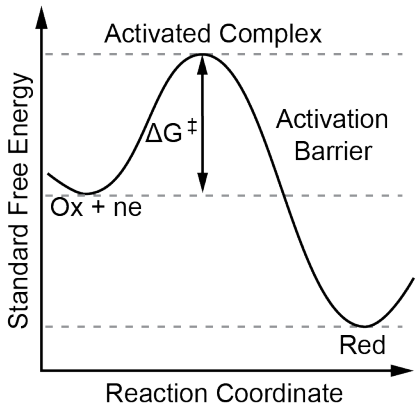


**Figure 40.** Reaction coordinate diagram that shows how the free energy of a system changes during a chemical reaction.

#### 3.3.2.3.2 Nernst Equation in Biological Application

In a galvanic cell, $E$ is the potential generated from the overall spontaneous redox reactions occurring inside a cell and where the Nernst equation can assist to estimate the cell potential, $E$. While in biological applications, Nernst equation can also thermodynamically describe the probability of electrolyzing a chemical species in a chemical reaction. In this application of the Nernst equation, $E$ is the potential applied onto the working electrode. $C_{Ox}$ and $C_{Red}$ are the bulk concentrations of $Ox$ and $Red$ present at the surface of the working electrode, respectively.

In this case, a carbon fiber microelectrode is typically employed as a working electrode to measure the current change derived from the content (e.g. neurotransmitters) released during exocytotic events at single cell level. This measurement is achieved by applying an external potential energy onto the working electrode surface to initiate the non-spontaneously electrochemical reaction (i.e. oxidation or reduction) of the released vesicle neurotransmitter content and to obtain information of electron transfer processes at the carbon-solution interface. For the case of forward reduction in $Equation\ 6$, the external potential energy applied is to reduce the energy barrier (or activation energy, $\Delta G^{\ddagger}$) that is needed to reach the transition state (or activated complex) of a chemical reaction along the reaction coordinate between reactant and product (Figure 40). The transition state represents the highest free energy along the reaction coordinate. A chemical species can be oxidized when a large enough positive potential is applied onto the working electrode, so that the barrier becomes negligible. Conversely, a reduction reaction happens when the potential applied on working electrode is negative enough.

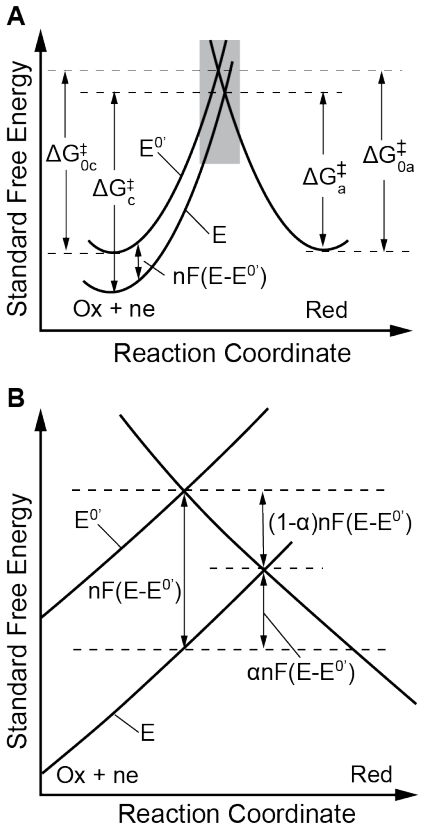


**Figure 41.** A potential change effects the standard free activation energy for a redox reaction (A). (B) is the magnification of the area in box in (A).

#### 3.3.2.4 Effects of Potential on the Energy Barrier

For a reversible reaction ($Equation\ 6$) at the working electrode surface, when $E$ is equal to formal potential ($E^{0'}$), this reversible reaction reaches equilibrium (Figure 41) and the potential is called $E_{eq}$, where anodic activation energy

($\Delta G_{Oa}^{\ddagger}$) for oxidation reaction and cathodic activation energy ($\Delta G_{Oc}^{\ddagger}$) for reduction reaction are the same. Polarization occurs, for example, when a more negative potential is applied on the working electrode ($E < E_{eq}$). The effect is to lower the energy of electrons as reactant by a change of $nF\Delta E = nF(E - E^{0\prime})$, the curve representing $Ox + ne$ decreases with respect to that representing $Red$, the energy barrier for reduction is decreased from $\Delta G_{Oa}^{\ddagger}$ to $\Delta G_{a}^{\ddagger}$ ($\Delta G_{Oa}^{\ddagger} > \Delta G_{a}^{\ddagger}$) by a fraction $(1 - \alpha)$ of the total energy change ($Equation\ 19$), $\alpha$ is the transfer coefficient, while the energy barrier for oxidation is increased from $\Delta G_{Oc}^{\ddagger}$ to $\Delta G_{c}^{\ddagger}$ ($\Delta G_{Oc}^{\ddagger} < \Delta G_{c}^{\ddagger}$) by a fraction ($\alpha$) of the total energy change ($Equation\ 19$). Hence,

$$\Delta G_{a}^{\ddagger} = \Delta G_{Oa}^{\ddagger} - (1 - \alpha)nF\left(E - E^{0\prime}\right) \qquad (16)$$

$$\Delta G_{c}^{\ddagger} = \Delta G_{c}^{\ddagger} + \alpha nF(E - E^{0\prime}) \qquad (17)$$

the extent of polarization can be measured by overpotential, $\eta$,

$$\eta = E - E_{eq} \qquad (18)$$

and the total energy change (or excess energy) can be calculated via the overpotential ($\eta$),

$$Changed\ energy = -nF\left(E - E_{eq}\right) = -nF\eta \qquad (19)$$

On the contrary, when a more positive potential is set on the working electrode ($E > E_{eq}$), the direction of the electrode reaction reverses to an oxidation reaction.

#### 3.3.2.4.1 Arrhenius Equation

Considering the same redox reaction ($Equation\ 6$) at the electrode-solution interface, the effect of the absolute temperature ($T$) on the rate constant ($k$) of a chemical reaction was summarized into a mathematical equation called Arrhenius equation, which was named after Svante

Arrhenius. Arrhenius equation reveals the generality of the dependence of rate constant with temperature and is commonly stated in the form:

$$k_f = B_f e^{\frac{-\Delta G_f^{\ddagger}}{RT}} = A_f e^{\frac{-\Delta G_c^{\ddagger}}{RT}} \quad (20)$$

$$k_b = B_b e^{\frac{-\Delta G_b^{\ddagger}}{RT}} = A_b e^{\frac{-\Delta G_a^{\ddagger}}{RT}} \quad (21)$$

where $\Delta G^{\ddagger}$ is the activation energy (energy barrier) that is the minimum free energy needed for a reaction to take place. The exponential form of (20) and (21) shows the probability of thermal energy crossing the energy barrier, whereas $B$ is the pre-exponential factor that relates to the attempt frequency of reaction. This is the *Arrhenius equation*, which relates rate constant ($k$) to activation energy of a chemical reaction when other parameters (e.g. $R$ and $T$) are constant. Inserting the activation energies ( $Equation\ 16$ and $Equation\ 17$ ) into the Arrhenius equation,

$$k_f = B_f e^{\frac{-\Delta G_{0c}^{\ddagger}}{RT}} e^{\frac{-\alpha F\left(E-E^{0\prime}\right)}{RT}} \quad (22)$$

$$k_b = B_b e^{\frac{-\Delta G_{0a}^{\ddagger}}{RT}} e^{\frac{(1+\alpha) F\left(E-E^{0}\right)}{RT}} \quad (23)$$

The first two factors $B_f e^{\frac{-\Delta G_{0c}^{\ddagger}}{RT}}$ and $B_b e^{\frac{-\Delta G_{0a}^{\ddagger}}{RT}}$ in $Equation\ 22$ and $Equation\ 23$ have the same value called standard rate constant ( $k^0$ ) at $E = E^{0\prime}$ when an equilibrium is achieved at the electrode-solution interface. At other applied potential, the rate constant can be re-written in the form of:

$$k_f = k^0 e^{\frac{-\alpha F\left(E-E^{0\prime}\right)}{RT}} \quad (24)$$

$$k_b = k^0 e^{\frac{(1-\alpha) F\left(E-E^{0\prime}\right)}{RT}} \quad (25)$$

Arrhenius equation shows that the rates of forward reaction ($k_f$) and backward reaction ($k_b$) rely on the potential ($E$) applied onto the electrode when a redox reaction ($Equation\ 6$) takes place at the electrode surface.

#### 3.3.2.4.2 Butler-Volmer Equation

The relation between the current ($i$) and the applied potential ($E$) at the electrode surface can be derived by inserting the Arrhenius equations ( $Equation\ 24$ and $Equation\ 25$ ) into the equation of the electrode net current ($Equation\ 10$, Section 3.3.2.2) that is the sum of cathodic current in the forward reduction and anodic current in the backward oxidation. The complete current-potential characteristic is yielded, which is called *Butler-Volmer equation*:

$$i = nFAk^0\left[C_{Ox}(0,t)e^{\frac{-\alpha F(E-E^{0\prime})}{RT}} - C_{Red}(0,t)e^{\frac{(1-\alpha)F(E-E^{0\prime})}{RT}}\right] (26)$$

Butler-Volmer equation is one of the most fundamental relationships in electrochemical kinetics to describe how the applied electrode potential affects the current on electrode. This equation is used to analyze almost every issue in the case of heterogeneous reactions. Meanwhile, Butler-Volmer equation also reveals the dependence of the electrode current on time-dependent surface concentrations of analytes when applied potential and other environmental parameters are constant.

#### 3.3.2.4.3 Cottrell Equation

To obtain quantitative information on electrode surface like faradaic current, which is dependent on mass-transfer efficiency, kinetic parameters like the rate of chemical reaction, structure of the double layer and experimental parameters such as the applied potential, and the analyte concentration, it is difficult, or even fails to use Butler-Volmer equation combined with Fick's laws (Section 3.3.1.1) to yield a solution, especially in the cases of more complicated processes like reactions with multi-step mechanisms.

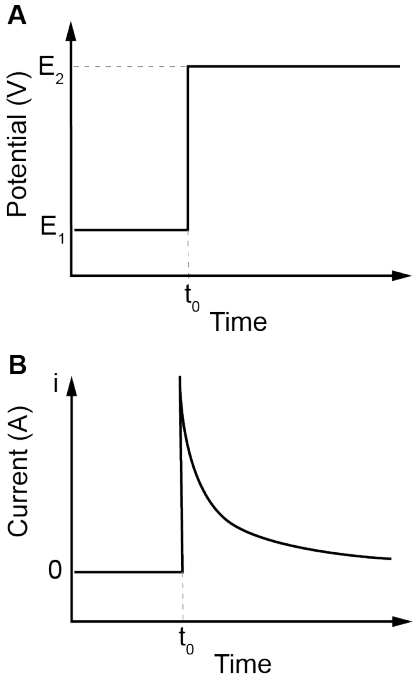


**Figure 42.** Illustration of a potential step method applied at the surface of planar macroelectrode. The applied potential is switched from $E_1$ to $E_2$ (A), which causes a current response from the redox reaction (B).

Usually, simpler theory, for example, the *Cottrell equation*, can be applied as an alternative to treat the designed experiment in practice. In an ideal condition, the linear diffusion of mass transport from one direction in an unstirred solution takes place at the planar macroelectrode surface when a potential step method is applied (Figure 42), where a potential is suddenly switched from $E_1$ to $E_2$, the responding current follows with a large initial increase due to the instantaneous faradaic process (oxidation), and continues with a rapid decay as function of time because of the consumption of analytes at the electrode surface and the depletion of analyte in the diffusion layer resulting into a concentration gradient from the bulk solution to the electrode surface, and eventually a steady-state current is approached when an equilibrium between the flux of mass transport by diffusion and the flux of electron transfer in a faradaic process is achieved. How in this process the current ( $i$ ) changes with respect to time ( $t$ ) is mathematically described by the Cottrell equation:

$$i\,(t) = \frac{nFA\sqrt{D}C^*}{\sqrt{\pi t}} \qquad (27)$$

where $A$ is the surface area of the planar electrode, $C^*$ is the concentration of $Red$ species in bulk solution, $D$ is the diffusion coefficient of $Red$ species, $n$ is the number of electrons transferred from the oxidation of one $Red$ molecule. A Cottrell-type of equation can also be derived for electrodes with other surface geometries than an (infinite) planar electrode, like spherical, cylindrical and rectangular.

Planar (disk) microelectrodes are widely used, especially in the *in vivo*, *in vitro* and *ex vivo* exocytosis measurements, however the current-time transients at the microelectrodes applied by chronoamperometry cannot be described by the Cottrell equation. Different to the one-dimension linear diffusion of mass transport that occurs on the planar macroelectrode (Figure 43A) that is regarded as an infinite plane, two-dimension spherical diffusion

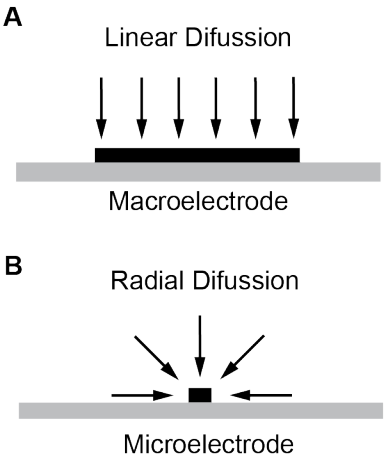


**Figure 43.** Different diffusion profiles of mass transport at planar (disk) electrode surface. (A) Linear diffusion occurs at macroelectrode. (B) Radial diffusion at a microelectrode.

dominates the mass transport process on the finite planar microelectrode in the ideal case (Figure 43B). Thus, the Shoup and Szabo equation (28 and 29) is usually used to describe the current changes with respect to time and with an error less than 0.6 %.[163]

$$i = 4nFrDC^{*}f(t) \tag{28}$$

$$f(t) = 0.7854 + 0.8862\sqrt{\frac{r^2}{4Dt}} + 0.2146e^{(-0.7823\sqrt{\frac{r^2}{4Dt}})} \tag{29}$$

where $r$ is the electrode radius, and the rest of the parameters have been described in the Cottrell equation ($Equation\ 27$). The Shoup and Szabo equation describes the current response at different temporal stages, a large immediate current rise is initiated by a potential switch (Figure 40) followed by a fast decay due to depletion of the diffusion layer, and a steady-state current response ($i_{ss}$) is eventually achieved when $t$ becomes very large. Therefore, the Shoup-Szabo equation ($Equation\ 28$) can be simplified as:

$$i_{ss} = 4nFrDC^{*} \tag{30}$$

Both of the Cottrell equation and Shoup-Szabo equation provide the faradaic information of initial non-steady state and later steady-state at the electrode surface. They also revealed the proportional relation between the faradaic current, the bulk concentration of analyte and the electrode surface area.

# 4. Enzyme-based Electrochemical Biosensors

Biosensor is an analytical device or instrument that is composed of a biological component and a transducer, with the aim to function as a detection scheme for sensing chemical or biological molecules. The biological recognition elements used for constructing a biosensor and sensing analytes can be macromolecules that very specifically recognize and bind to a target analyte such as antibodies, nucleic acids and enzymes. There are also different types of transducer employed in biosensor fabrication like optical, massed-based, piezoelectric and electrochemical transducers. Biosensor can be categorized into several types according to different transduction processes. The principle of electrochemical biosensor is to convert the chemical or biological signal into an electrical signal (Figure 44). This type of biosensor is one of the most widespread types among various biosensors, where numerous of electrochemical biosensors have been commercialized.[164] In this thesis, the enzyme-based electrochemical biosensor with nanomaterial supports for enzyme immobilization will be mainly discussed.

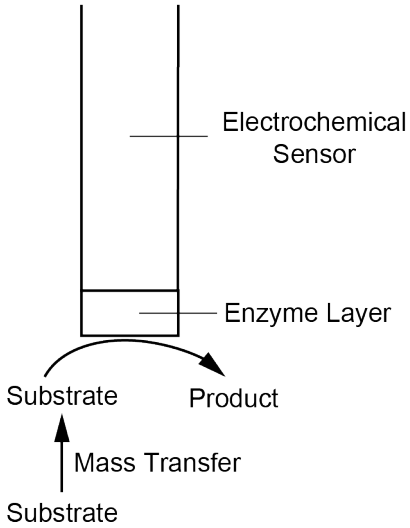


**Figure 44.** Illustration of the basic principle of an enzyme-based electrochemical biosensor.

Nowadays, enzyme-coupled electrochemical biosensors are widely utilized in, for instance, food analysis, health care and environmental safety.[165–167] The first glucose sensor, actually was the first biosensor among all types, and was invented by Clark and Lyons in 1962 via immobilizing the enzyme glucose oxidase onto the surface of an amperometric electrode.[166] The glucose biosensor was initially aimed to monitor blood glucose for surgical patients, and currently it is mainly used to measure and monitor blood glucose levels at especially diabetes patients. It can also be utilized in, for example, food industry to monitor the glucose concentration in fermentation processes. In the development of an enzyme-based electrochemical biosensors, several approaches have been established and are generally summarized into three generations by their order in time for development. Due to glucose biosensor is of importance in the development of

enzyme-based electrochemical biosensor, it is chosen to illustrate the evolution of electrochemical biosensors from the first to the third generation.

The first-generation of enzyme-based electrochemical biosensor (Figure 45A) is constructed with the simplest design concept. Here, enzymes are immobilized onto the surface of an electrode and the target of interest (i.e. substrate) is monitored via the detection of enzymatic product (e.g. $H_2O_2$).[166] In the first-generation glucose biosensor, the immobilized glucose oxidase (GOx) oxidizes glucose (i.e. substrate) to gluconolactone (i.e. product), meanwhile flavin adenine dinucleotide (FAD) that is a coenzyme or cofactor of GOx is reduced to its hydroquinone form $FADH_2$ by two electrons. Next, $H_2O_2$ (i.e. second product) is produced by dissolved $O_2$ when $FADH_2$ is reformed to FAD. Finally, oxidation of $H_2O_2$ occurs at the electrode surface when a positive potential is applied. The oxidation of glucose is eventually achieved by the sensor after several steps, and the amplitude of the resulting current is proportional to the concentration of glucose. Although the first-generation biosensor works with high sensitivity, there are still some disadvantages with this sensor layout.[168] For example, it requires a protein that possesses a flavin group, and it is highly dependent on the concentration of electron acceptor (e.g. dissolved $O_2$) that usually has a limited solubility in aqueous solution, which probably limits its utilization in biological samples.[169] Besides, the large oxidation potential applied to the electrode surface that is needed to induce an oxidation reaction of the enzymatic product (e.g. $H_2O_2$) can also results in redox reaction of other interfering electroactive molecules commonly present in biological samples, such as uric acid, ascorbic acid and paracetamol, which, in turn, can lead to a large and noisy background thereby decreasing the sensor's limit of detection.[169] Fortunately, the introduction of, for example, selective and permeable membranes like Nafion or cellulose acetate between the immobilized enzyme and substrate in aqueous solution can help minimize the electroactive interferences.[170]

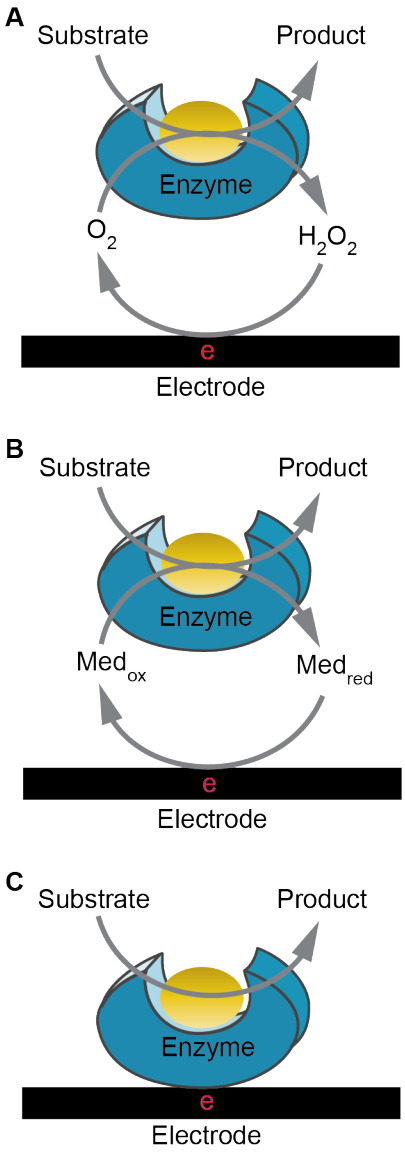


**Figure 45.** Schematic illustration of three generations of amperometric enzyme-based biosensors.

The second-generation of enzyme-based electrochemical biosensor (e.g. glucose biosensor) has addressed many issues in the first-generation by, for example, using a mediator as electron acceptor to eliminate the dependency of dissolved $O_2$ for $H_2O_2$ production (Figure 45B). In this new sensor layout, a mediator instead of dissolve $O_2$ is associated with the FAD regeneration and producing electric signal at the electrode surface.[169] The mediator is a small molecule, such as ferrocyanide, conducting organic salts or ferrocene derivative, which are redox active and rapidly associates with the enzymes.[171] Ideally, the mediator incorporated in the sensor construction is expected to be chemically stable and nontoxic, and have low solubility in aqueous solution and low detection potential. Although the second-generation electrochemical biosensor has resulted in improvements and became $O_2$ independent, the issue of mediator leaching at the electrode surface is a problem that often occurs over time.

The layout of the third-generation enzyme-based electrochemical biosensor is based on the principle of direct electron transfer between the enzyme and the electrode.[172] In this design, electron transfer occurs during the enzymatic transformation of substrate to product via the active site of the redox enzyme without the assistance of co-substrates or mediators (Figure 45C). The absence of mediator leads the third-generation biosensor to have very high selectivity especially at low potential applied onto the electrode surface with less interference. The function of the third-generation biosensor depends on direct mass transfer that strongly relies on the orientation of the immobilized enzyme at the electrode surface, and the optimal design is to ensure that the distance between the active site of the enzyme and the electrode surface to be as short as possible. The third-generation biosensor allows efficient electron transfer that can result in higher signal density with higher detection speed. However, only a few redox enzymes such as horseradish peroxidase have been reported to be able to perform the direct electron transfer to the electrode.[173,174]

### 4.1 Enzyme

In the design and construction of an enzyme-based electrochemical biosensor, enzymes are usually employed to catalyze the non-electroactive molecules of interest like glucose, acetylcholine and glutamate into forming a reporting molecule like hydrogen peroxide ($H_2O_2$) that is electroactive and can offer electric signals with the assistance of an electrochemical instrument.

Enzymes are macromolecules that serve as biological catalysts to increase the rate of chemical reactions by decreasing their activation energy that has been mentioned in Section 3.3.2.3.2 and as shown in Figure 40. Although few enzymes are catalytic RNA molecules called ribozymes, most of the enzymes are proteins. Enzyme can convert one chemical species called a substrate into another chemical species called a product. The unique three-dimensional structure of an enzyme determines its specificity. The enzyme activity is affected by the experimental conditions like temperature and pH in aqueous solution, where the optimal enzymatic activity usually is associated with an optimal temperature and pH value, and where the enzyme activity decreases significantly beyond its optimal range of conditions. Other molecules can affect the enzymatic activity as well. Molecules called inhibitors decrease the enzyme's activity, and molecules called activators increase the enzyme's activity. Before catalysis, substrate must bind to the cavity in the enzyme structure called the active site where it binds with high specificity. The active site contains one or more binding sites that can orient the bound substrate, and a catalytic site usually sits next to the bind site. The mechanism of the whole catalytic process of a chemical reaction is illustrated in Figure 46.

Enzyme can accelerate the conversion of a substrate to a product multi-millions of times faster than the speed of a native spontaneous chemical reaction. For example, the enzyme orotidine 5'-phosphate decarboxylase catalyzes the convention of orotidine monophosphate to uridine monophosphate via decarboxylation in millisecond timescale, otherwise the same chemical reaction

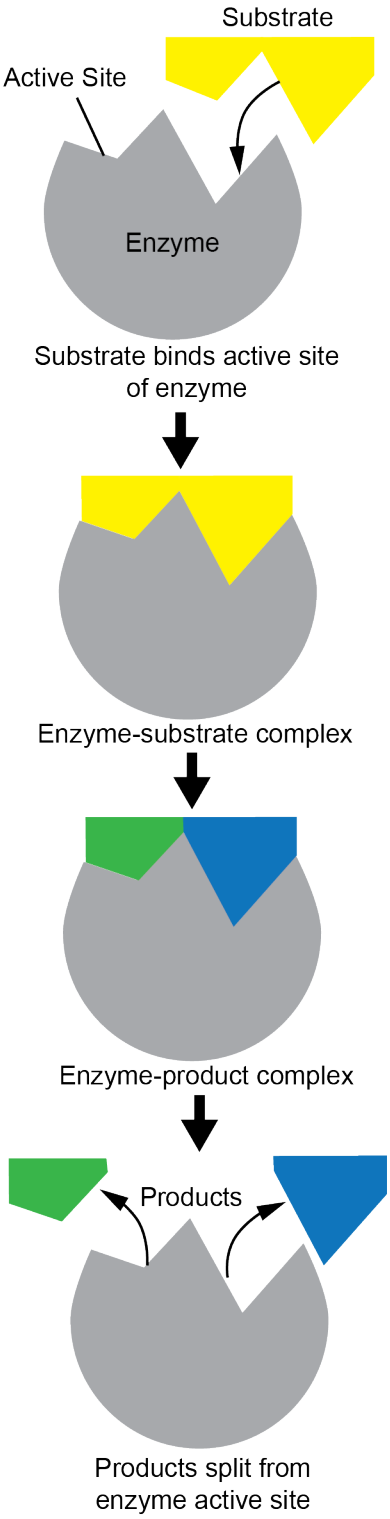


**Figure 46.** A simple mechanism of an enzyme-substrate reaction.

spontaneously occurs with a half-time of 78 million years in the same experimental conditions at the room temperature in the neutral aqueous solution.[175,176] Carbonic anhydrase is reported as one of the fastest enzymes according to current knowledge. Each carbonic anhydrase enzyme can hydrate around 1000 molecules of $CO_2$ per millisecond.[177] One type of acetylcholinesterase can hydrolyze about 25 molecules of neurotransmitter acetylcholine to acetate and choline per second.[178,179]

### 4.1.1 Enzyme Assays

The rate of enzyme reactions is measured by laboratory procedures called enzyme assays, which usually measures the concentration changes of products or substrate with time. Figure 47 is an example of the progress curve for an enzymatic reaction in an enzyme assay. The rate of reaction is actually the slope of curve in Figure 47. The initial product formation increases linearly versus time with constant (and maximal) rate of enzyme reaction for a short time period upon the reaction initiation, and the rate slows down as the reaction continuously carries on with the consumption of substrate. The time of constant initial rate depends on the experimental conditions, and it can vary from hours to milliseconds.

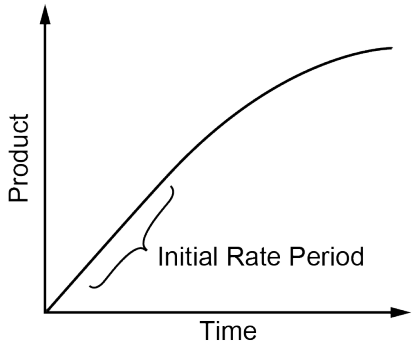


**Figure 47.** The progress curve of an enzymatic reaction.

### 4.1.2 Michaelis-Menten Kinetics

Enzyme kinetics is the study of how enzymes catalyze chemical reactions. A quantitative theory about enzyme kinetics was proposed by Leonor Michaelis and Maud Leonora Menten in 1913, and is called Michaelis-Menten kinetics,[180] which is the well-known model of enzyme kinetics. They proposed that the enzymes firstly bind to the substrate to form an enzyme-substrate complex, and then proceed the catalysis of the chemical reaction to produce the products as illustrated in Figure 46.

The Michaelis-Menten equation ($Equation\ 31$) describes the variation of reaction rate ($v$, i.e. the slope of curve in Figure 48) with the substrate concentration ($[S]$) as follows:

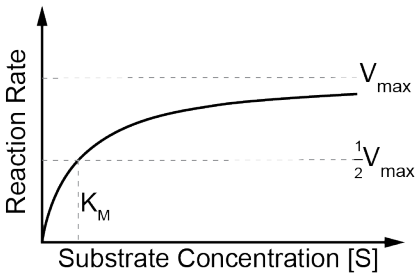


**Figure 48.** Michaelis-Menten saturation curve that shows the relation between the reaction rate and substrate concentration of an enzyme reaction.

$$v = \frac{V_{max}\,[S]}{K_M + [S]} \qquad (31)$$

As shown in Figure 48, enzyme rate increases with the increasing substrate concentration at constant solution conditions until approaching a steady state. This steady state is called $V_{max}$ and stands for the maximum rate of an enzyme catalytic reaction. At the state of $V_{max}$, all enzymes are bound with a substrate and their total amount is the same as the amount of enzyme-substrate complex. $K_M$ is called Michaelis-Menten constant, and it represents the substrate concentration when the enzyme reaches the half of its maximum reaction rate ( $V_{max}$ ). For a certain substrate, each enzyme is associated with a characterized $K_M$ value.

### 4.1.3 Immobilization of Enzymes

It has been realized that enzymes have enormous potentials of practical usage in different fields and applications, such as widespread industrial processes, pharmaceuticals, biofuel cells and biosensors. Since enzymes have a short lifetime that limits their usefulness, improving the enzyme stability is highly needed for further applications and it also becomes an interesting topic that draws substantial attention of scientists. Except protein engineering, enzyme modification and medium engineering, the strategy of enzyme immobilization is one well-used approach to maintain and improve the stability of enzymes.[181] The concerns of enzyme stability are generally about thermal stability, pH stability, storage stability and recycling stability. And the stability of immobilized enzymes is usually enhanced compared to that of free enzyme in solution.

Enzyme immobilization is a procedure that fixes an enzyme to a support or matrix of a solid surface. Especially in the process of enzyme-based biosensor construction, enzyme immobilization is an important step. The operation of enzyme immobilization can affect the sensor's performance like the working efficiency, temporal resolution, sensitivity, selectivity, stability, reproducibility

and reusability. In detail, there are several different strategies and techniques of enzyme immobilization onto electrode surface that have been developed and the major ones are briefly described and discussed as follows.

#### 4.1.3.1 Adsorption

Adsorption is probably the easiest and simplest method to immobilize enzymes onto an electrode surface (Figure 49A). It is a straightforward method that is usually performed via dissolving enzymes in solution and placing the solid support into enzyme solution for a certain period of time, or drying enzyme solution on the electrode surface. In general, the mechanism of adsorption is based on weak non-covalent interactions such as van der Waals forces, hydrophobic effects and electrostatic interactions.[182] Physical adsorption occurs through weak bond mainly via Van der Waals forces. Adsorption relies on electrostatic interaction when the enzyme and the support display opposite charges. The net charge of an enzyme can be adjusted by the pH value of its surrounding dissolving solution. Enzyme carries a net of positive charge when the surrounding pH is lower than the enzyme's isoelectric point where enzyme is electrically neural. If the support is negatively charged, enzyme that carries a net positive charge can be electrostatically immobilized onto it.

Since there is no chemical reaction involved in the adsorption process, the support surface may block the active site of the immobilized enzyme, which leads to the loss of enzyme activity. And the fact that the enzymes are loosely adsorbed onto the support via this immobilization method, it can cause the enzyme desorption due to the changes of environmental factors like temperature and pH value of surroundings. Besides, since the bonding between enzyme and support is not specific, adsorption of contaminants like other substance and proteins is another drawback of this immobilization method.

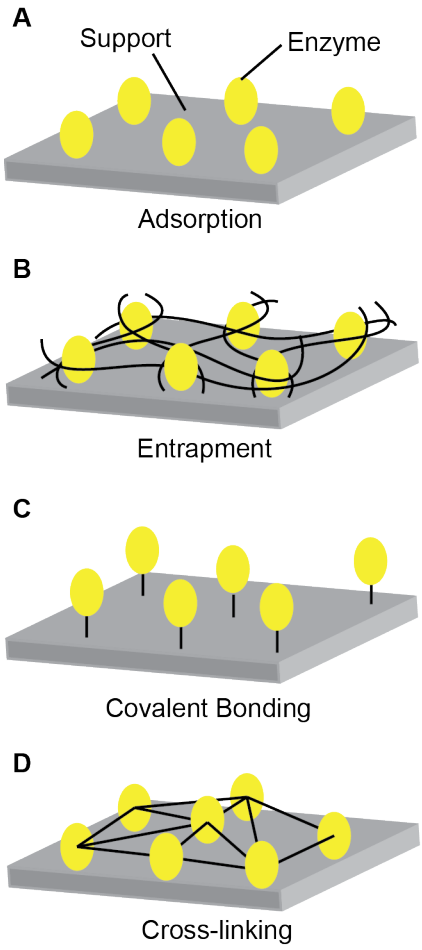


**Figure 49.** Schematics of different enzyme immobilization strategies.

#### 4.1.3.2 Entrapment

Entrapment is another immobilization method that traps the enzymes in a porous matrix such as polymer and sol-gel

glass.[183] It is performed by initially co-culturing enzymes with monomer molecules of the support material in an aqueous solution, thereby simultaneously immobilizing them in the same sensing layer via polymerization process of the monomers added (Figure 49B). The polymerization process usually includes (1) electropolymerization using mostly conductive polymers such as polyaniline, polypyrrole or polythiophene;[182] (2) photopolymerization using pre-polymer containing photo cross-linking groups with initiation of light exposition;[184,185] (3) sol-gel process using for example, highly porous silica gels. Other materials are also often used in the entrapment method, for instance, polysaccharide-based hydrogels such as agarose, chitosan and alginate, carbon paste[182] and amphiphilic network composed of an hydrophobic phase of poly-dimethylsiloxane and an hydrophilic phase of poly(2-dydropxyethyl acrylate).[186,187]

Although the polymerization process sometimes relies on highly reactive monomers that may react with amino acid residues of the enzymes, in the most cases, enzymes are physically entrapped in the support matrix without modification, thus the activity of enzyme and its stability are usually well retained compared to other immobilization methods. However, when the pore size of matrix is too big the enzyme leakage may occur.[188] Besides, the diffusion barriers limit the mass transfer of the substrate or analyte, which leads to a reaction delay and this barrier can cause signal detection postponement.[182]

#### 4.1.3.3 Covalent Bonding

Immobilization via covalent bonding depends on the strong chemical bond formed between a support and the enzyme (Figure 49C). The bonding strength relies on the amino acid side chain of the enzyme like histidine, aspartic acid and arginine. The degree of bonding reactivity is affected by different functional groups such as phenolic hydroxyl group (–OH) and imidazole ($C_3N_2H_4$) that do not have a function in the catalytic activity.[189] Covalent immobilization can occur on both uncoated support surface and a modified

support. For example, a peptide-modified surface offers precise control of protein orientation and position, thereby improving the affinity, specific activity and stability of immobilized enzyme.[190] The detail mechanism of covalent immobilization and the activation methods between enzyme and support surface via different functional groups have been well summarized in a review paper from Sassolas *et al.*[182]

Covalent immobilization has been widely used in the development of enzymatic sensors. This method offers the strongest bond between enzyme and support among different immobilization methods and it leads to the lowest leakage of enzyme during applications.[191]

#### 4.1.3.4 Cross-linking

Enzymes immobilized via cross-linking methods are also result in enzymes that are covalently bound to each other via the means of bi- or multifunctional reagents such as glyoxal and hexamethylenediamine (Figure 49D). Among all reagents, glutaraldehyde is the most commonly used cross-linking reagent since it can be economically and easily obtained in large quantities. The cross-linkers used in this method are usually aiming to ensure that their binding sites on enzyme do not occupy the enzyme active site where analyte catalysis occurs.

This method usually causes very little desorption from the support surface due to the strong chemical binding between biomolecules, which, in turn, leads to loss of enzymatic activity due to the distortion of enzyme conformation.

## 4.2 Nanomaterials as Immobilization Support for Enzyme and Applications in Electrochemical Biosensors

To improve the enzyme stability and catalytic efficiency for especially small-scale applications, modifying the structure of carrier materials to nanoscale has become a popular strategy for enzyme immobilization (Figure 50). Nanomaterials are referred to materials of which every single unit is between 1 to 1000 nm (however usually is between 1 to 100 nm) in size. Many types of nanomaterials

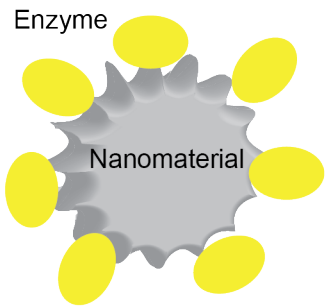


**Figure 50.** Immobilization of enzyme at nanomaterial support.

such as nanoparticles, nanofibers or nanotubes and materials with nanoporous structure have remarkably captured people's attention and been introduced for enzyme immobilization as support. Compared to materials with larger size, 1) nanomaterials offer high surface to volume ratio (or large surface area per unit mass), which can lead to high yield of enzyme immobilization per unit of support in weight; 2) the surface curvature of nanomaterials can assist resisting denaturation of immobilized biological macromolecules like proteins; 3) enzymes immobilized on nanomaterials create less possibilities of steric hindrances; 4) nanomaterials also fit in the requirement of design for reducing the size of applications like bioreactors and biosensors.[192] Besides, nanomaterials have enormous potential in broad applications such as drug delivery as vehicles and electromechanical systems as components.

Moreover, in the application of electrochemistry, nanomaterials play an important role and are often employed in the novel design of enzyme-based biosensors. Specifically, to increase the surface area that can improve electrode sensitivity, to enable the detection of certain analytes (e.g. hydrogen peroxide), and/or to avoid enzyme denaturation in the case when an electrode is applied to construct an enzyme-based biosensor, the surface of electrode can be modified with nanoparticles such as silver (Ag) nanoparticles, gold (Au) nanoparticles,[63,64] platinum (Pt) nanoparticles[193] and alloy nanoparticles,[194] and nanotubes like carbon nanotubes.[195]

### 4.2.1 Nanoparticles

Nanoparticles (NPs) describe particles of which all three external dimensions are sized to nanoscale, usually within 100 nm, and there is no significant difference between the shortest and the longest axes. Nanoparticle synthesis has been explored with different types of materials including high-purity oxide ceramics such as aluminum oxide and copper oxide, polymers, composite materials like silicon carbides and aluminum nitrides, metals like Au and Ag and non-metals. Many researches have reported that enzyme

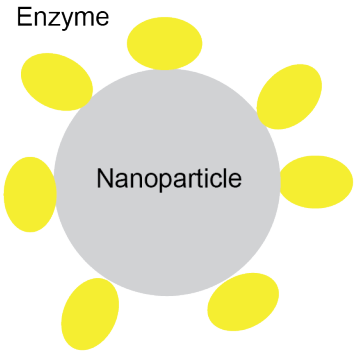


**Figure 51.** Immobilization of enzyme at nanoparticle.

immobilization onto NPs (Figure 51) can reduce enzyme denaturation, improve enzyme stability and resistance to the changes of chemical environment (e.g. pH, temperature and ionic strength) and enzyme catalytic activities.[196] Because of the unique characteristics of NPs like high surface-to-volume ratio, high curvature, overall low mass transfer resistance, high enzyme loading efficiency and fast electron transport rate for metal materials, it allows the enzyme-nanoparticle conjugates to apply into a wide range of applications. In addition, magnetic NPs have another property that they can be easily separated when an external magnetic power is applied.

The conjugation of protein to especially AuNPs that are electron dense has been widely employed in applications, for example, for visualizing immunostaining methods using electron microscopy, atomic force microscopy or light microscopy,[197,198] and also has drawn a lot attention on the effect of conjugation to stability and activity of immobilized proteins.[199] For example, the efficiency of trypsin increased by about 12% when immobilized onto AuNPs and maintained a higher stability compared to that of free trypsin in solution as shown by Lv *et al.*[200] While Huang *et al.* observed that the biocatalytic activity of AuNP-trypsin was lower than that of native trypsin.[201] The effects of conjugation to NPs on the activity and stability of immobilized proteins are not limited to AuNP, other NPs have also been reported. When trypsin was immobilized onto chitosan $Fe_3O_4$ magnetic NPs via covalent bonding, it performed active in a wider pH range and with a higher thermal stability than when free in solution.[202] Besides, impact from other aspects of nanoparticle properties on the enzymatic performance was considered as well. The work from Vertegel *et al.* showed that the surface curvature of NPs contributed from their size may affect the catalytic activity of immobilized enzyme as well, better enzymatic activity was obtained when lysozymes were immobilized onto smaller silica NPs with higher curvature in comparison with bigger silica NPs with flatter surface.[203]

The Cans group initiate the work on enzyme-nanoparticle bioconjugates from 2007 by immobilizing HRP and fluorophore-labeled HRP onto AuNP and comparing the enzymatic activities. Then the focus of bioconjugates work in Cans group was moved to the cases of monolayer enzyme immobilization and its applications in fabricating rapid enzyme-based electrochemical biosensors, based on the hypothesis that thin enzyme layer should minimize the distance of diffusion limited distance for detection of electrochemical reporter molecules. Specifically, enzyme-AuNP conjugates with monolayer coating of a two-enzyme system (i.e. acetylcholinesterase and choline oxidase) at their optimum ratios were built in 2014.[204] The findings from this work and implementing a monolayer enzyme coating onto AuNP-modified carbon fiber surface for constructing a fast acetylcholine amperometric biosensor, showed that recording speed could be improved from seconds down to millisecond timescale using this strategy (**Paper I**).[63] By employing the same concept, an ultrafast glutamate enzyme-based biosensor was developed in **Paper III,** which displays that temporal resolution could be improved and fast enough for real-time detection of individual sub-millisecond exocytosis events from spontaneous glutamate release in the nucleus accumbens of rodent brain tissue.[64] Moreover, from the characterization of the glucose oxidase interaction when immobilized to the surface of AuNPs, we found that enzymes in crowdedness when attached as monolayer coatings at AuNP surface significantly improve the catalytic activity and stability of immobilized enzyme (**Paper IV**).

### 4.2.2 Nanotubes

Nanotubes are structures with tube-like shape and with cross-section in nanometer scale. There are nanotubes in different materials like silicon nanotube,[205] titanium nanotube[206] and even DNA nanotube[207]. One example was recently reported that lipases immobilized onto glutaraldehyde functionalized $SnO_2$ nanotubes[208] showed good activity with broader pH range and broader temperature range, in contrast to free lipases in solution.

Especially the thermal stability (or monitored by the residual activity) of lipases was improved using different immobilization methods from 4% (free lipase) to 42 % (lipase immobilized via covalent binding) and 61 % (immobilized lipase with additional cross-linking) at 70 ℃, additionally the pH stability of the immobilized lipases was enhanced to 38% whereas free lipases totally lost its activity.

Among the wide varieties of nanotubes, carbon nanotube (CNT) is probably the most popular and well-known one. It is conductive and can be considered as a cylinder made up of rolled-up graphene sheets with diameter on the nanoscale and a length usually in microscale. In general, CNTs can be formed in either single-walled carbon nanotubes (SWCNT) or multi-walled carbon nanotubes (MWCNT). Since CNTs display excellent thermal, electrical, mechanical and biocompatible properties, they are used for enzyme immobilization in the applications, especially in constructing biofuel cells or biosensors. As illustrated, SWCNTs have a diameter roughly in 1-2 nm with a length of 0.2-5 μm (Figure 52A),[209] while the diameter of MWCNTs varies between 2 to 25 nm (Figure 52B).[210] Both SWCNT and MWCNT have been employed for immobilization of proteins or enzymes like horseradish peroxidase, trypsin, soybean peroxidase and proteinase K via adsoprtion.[211] In the study of immobilizing phytase onto functionalized MWCNT via covalent bonding,[212] the thermal stability of immobilized phytase was improved from 3% to 33% and from 27% to 51% at 90 ℃ and 80 ℃, respectively, in comparison to the free phytase in bulk solution. Besides, the activity of immobilized phytase is higher than that of free phytase in pH 8-10.

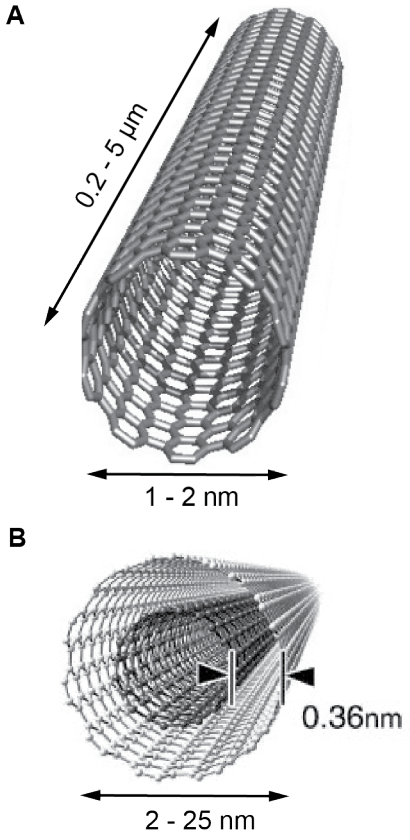


**Figure 52.** Illustration of single-walled carbon nanotube (A) and multi-walled carbon nanotube (B). Reprinted and adapted with permission from Reference 209 and 210.

#### 4.2.2.1 Carbon Nanotubes in Electrochemistry

Because of the unique structures and excellent electrical, electrochemical and mechanical properties, for instance, CNT is able to behave as a semi-conductive or conductive materials due to the variations of structure (i.e. mainly regarding helicity and diameter),[213–215] CNTs have been

integrated into the design of electrochemical sensor as key components.[216] Basically, CNT-based sensors can offer faster electron transfer kinetics and higher sensitivity compared to traditional electrodes. There are several strategies to construct the CNT–based biosensors as following.[217]

CNT paste electrodes are made by mixing CNT powder with bromoform, mineral oil and deionized water.[217–219] For example, by using bromoform as binder, the CNT-paste electrode was constructed for detecting dopamine with both *in vivo* and *in vitro* models in 1996.[218] CNTs can also be used to modify the surface of glassy carbon electrodes or metal electrode for electrochemical detection of analyte, to improve the electrodes' sensitivity and stability, due to CNT's ability to resist surface fouling and process fast electron transfer. Besides, electrodes composed of CNTs can be further fabricated with metallic nanoparticles (e.g. gold nanoparticles and platinum nanoparticles) nanowires via electrodeposition or other adsorption methods.[220]

Besides, by immobilizing enzymes via different methods like direct adsorption, covalent-bonding, entrapment and encapsulation to CNT-based electrode, the sensitivity and selectivity of electrodes can be improved for detecting inert-electroactive compounds.[217] For instance, enzymes lactate oxidase and polyphenol oxidase are immobilized within CNT paste electrode by dispersing into CNT with mineral oil to detect lactate and phenols and catechols with high sensitivity.[219] As a further example, covalent attachment has been employed to immobilize glucose oxidase to CNT-modified gold electrode via flavin adenine dinucleotide as linker in between.[221]

### 4.2.3 Nanopores

Nanopores describe the porous surface in solid materials, and the size of these pores or cavities is on the nanoscale. Specifically, porous materials with pore size among 2 nm to 50 nm are defined as mesoporous materials, which are usually made by different oxides like aluminum oxide ($Al_2O_3$),[222] titanium dioxide ($TiO_2$)[223] and silicon dioxide ($SiO_2$)[224]. The pore size is one of the key factors that can

affect the immobilized enzyme activity, loading efficiency and stability.

Mesoporous silica (Figure 53) is one of the promising nanoporous materials for enzyme immobilization as solid support. Improvement of thermal stability, storage stability, resistance to harsh conditions (e.g. high temperature and pH value) and catalytic activity of enzymes immobilized onto mesoporous silica via covalent binding has achieved in many reseaches.[225] In the study of Åkerman group, enzymes were successfully immobilized and evenly distributed into the mesoporous silica.[226,227] In their continued work, by co-immobilizing two enzymes (i.e. formate dehydrogenase and formaldehyde dehydrogenase) in siliceous mesostructured cellular foams, the activity of converting $CO_2$ to formaldehyde is increased to approximately 4 times compared to the free enzymes in the bulk solution state.[228] Mesoporous silica with immobilized enzymes (e.g. HRP and GOx) has also been applied in the design of electrochemical biosensors with high stability.[225] Dai *et al.* developed a phenol sensor that was constructed by fabricating the carbon electrode using mesoporous silica that had been loaded with HRP and tyrosinase,[229] and provided a sensor with a long-term stability about 80 days.

In the study of protein immobilization with other porous materials, α-amylase immobilized onto nanoporous zeolite was retained around 48 % of its native activity, and its stability in wide range of pH, higher temperature and storage was improved as well compared to enzyme in free solution.[230]

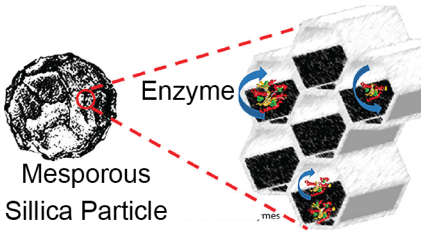


**Figure 53.** Illustration of mesoporous silica particles with enzyme loading. Reprinted and adapted with permission from Reference 227.

# 5. Methods for Nanomaterial Analysis

The studies of nanomaterials (e.g. nanoparticles and enzyme) presented in this thesis were fundamental to enable the design and construction of novel ultrafast enzyme-based electrochemical biosensors with nanomaterial-coated surfaces. The amount of enzyme needed for monolayer coating onto the AuNP-modified electrode surfaces was determined in three steps. 1) The study of enzyme-nanoparticle interaction using ultraviolet-visible spectrophotometry; 2) The size measurements of AuNP and enzyme-AuNP conjugates using the technique of dynamic light scattering (DLS) and nanoparticle tracking analysis (NTA); 3) The quantification measurement of the number of enzymes bound per AuNP in conjugates in bulk solution using fluorescence spectrophotometry.

### 5.1 Ultraviolet-Visible Spectroscopy

Ultraviolet-visible (UV-Vis) spectroscopy is a spectroscopy method that measures the absorbance of light in the region of ultraviolet (190 nm – 400 nm) and the near visible spectral region (400 nm-800 nm), by a sample containing molecules that absorb light at a certain wavelengths or a range of wavelengths.

Figure 54 illustrates the basic setup and principle of a UV-Vis spectrophotometer. A light source provides light covering visible and adjacent ultraviolet spectral regions (200 - 800 nm) and passes through a monochromator, which can split the incident light into narrow band of wavelengths. The split light then passes through the essentially transparent cuvette, which serves as the sample container, one wavelength at the time, or the light is passed through a reference cuvette, which functions as the blank and usually contains the sample solvent. When the intensity of transmitted light in the reference cuvette ($I_o$) is larger than that in the cuvette containing the sample solution ($I$), it indicates that the sample is absorbing some of the light at that specific wavelength. The sample absorbance ($A$) is related to the transmitted light intensity

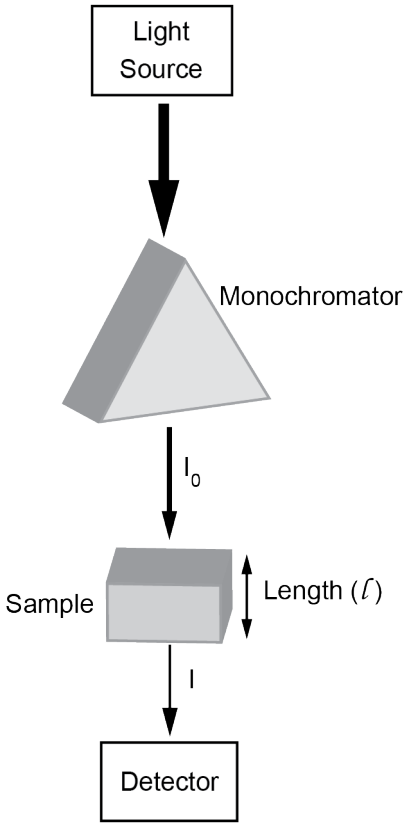


**Figure 54.** General schematic of a typical UV-Vis absorption spectrophotometer.

via $Equation\ 32$:

$$A = \log_{10} \frac{I_o}{I} \qquad (32)$$

This technique can also be further quantitatively used to determine the sample concentration that is proportional to the sample absorbance based on the Beer-Lambert law ($Equation\ 33$):

$$A = \varepsilon \cdot l \cdot c \qquad (33)$$

where $c$ is the sample concentration, $l$ is the length the light is passing through the sample, $\varepsilon$ is the molar extinction coefficient that is constant for a certain molecule at a particular wavelength.

**5.2 Dynamic Light Scattering**

Dynamic light scattering (DLS) is a technique that allows measuring the size distribution of small particles in suspension in the nano-range. The samples typically include micelles, emulsions, proteins, polymers and nanoparticles. The basic principle of DLS is to illuminate the sample under Brownian motion using a light source such as a laser beam, and the intensity fluctuations of the scattered light are captured at a certain scattering angle (e.g. 173°) via a photon detector to obtain the details on particle size (Figure 55). A fixed angle for detecting scattered light allows measuring the mean size of particles but in a limited range of sizes, multi-angle measurements might assist to further infer the particle size distribution. Analyzing the intensity fluctuation of scattered light can provide further information about particle physical properties, for instance, the diffusion coefficient of particles under Brownian motion.

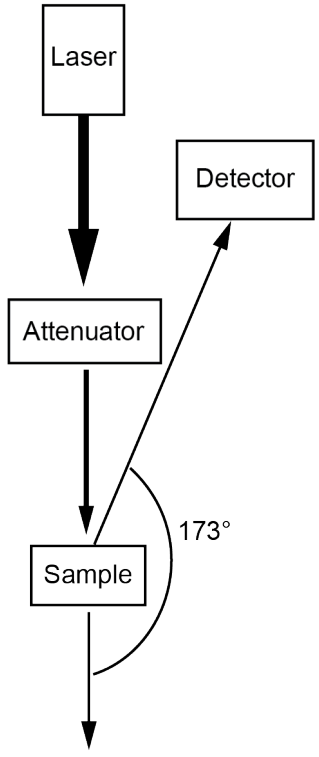


**Figure 55.** Schematic of the basic parts for a typical dynamic light scattering with backscatter detection.

Brownian motion describes the fast and random movement of nanoparticles in suspension due to their collision with solvent molecules. Usually smaller particles move faster than larger particles. The relation between the particle size and the nanoparticle movement under

Brownian motion can be linked by *Stokes-Einstein equation* ($Equation\ 34$),

$$D = \frac{k_B T}{6\pi\eta r} \qquad (34)$$

where $D$ is the diffusion coefficient of particles, determination of $D$ depends on particle size and other properties as well as temperature and pressure, $r$ stands for the hydrodynamic radius of particle, $\eta$ is the dynamic viscosity of the fluid, $T$ is the absolute temperature, $k_B$ is the Boltzmann's constant.

Figure 55 illustrates the basics of a typical DLS instrument. In order to generate a measurable scattered light, the intensity of the scatted light can be adjusted via modulating the sample concentration to optimum. Since the particles can scatter light in all direction after illuminated, the detector can theoretically be placed in the any locations. However, the intensity of scattered light generated by particles with the same size depends on the scattering angle, which means that there is an optimal angle for detecting each size of particles. In this thesis, a detector located at 173° (Figure 55) was chosen for measurement of light scattering from enzyme-AuNP conjugates to avoid, for example, the signals from incident light that passes through sample, the side effects of contaminants and contributions from multiple scattering, which can lead to large errors in measurements.

### 5.3 Nanoparticle Tracking Analysis

Nanoparticle tracking analysis (NTA) is a technique that can profile the size distribution of particles and determine the particle concentrations in liquid suspension under Brownian motion, which is achieved by visualizing the individual particle movements and analyzing the information of Brownian motion and light scattering.[231] The particle hydrodynamic radius related to the rate of particle movements can be calculated via the Stokes-Einstein equation. NTA allows determining the particle size distribution in the range of approximately 10 to 1000 nm in

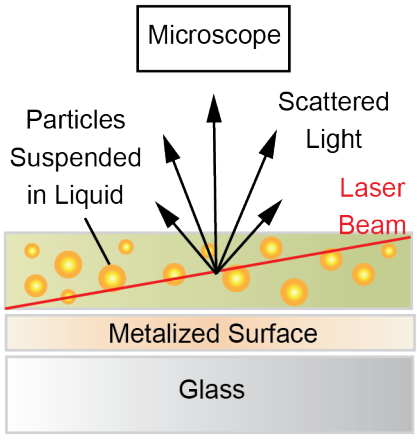


**Figure 56.** Schematic of the main setup for nanoparticle tracking analysis system (NTA).

diameter. Compared to DLS that is an ensemble technique, NTA collects information from individual particles.[232]

Figure 56 shows the basic mechanism of a NTA system. A laser beam passes through the sample chamber and illuminates individual particles suspended in a solvent using scattered light. The illuminated particles will scatter light to enable the microscope that is equipped with a video camera to visualize and track the particle movements. The recorded videos are used for data analysis using a software based on Stokes-Einstein equation. The NTA measurements of enzyme-AuNP conjugates performed in projects mentioned in this thesis were made in order to complement the information collected from DLS measurements. The data obtained via both of DLS and NTA measurements are similar and consistent for each experimental condition.

### 5.4 Fluorescence Spectroscopy

Fluorescence spectroscopy is a technique that measures the intensity of emitted fluorescent light from an analyte after absorbing light energy. By creating a calibration curve of fluorescence intensities versus standard solutions containing a series of analyte concentration, or knowing the absorbance and quantum yield, the concentration of an analyte in a sample solution can be determined. Usually a beam of ultraviolet light is used as light source to excite the molecules in sample. As illustrated in Figure 57, after absorbing a photon from the light source at a particular wavelength, the electrons in molecules are excited from the ground electronic state ($S_0$) at a low energy level to one of the vibrational states that are at higher electronic energy levels ($S_1$ and $S_2$). After that, there are several mechanisms for the absorbed energy of excited electrons to dissipate their energy. For example, vibrational relaxation, which is a nonradiative transition, usually relaxes the energy to the lowest vibrational level within the same excited state. Another type of nonradiative transition is called internal conversion, which is a process where the excited electron from one vibration level of a higher excited electronic state ($S_2$) can transit to another vibration

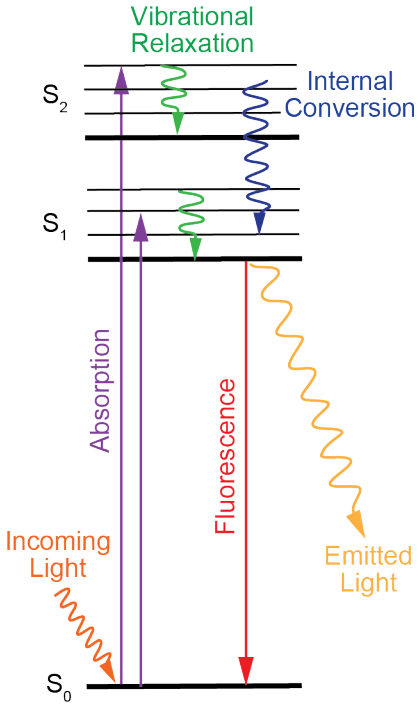


**Figure 57.** A Jablonski diagram including vibrational levels at excited states illustrates the absorbance, vibrational relaxation, internal conversion and light emission from a fluorescent molecule.

level of a lower electronic state ($S_1$). When the energy of molecules drops from the lowest vibrational level in the excited electronic state to any vibrational levels of the ground state, a photon is emitted. This optical phenomenon is called fluorescence. The whole process is illustrated in the Jablonski diagram (Figure 57).

Figure 58 shows the schematic diagram of a fluorescence spectrophotometer. A monochromator is placed before the sample cuvettes to subject the sample to light at a fixed wavelength. The emitted fluorescent light is examined by another monochromator to scan a range of wavelengths of light and to search for the optimal fluorescent wavelength. The other way around, an optimal wavelength of incident light for exciting an analyte can be found out by fixing the wavelength to collect the emitted light. At a fixed wavelength of incident light and a fixed wavelength of emitted light, the intensity of fluorescence is proportional to the sample concentrations. Thus, the fluorescent spectroscopy can perform quantitative measurements. To avoid the interferences from the incident light and optimize sensitivity, the detector is often positioned at 90° to the excitation light beam.

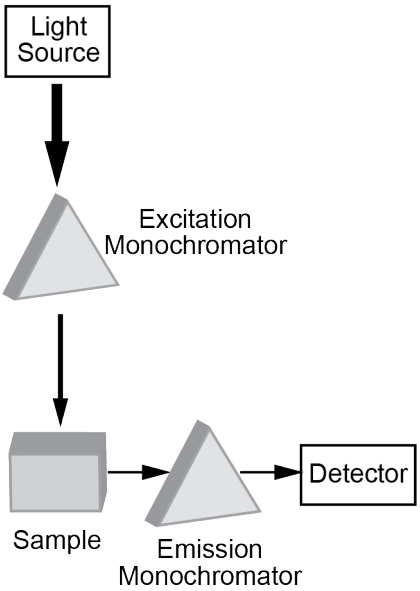


**Figure 58.** Schematic diagram of a typical fluorescence spectrophotometer with its basic components.

# 6. Summary of Papers

The projects presented in this thesis mainly focus on developing new analytical tools to the neuroscience field where there has been a limitation to what measurements current technology can achieve. We have in these projects presented aimed to improve the temporal resolution of sensors to allow real-time detection of rapid sub-millisecond fluctuations of key molecules in the brain that need detection schemes based on chemically selective biosensors. To meet this challenge, we have used a new approach for the development of ultrafast enzyme-based electrochemical biosensors where we used our knowledge in nanomaterial science, analytical chemistry, surface chemistry, physical chemistry and neuroscience to succeed. Amperometric microelectrodes have been one of the most popular tools for monitoring neuronal activity in brain tissue for detection of the sub-millisecond to millisecond events of neurotransmitter release at single cell exocytosis activity. However, conventional amperometry techniques are limited to detection of electroactive molecules like the catecholamines. The detection of non-electroactive neurotransmitters (e.g. acetylcholine and glutamate) and other important non-electroactive brain analytes e.g. glucose is only possible through the introduction of a biosensor scheme. However, the temporal resolution of traditional enzyme-based electrochemical biosensors has for long suffered from a temporal resolution that is on three orders of magnitude slower than needed to temporally resolve single exocytotic events. As presented by this thesis, we here introduce a new concept of improving the speed for enzyme-based biosensors. This was realized by limiting the coating of enzyme at the electrode surface into an ultrathin layer or monolayer, in comparison to the thick enzyme layers that are traditionally employed. Using this strategy, we improved detection speed of glucose, acetylcholine and glutamate 2-3 orders of magnitude compared to existing technology. The success of this sensor development was based on performing detailed studies of enzyme interactions to nanoparticle surfaces in bulk solution, where key knowledge on how to limit enzymes into ultrathin layers while maintaining optimal retained enzyme activity by the immobilized enzymes was implemented when designing and fabricating these novel enzyme-based nanoparticle-coated microelectrode sensors. Moreover, with this invention, the ultrafast sensors were used to show that the real-time detection of rapid single exocytosis events was possible. These new analytical biosensor tools were also used for establishing a novel method for quantifying glutamate content in single synaptic vesicles and to determine the amount of glutamate released at various different types of dynamic single exocytotic events.

In **Paper I**, a fast acetylcholine sensor was fabricated using a two-enzyme system to detect the non-electroactive neurotransmitter, acetylcholine. The sensor was made up by a 33 μm (in diameter) carbon fiber microelectrode that was modified with electrochemically deposited AuNP hemispheres using a protocol, which we established and aimed to achieve a homogenous size distribution of 20 nm AuNPs at the carbon electrode surface. Then a two-

enzyme system composed of acetylcholinesterase (AChE) and choline oxidase (ChO) was immobilized onto the surface of the AuNP hemisphere at the electrode surface, using the findings from a previous study on what ratio of immobilized enzymes (i.e. 1:10 AChE/ChO) [204] that provide the optimal efficiency of the sequential reaction by these two immobilized enzymes. The limit of detection for this acetylcholine sensor reached 10 μM and a linear detection range at physiological relevant concentrations. The sensor provided good chemical selectivity in the presence of other common interfering molecules in the brain like norepinephrine and dopamine, glutamate, glucose and ascorbic acid. Moreover, by testing the sensor using an artificial cell model for exocytosis, single vesicle release events of acetylcholine were temporally resolved on the millisecond timescale. The detection of acetylcholine was based on monitoring the reduction reaction for the enzymatic product $H_2O_2$ as a result to the enzyme sequential reactions of acetylcholine. This achievement showed that this new design of an ultrafast sensor allows detection of vesicular acetylcholine release and inspired us to the continuous work on applying this biosensor concept to other enzyme-based biosensor systems for detection of other important brain analytes.

In the development of these enzyme-based AuNP coated biosensors, it is important to characterize the AuNP size and density at the electrode surface while studying the interaction between enzymes and AuNPs for maximizing the sensor's detection ability. Usually, nanoparticle density and size are characterized via imaging technique such as scanning electron microscopy, which is a time-consuming process. To quantify enzyme immobilized onto metal nanoparticles, enzymes were commonly labeled with fluorophore before immobilization, and then by dissolving the metal nanoparticle support using cyanide solution (e.g. potassium cyanide). Thereafter the number of enzymes left in solution is measured via fluorescent spectrophotometry. However, this process is toxic because of the cyanide used in this process and therefore the work in **Paper II** propose a faster, non-toxic and cheaper analytical method to characterize immobilized enzymes at the surface of AuNPs that were electrodeposited at glassy carbon electrode surface. Here AuNP size and density were characterized and enzymes immobilized onto this nanoparticle support were quantified. In this method, the size and density of nanoparticles deposited at a glassy carbon electrode were determined by electrochemically stripping off AuNPs from the electrode surface. Fluorophore-labeled enzymes immobilized onto the AuNP surface were collected into the stripping solution, and were quantified using fluorescence spectroscopy. By correlating the number of deposited AuNPs and immobilized enzymes, the average number of enzymes bound per AuNP was determined.

In **Paper III**, an ultrafast biosensor based on a carbon fiber microelectrode with AuNP modification for detection of glutamate, which is a non-electroactive neurotransmitter, was constructed by applying the concept of limiting the enzyme coating at the electrode surface to a monolayer. Before this achievement, there was a lack of a technique that was capable

to monitor real-time single exocytosis activity of glutamate during neuronal communication. In this work, the performance of monolayer enzyme coating onto AuNPs modified electrode was guided by the detail characterization of glutamate oxidase interaction with AuNP in bulk solution using a UV-Vis based flocculation assay and enzyme-AuNP size measurements using NTA and DLS technique. The glutamate sensor was then implemented for detection of glutamate activity *ex vivo* in brain slices of two rodent models. Here, detection of random bursts of single half-millisecond exocytosis events were temporally resolved from spontaneous glutamate activity in the core region of the nucleus accumbens of mouse and rat brain slice. The kinetics of glutamate exocytotic release events were carefully examined and summarized into six categories of current spikes depending on their shape. The relative quantification of the quantal content of these spikes suggested that more than one mode of exocytosis was detected and that the frequency of the different kinds of spikes were strikingly similar in both rodents.

Immobilization of enzymes onto the nanomaterial support is often utilized in catalysis and different biotechnological applications including biosensor technologies. For example, the construction of an electrochemical glucose biosensor, the enzyme glucose oxidase (GOx) is incorporated in the detection scheme for blood sugar. For the sensor's function and working efficiency, the stability and retained enzyme activity of immobilized enzymes is of great importance. However, enzymes often suffer from denaturation upon immobilization at solid surfaces, especially at flat surfaces, due to deformation of their tertiary structure upon binding. To optimize the performance of sensors coated with enzyme-nanomaterial conjugates, the interaction of enzyme to AuNP needs to be considered. The interactions of GOx with AuNPs are explored in **Paper IV** and showed how a careful pre-study of the enzyme interaction can have significant outcome on the efficiency of the final enzyme-AuNP conjugate. By increasing the density of immobilized enzymes onto 20 nm AuNPs while limiting the coating to a monolayer, the activity of immobilized enzymes was studied as a function of enzyme density at the AuNP surface. Here we found that when enzymes are bound at molecularly crowded conditions, where the enzyme was attached with a minimal size of its molecular footprint at a AuNP surface, the specific enzyme activity was improved approximately 300% compared to that of native GOx in aqueous solution. A glucose electrochemical biosensor that relies on such stable enzymes with excellent catalytic performance was implemented and was tested using the vesicle content analysis method developed in **Paper V,** which showed that glucose release from individual glucose-loaded liposome could be temporally resolved on the sub-millisecond timescale.

After creating an ultrafast sensor for glutamate, we utilized our new technology to address another challenge in neurochemistry regarding quantification of rapid glutamate fluctuations. In **Paper V**, the ultrafast glutamate sensor (**Paper III**) was utilized to establish a new method for quantification of glutamate in single synaptic vesicles. This method was based on the placement of the glutamate sensor in a solution of either isolated synaptic vesicles or glutamate-loaded LUVs and by applying a negative potential to the sensor surface,

vesicles in contact with the sensor surface randomly were triggered to burst and release their glutamate content onto the electrode surface upon rupture. Here the vesicle quantal content of glutamate was detected by the sensor. These measures were then related to a calibration curve that was generated from monitoring the charge detected from the glutamate released by LUVs pre-filled with different concentrations of glutamate. This calibration was then also used to determine the amount of vesicular content in isolated synaptic vesicles and the amount of vesicular glutamate released at different categories of single exocytotic release events in rodent brain slice.

# 7. Future Outlook

The brain is the most complex organ in human body and together with the central nervous system. It regulates most of the body activities, such as speech, emotion, cognition, motion and senses of smell, hearing, vision and taste. To deeper understand the brain function and malfunction especially in neurologic diseases, further development of advanced analytical tools is really needed and is of great importance for clinical diagnosis and medical treatment. The development of novel enzyme-based ultrafast electrochemical biosensors in our group allows for the real-time detection of vesicular release of non-electroactive neurotransmitters glutamate and acetylcholine during exocytotic events in neuronal communication using amperometry, which previously was limited to electroactive neurotransmitters (e.g. dopamine) detection only.

The real-time *ex vivo* measurements of single glutamate vesicular releases in rodent brain slices was achieved in **Paper III**, which showed a variety of current shape spikes with various quantal release that indicates more than one type of mechanism are involved, and the relative occurrence and magnitude of amperometric spikes were very similar on both types of rodent recordings. To deepen the understanding of the exocytosis mechanisms behind these categorized events and what they mean, more work is needed, the collected amperometric data need to be further characterized and connected to what mechanisms are behind altering the dynamic of spikes and the quantal release. In addition, the release patterns identified not only need to be better understood, but also find how alterations of these might correlate to neuronal activity and disease. Moreover, for gaining better knowledge of brain related diseases and behavior with neurologic pathways with glutamate, the ultrafast biosensor schemes developed in our group provide great promise for application to *in vivo* measurements using living animal models such as rodents to study glutamate activity coupled to behavior. Although the damage on biological tissue caused by our ultra-small sensors that were constructed by biocompatible materials is negligible, to eliminate the low possibilities of tissue damage and immune response, the size of sensor surface can be further reduced.

To ensure and enhance the stability and sensitivity of enzyme-based biosensor for *in vivo* or *ex vivo* measurements, it is of importance to maximize the activity of immobilized enzyme and that the enzymes are well protected during long periods of measurement. Herein, we are interested in exploring different strategies to modify the sensor surface to physically protect the immobilized enzymes at the sensor surface before the insertion process and measurement in tissue, where some of key findings we would like to implement relate to our studies in **Paper IV**. Here, both physical and chemical protection strategies for the sensor electrode surface can be explored, where we can combine our expertise in nanomaterial science, surface chemistry and analytical chemistry to find new solutions and create robust and reliable *in vivo* sensor probes.

As we know, neurotransmitters and related chemical compounds are deeply involved in various neuronal pathways in the brain, and many are strongly correlated with the neurological diseases and disorders. The needs for early diagnosis via real-time monitoring device as implant in the brain are an interesting thought. Because the sensors developed in this thesis are made of electrodes that have the ability also for multi-analyte detection with ultrahigh temporal and spatial resolution, these sensors have great potential to be integrated into future brain microchip as a multi-sensing array to perform brain or mind reading with efficient feedback in real-time to computers or mobile phones. In addition，this device can also be exploited with other functions like monitoring the general health, such as combining daily read-out of physiological compounds that are electroactive and blood sugar fluctuations through-out the days.

# 8. Acknowledgement

I would like to take this opportunity to express my sincere thanks to all of you that has been there for me offering your warmly help and continuous support during my PhD time.

Firstly, there are not enough words to express my sincere gratitude to my supervisor **Ann-Sofie**. Ann-Sofie, you provided me with the opportunity to join your team and to dive into the world of scientific research. To finish the almost 5 years of work and writing of this thesis, you have supported me with all the support I needed, by sharing your motivation, immense knowledge and provided patient guidance. Besides, the rock'n'roll tutorials in Hard Rock with the wonderful salad are one of the best moments for me during the last five years. Moreover, thank you so much for taking care of me, made sure I visited medical doctors when I needed to, and took me to hospital in person when I had fever with infection. Thank you so much Ann-Sofie! You hold me all the way to achieve here.

Besides, I would like to thank my co-supervisor **Björn**. Thank you so much for looking after me and provided me with encouragement and guidance during the last five years. It is not forgettable that you took me to hospital and stayed with me at the hospital when the emergency took place. Many thanks for day and night working on providing feedback on my thesis with insightful and funny comments, even when travelling. You are always there when I have difficulties and help me solve any problems.

My sincere thanks also go to my co-supervisor **Tanya**. Thank you so much for taking care of me no matter where we are. Thanks a lot for the support in the lab and for all feedback on my thesis writing, even when you had a large pile of tasks to do.

To my co-supervisor **Aldo**, thank you so much for passing on all of your valuable and practical knowledge and your great experience in the lab. I really appreciated your support when I felt extremely down and needed support the most. Thank you!

I would like to thank **Jerker**. I could not express more of my appreciation for your great support and guidance in overcoming the numerous of obstacles I have been facing through my entire last five years of PhD studies. Thank you so much!

My sincere appreciation goes to **Nina Kann** as well. You bring warmth and light to everyone around. Thank you so much for helping me solve problems one by one these years. Your support means a lot to me.

To **Per Lincoln**, I appreciate very much your great support and on going attention to my PhD studies, especially in the final stage that was extremely crucial for finalizing all tasks. Thank you!

Thank you **Bosse** for being my examiner, your support and running all the big events for me!

A very special gratitude goes to **Maria**, who provided me with moral and emotional support these last five years especially at the moment when I was close to collapse, your encouragement and guidance cheered me up and helped me get back to research life and with faith again! And thanks a lot for providing lab instrument support!

To my dear collaborators, **Jackie, Joakim, Jenny, Hoda, Devesh, Karolina, Thomas, Hampus and Rima**, thank you for the sleepless nights that we were working together to push out the work, for inspiring and stimulating brainstorming discussions, and for all the fun and stories we have had. Without your precious support, it would not be possible to accomplish all the research work the last five years.

I also would like to thank **everyone** who ever offered me support in the lab with instrument guidance, problem solving and answering many questions.

In particular, thank you **Lulu** for enlightening my research work when I was suffering from lab experiments for a half year without any outcomes. Thank you for patient listening and guidance along the way these years.

I would like to thank **Sandra** in special. I could not remember how many times I have come to you and asked millions of questions about science, I always get detailed and excellent answers, and you provide patient support and guidance. Thank you so much for all the help!

I am also grateful to all my dear colleagues that I have run across the past 5 years from analytical and physical chemistry, biological physics and the MC2 team that made my days more enjoyable and fun, by sharing knowledge and good times. The list of all your names would be a very long one- thank you all!

**Gunilla**, **Anna** and **Lotta**, thank you so much for all the support and help with the administration these last five years. **Sara**, you are always so nice and supportive to everyone and help me get the stuff that I need as fast as possible. **Lynga**, you are an amazing girl with talents in organization. I appreciate very much your effort in supporting our teaching.

**Marcel**, **Catherine** and **Richard**, thank you so much for being my “body guards” to ensure my well-being and health, which allow me to face all the challenges.

My external cheerleader, **Aline**, you are always there to back me up without leaving me alone these years, although I was always occupied by different things and could not contribute enough time and energy to our friendship. Thank you so much for understanding me. I miss your enthusiastic encouragement ‘Momo, Momo…… Momo, finish your PhD study……’.

Thank you **Mikael** and **Bernt** for supporting me and treating me as a family member during the toughest time of my PhD study.

Finally, I must express my profound gratitude to my life-coach, **Mom**, for cheering me up with continuous encouragement and unfailing support throughout my entire life. I could not image to accomplish this big task without you. Thank you Mom!

妈妈，谢谢您一直以来的支持与陪伴， 聆听与教导， 信任与尊重！

# 9. References


(1) Herculano-Houzel, S. The Human Brain in Numbers: A Linearly Scaled-up Primate Brain. *Front. Hum. Neurosci.* **2009**, *3*, 31.

(2) Azevedo, F. A. C.; Carvalho, L. R. B.; Grinberg, L. T.; Farfel, J. M.; Ferretti, R. E. L.; Leite, R. E. P.; Filho, W. J.; Lent, R.; Herculano-Houzel, S. Equal Numbers of Neuronal and Nonneuronal Cells Make the Human Brain an Isometrically Scaled-up Primate Brain. *J. Comp. Neurol.* **2009**, *513* (5), 532–541.

(3) Oishi, Y.; Xu, Q.; Wang, L.; Zhang, B.-J.; Takahashi, K.; Takata, Y.; Luo, Y.-J.; Cherasse, Y.; Schiffmann, S. N.; de Kerchove d'Exaerde, A.; et al. Slow-Wave Sleep Is Controlled by a Subset of Nucleus Accumbens Core Neurons in Mice. *Nat. Commun.* **2017**, *8* (1), 734.

(4) Shirayama, Y.; Chaki, S. Neurochemistry of the Nucleus Accumbens and Its Relevance to Depression and Antidepressant Action in Rodents. *Curr. Neuropharmacol.* **2006**, *4* (4), 277–291.

(5) *Neuroscience*, 3rd ed.; Purves, D., Augustine, G. J., Fitzpatrick, D., Hall, W. C., Lamantia, A.-S., Mcnamara, J. O., Willians, S. M., Eds.; Sinauer Associates, Inc: Sunderland, Massachusetts U.S.A., 2004.

(6) Glickstein, M. *Neuroscience : A Historical Introduction*; The MIT Press: Cambridge, UNITED STATES, 2014.

(7) Moore, K. L.; Dalley, A. F.; Agur, A. M. R. *Clinically Oriented Anatomy*, 6th ed.; Taylor, C., Heise, J., Montalbano, J., Eds.; Philadelphia Wolters Kluwer/Lippincott Williams & Wilkins: Baltimore, U.S.A., 2010.

(8) Pannese, E. III. Shape and Size of Neurons. In *Neurocytology*; Springer International Publishing: Cham, Switzerland, 2015; pp 13–23.

(9) Haug, H. Die Gestalt Des Neurons Aus Der Sicht Quantitativer Untersuchungen (Referat). *Verh. Anat. Ges.* **1982**, *76*, 73–80.

(10) Overview of Neuron Structure and Function https://www.khanacademy.org/science/biology/human-biology/neuron-nervous-system/a/overview-of-neuron-structure-and-function.

(11) *Principles of Neural Science*, 4th ed.; Eric R. Kandel, James Schwartz, T. J., Ed.; McGraw Hill Companies: New York City, New York, 2000.

(12) Newman, E. A. New Roles for Astrocytes: Regulation of Synaptic Transmission. *Trends Neurosci.* **2003**, *26* (10), 536–542.

(13) Fiacco, T. A.; Agulhon, C.; McCarthy, K. D. Sorting Out Astrocyte Physiology from Pharmacology. *Annu. Rev. Pharmacol. Toxicol.* **2009**, *49* (1), 151–174.

(14) Verkhratsky, A.; Butt, A. Neuroglia: Definition, Classification, Evolution, Numbers, Development. In *Glial Physiology and Pathophysiology*; John Wiley & Sons, Ltd: Chichester, UK, 2013; pp 73–104.

(15) Çakır, T.; Alsan, S.; Saybaşılı, H.; Akın, A.; Ülgen, K. Ö. Reconstruction and Flux Analysis of Coupling between Metabolic Pathways of Astrocytes and Neurons: Application to Cerebral Hypoxia. *Theor. Biol. Med. Model.* **2007**, *4* (1), 48.

(16) Bruce Alberts, Alexander D. Johnson, Julian Lewis, David Morgan, Martin Raff, Keith Roberts, P. W. *Molecular Biology of the Cell*, 6th ed.; Garland Science, Ed.; Taylor and Francis Group: New York, NY, 2014.

(17) Lewis, R.; Asplin, K. E.; Bruce, G.; Dart, C.; Mobasheri, A.; Barrett-Jolley, R. The Role of the Membrane Potential in Chondrocyte Volume Regulation. *J. Cell. Physiol.* **2011**, *226* (11), 2979–2986.

(18) Steinbach, H. B.; Spiegelman, S. The Sodium and Potassium Balance in Squid Nerve Axoplasm. *J. Cell. Comp. Physiol.* **1943**, *22* (2), 187–196.
(19) HODGKIN, A. L. THE IONIC BASIS OF ELECTRICAL ACTIVITY IN NERVE AND MUSCLE. *Biol. Rev.* **1951**, *26* (4), 339–409.
(20) Drachman, D. A. Do We Have Brain to Spare? *Neurology* **2005**, *64* (12), 2004–2005.
(21) Hormuzdi, S. G.; Filippov, M. A.; Mitropoulou, G.; Monyer, H.; Bruzzone, R. Electrical Synapses: A Dynamic Signaling System That Shapes the Activity of Neuronal Networks. *Biochim. Biophys. Acta - Biomembr.* **2004**, *1662* (1–2), 113–137.
(22) Bennett, M. V. .; Zukin, R. S. Electrical Coupling and Neuronal Synchronization in the Mammalian Brain. *Neuron* **2004**, *41* (4), 495–511.
(23) Bello, O. D.; Jouannot, O.; Chaudhuri, A.; Stroeva, E.; Coleman, J.; Volynski, K. E.; Rothman, J. E.; Krishnakumar, S. S. Synaptotagmin Oligomerization Is Essential for Calcium Control of Regulated Exocytosis. *Proc. Natl. Acad. Sci.* **2018**, *115* (32), E7624–E7631.
(24) Südhof, T. C. Neurotransmitter Release: The Last Millisecond in the Life of a Synaptic Vesicle. *Neuron* **2013**, *80* (3), 675–690.
(25) Van Liefferinge, J.; Massie, A.; Portelli, J.; Di Giovanni, G.; Smolders, I. Are Vesicular Neurotransmitter Transporters Potential Treatment Targets for Temporal Lobe Epilepsy? *Front. Cell. Neurosci.* **2013**, *7*.
(26) Gasnier, B. The Loading of Neurotransmitters into Synaptic Vesicles. *Biochimie* **2000**, *82* (4), 327–337.
(27) Hua, Y.; Scheller, R. H. Three SNARE Complexes Cooperate to Mediate Membrane Fusion. *Proc. Natl. Acad. Sci.* **2001**, *98* (14), 8065–8070.
(28) Hanson, P. I.; Roth, R.; Morisaki, H.; Jahn, R.; Heuser, J. E. Structure and Conformational Changes in NSF and Its Membrane Receptor Complexes Visualized by Quick-Freeze/Deep-Etch Electron Microscopy. *Cell* **1997**, *90* (3), 523–535.
(29) Weber, T.; Zemelman, B. V; McNew, J. A.; Westermann, B.; Gmachl, M.; Parlati, F.; Söllner, T. H.; Rothman, J. E. SNAREpins: Minimal Machinery for Membrane Fusion. *Cell* **1998**, *92* (6), 759–772.
(30) Jahn, R.; Lang, T.; Südhof, T. C. Membrane Fusion. *Cell* **2003**, *112* (4), 519–533.
(31) Borisovska, M.; Zhao, Y.; Tsytsyura, Y.; Glyvuk, N.; Takamori, S.; Matti, U.; Rettig, J.; Südhof, T.; Bruns, D. V-SNAREs Control Exocytosis of Vesicles from Priming to Fusion. *EMBO J.* **2005**, *24* (12), 2114–2126.
(32) Sutton, R. B.; Fasshauer, D.; Jahn, R.; Brunger, A. T. Crystal Structure of a SNARE Complex Involved in Synaptic Exocytosis at 2.4 Å Resolution. *Nature* **1998**, *395* (6700), 347–353.
(33) Hayashi, T.; McMahon, H.; Yamasaki, S.; Binz, T.; Hata, Y.; Südhof, T. C.; Niemann, H. Synaptic Vesicle Membrane Fusion Complex: Action of Clostridial Neurotoxins on Assembly. *EMBO J.* **1994**, *13* (21), 5051–5061.
(34) Südhof, T. C. A Molecular Machine for Neurotransmitter Release: Synaptotagmin and Beyond. *Nat. Med.* **2013**, *19* (10), 1227–1231.
(35) Chapman, E. R. Synaptotagmin: A $Ca^{2+}$ Sensor That Triggers Exocytosis? *Nat. Rev. Mol. Cell Biol.* **2002**, *3* (7), 498–508.
(36) Sudhof, T. C.; Rothman, J. E. Membrane Fusion: Grappling with SNARE and SM Proteins. *Science (80-. ).* **2009**, *323* (5913), 474–477.
(37) Zhou, Q.; Zhou, P.; Wang, A. L.; Wu, D.; Zhao, M.; Südhof, T. C.; Brunger, A. T. The Primed SNARE–Complexin–Synaptotagmin Complex for Neuronal Exocytosis. *Nature*

**2017**, *548* (7668), 420–425.
(38) del Castillo, J.; Katz, B. Quantal Components of the End-Plate Potential. *J. Physiol.* **1954**, *124* (3), 560–573.
(39) del Castillo, J.; Katz, B. Local Activity at a Depolarized Nerve-Muscle Junction. *J. Physiol.* **1955**, *128* (2), 396–411.
(40) del Castillo, J.; Katz, B. Biophysical Aspects of Neuro-Muscular Transmission. *Prog. Biophys. Biophys. Chem.* **1956**, *6*, 121–170.
(41) Ceccarelli, B. DEPLETION OF VESICLES FROM FROG NEUROMUSCULAR JUNCTIONS BY PROLONGED TETANIC STIMULATION. *J. Cell Biol.* **1972**, *54* (1), 30–38.
(42) Ceccarelli, B. TURNOVER OF TRANSMITTER AND SYNAPTIC VESICLES AT THE FROG NEUROMUSCULAR JUNCTION. *J. Cell Biol.* **1973**, *57* (2), 499–524.
(43) Heuser, J. E. EVIDENCE FOR RECYCLING OF SYNAPTIC VESICLE MEMBRANE DURING TRANSMITTER RELEASE AT THE FROG NEUROMUSCULAR JUNCTION. *J. Cell Biol.* **1973**, *57* (2), 315–344.
(44) Heuser, J. E.; Reese, T. S.; Landis, D. M. D. Functional Changes in Frog Neuromuscular Junctions Studied with Freeze-Fracture. *J. Neurocytol.* **1974**, *3* (1), 109–131.
(45) Heuser, J. E. Synaptic Vesicle Exocytosis Captured by Quick Freezing and Correlated with Quantal Transmitter Release. *J. Cell Biol.* **1979**, *81* (2), 275–300.
(46) Miller, T. M. Endocytosis of Synaptic Vesicle Membrane at the Frog Neuromuscular Junction. *J. Cell Biol.* **1984**, *98* (2), 685–698.
(47) Cremona, O.; De Camilli, P. Synaptic Vesicle Endocytosis. *Curr. Opin. Neurobiol.* **1997**, *7* (3), 323–330.
(48) Ceccarelli, B.; Grohovaz, F.; Hurlbut, W. P. Freeze-Fracture Studies of Frog Neuromuscular Junctions during Intense Release of Neurotransmitter. II. Effects of Electrical Stimulation and High Potassium. *J. Cell Biol.* **1979**, *81* (1), 178–192.
(49) Torri-Tarelli, F.; Grohovaz, F.; Fesce, R.; Ceccarelli, B. Temporal Coincidence between Synaptic Vesicle Fusion and Quantal Secretion of Acetylcholine. *J. Cell Biol.* **1985**, *101* (4), 1386 LP – 1399.
(50) Torri-Tarelli, F.; Haimann, C.; Ceccarelli, B. Coated Vesicles and Pits during Enhanced Quantal Release of Acetylcholine at the Neuromuscular Junction. *J. Neurocytol.* **1987**, *16* (2), 205–214.
(51) Valtorta, F.; Jahn, R.; Fesce, R.; Greengard, P.; Ceccarelli, B. Synaptophysin (P38) at the Frog Neuromuscular Junction: Its Incorporation into the Axolemma and Recycling after Intense Quantal Secretion. *J. Cell Biol.* **1988**, *107* (6), 2717 LP – 2727.
(52) Torri-Tarelli, F.; Villa, A.; Valtorta, F.; De Camilli, P.; Greengard, P.; Ceccarelli, B. Redistribution of Synaptophysin and Synapsin I during Alpha-Latrotoxin-Induced Release of Neurotransmitter at the Neuromuscular Junction. *J. Cell Biol.* **1990**, *110* (2), 449 LP – 459.
(53) Tarelli, F. T.; Bossi, M.; Fesce, R.; Greengard, P.; Valtorta, F. Synapsin I Partially Dissociates from Synaptic Vesicles during Exocytosis Induced by Electrical Stimulation. *Neuron* **1992**, *9* (6), 1143–1153.
(54) Valtorta, F.; Meldolesi, J.; Fesce, R. Synaptic Vesicles: Is Kissing a Matter of Competence? *Trends Cell Biol.* **2001**, *11* (8), 324–328.
(55) Fesce, R.; Grohovaz, F.; Valtorta, F.; Meldolesi, J. Neurotransmitter Release: Fusion or 'Kiss-and-Run'? *Trends Cell Biol.* **1994**, *4* (1), 1–4.
(56) Chow, R. H.; von Rüden, L.; Neher, E. Delay in Vesicle Fusion Revealed by Electrochemical Monitoring of Single Secretory Events in Adrenal Chromaffin Cells.

*Nature* **1992**, *356* (6364), 60–63.
(57) de Toledo, G. A.; Fernández-Chacón, R.; Fernández, J. M. Release of Secretory Products during Transient Vesicle Fusion. *Nature* **1993**, *363* (6429), 554–558.
(58) Staal, R. G. W.; Mosharov, E. V.; Sulzer, D. Dopamine Neurons Release Transmitter via a Flickering Fusion Pore. *Nat. Neurosci.* **2004**, *7* (4), 341–346.
(59) Takei, K. The Synaptic Vesicle Cycle: A Single Vesicle Budding Step Involving Clathrin and Dynamin. *J. Cell Biol.* **1996**, *133* (6), 1237–1250.
(60) Gandhi, S. P.; Stevens, C. F. Three Modes of Synaptic Vesicular Recycling Revealed by Single-Vesicle Imaging. *Nature* **2003**, *423* (6940), 607–613.
(61) Wu, X.-S.; Xue, L.; Mohan, R.; Paradiso, K.; Gillis, K. D.; Wu, L.-G. The Origin of Quantal Size Variation: Vesicular Glutamate Concentration Plays a Significant Role. *J. Neurosci.* **2007**, *27* (11), 3046–3056.
(62) Aravanis, A. M.; Pyle, J. L.; Tsien, R. W. Single Synaptic Vesicles Fusing Transiently and Successively without Loss of Identity. *Nature* **2003**, *423* (6940), 643–647.
(63) Keighron, J. D.; Wigström, J.; Kurczy, M. E.; Bergman, J.; Wang, Y.; Cans, A.-S. Amperometric Detection of Single Vesicle Acetylcholine Release Events from an Artificial Cell. *ACS Chem. Neurosci.* **2015**, *6* (1), 181–188.
(64) Wang, Y.; Mishra, D.; Bergman, J.; Keighron, J. D.; Skibicka, K. P.; Cans, A.-S. Ultrafast Glutamate Biosensor Recordings in Brain Slices Reveal Complex Single Exocytosis Transients. *ACS Chem. Neurosci.* **2019**, *10* (3), 1744–1752.
(65) Majdi, S.; Berglund, E. C.; Dunevall, J.; Oleinick, A. I.; Amatore, C.; Krantz, D.; Ewing, A. G. Electrochemical Measurements of Optogenetically Stimulated Quantal Amine Release from Single Nerve Cell Varicosities in Drosophila Larvae. *Angew. Chem. Int. Ed. Engl.* **2015**, *54* (46), 13609–13612.
(66) Takamori, S.; Holt, M.; Stenius, K.; Lemke, E. A.; Grønborg, M.; Riedel, D.; Urlaub, H.; Schenck, S.; Brügger, B.; Ringler, P.; et al. Molecular Anatomy of a Trafficking Organelle. *Cell* **2006**, *127* (4), 831–846.
(67) Budzinski, K. L.; Allen, R. W.; Fujimoto, B. S.; Kensel-Hammes, P.; Belnap, D. M.; Bajjalieh, S. M.; Chiu, D. T. Large Structural Change in Isolated Synaptic Vesicles upon Loading with Neurotransmitter. *Biophys. J.* **2009**, *97* (9), 2577–2584.
(68) Benfenati, F. Electrostatic and Hydrophobic Interactions of Synapsin I and Synapsin I Fragments with Phospholipid Bilayers. *J. Cell Biol.* **1989**, *108* (5), 1851–1862.
(69) Masson, J.; Sagné, C.; Hamon, M.; El Mestikawy, S. Neurotransmitter Transporters in the Central Nervous System. *Pharmacol. Rev.* **1999**, *51* (3), 439–464.
(70) *Principles of Neural Science*, 4th ed.; Kandel, E. R., Schwartz, J. H., Thomas M Jessell, Eds.; McGraw-Hill: New York, 2000.
(71) Khalil, O. S. Noninvasive Photonic-Crystal Material for Sensing Glucose in Tears. *Clin. Chem.* **2004**, *50* (12), 2236 LP – 2237.
(72) FULDNER, H. H.; STADLER, H. 31P-NMR Analysis of Synaptic Vesicles. Status of ATP and Internal PH. *Eur. J. Biochem.* **1982**, *121* (3), 519–524.
(73) Ahdut-Hacohen, R.; Duridanova, D.; Meiri, H.; Rahamimoff, R. Hydrogen Ions Control Synaptic Vesicle Ion Channel Activity in Torpedo Electromotor Neurones. *J. Physiol.* **2004**, *556* (2), 347–352.
(74) Fei, H.; Grygoruk, A.; Brooks, E. S.; Chen, A.; Krantz, D. E. Trafficking of Vesicular Neurotransmitter Transporters. *Traffic* **2008**, *9* (9), 1425–1436.
(75) Eiden, L. E.; Schäfer, M. K.-H.; Weihe, E.; Schütz, B. The Vesicular Amine Transporter Family (SLC18): Amine/Proton Antiporters Required for Vesicular Accumulation and

Regulated Exocytotic Secretion of Monoamines and Acetylcholine. *Pflügers Arch. Eur. J. Physiol.* **2004**, *447* (5), 636–640.
(76) Gasnier, B. The SLC32 Transporter, a Key Protein for the Synaptic Release of Inhibitory Amino Acids. *Pflügers Arch. Eur. J. Physiol.* **2004**, *447* (5), 756–759.
(77) Reimer, R. J.; Edwards, R. H. Organic Anion Transport Is the Primary Function of the SLC17/Type I Phosphate Transporter Family. *Pflügers Arch. Eur. J. Physiol.* **2004**, *447* (5), 629–635.
(78) Bally, M.; Bailey, K.; Sugihara, K.; Grieshaber, D.; Vörös, J.; Städler, B. Liposome and Lipid Bilayer Arrays Towards Biosensing Applications. *Small* **2010**, *6* (22), 2481–2497.
(79) Simonsson, L.; Kurczy, M. E.; Trouillon, R.; Hook, F.; Cans, A.-S. A Functioning Artificial Secretory Cell. *Sci. Rep.* **2012**, *2* (1), 824.
(80) Kuhar, M. J.; Minneman, K.; Muly, E. C. Catecholamines. In *Basic Neurochemistry MOLECULAR, CELLULAR AND MEDICAL ASPECTS*; Siegel, G. J., Albers, R. W., Brady, S. T., Price, D. L., Eds.; Elsevier Academic Press: San Diego, 2006; pp 211–225.
(81) Eisenhofer, G.; Rosano, T.; Whitley, R. J. Catecholamines and Serotonin. In *Tietz Fundamentals of Clinical Chemistry and Molecular Diagnostics*; Rifai, N., Horvath, A. R., Wittwer, C. T., Eds.; Elsevier Health Sciences: St. Louis, 2019; p 1088.
(82) Harris, R. C.; Zhang, M.-Z. Dopamine, the Kidney, and Hypertension. *Curr. Hypertens. Rep.* **2012**, *14* (2), 138–143.
(83) Chamberlain, S. R.; Robbins, T. W. Noradrenergic Modulation of Cognition: Therapeutic Implications. *J. Psychopharmacol.* **2013**, *27* (8), 694–718.
(84) Sara, S. J. The Locus Coeruleus and Noradrenergic Modulation of Cognition. *Nat. Rev. Neurosci.* **2009**, *10* (3), 211–223.
(85) Nathan Herrmann, Krista L. Lanctôt, and L. R. K. The Role of Norepinephrine in the Behavioral and Psychological Symptoms of Dementia. *J. Neuropsychiatry Clin. Neurosci.* **2004**, *16* (3), 261–276.
(86) Maletic, V.; Eramo, A.; Gwin, K.; Offord, S. J.; Duffy, R. A. The Role of Norepinephrine and Its α-Adrenergic Receptors in the Pathophysiology and Treatment of Major Depressive Disorder and Schizophrenia: A Systematic Review. *Front. psychiatry* **2017**, *8*, 42.
(87) Moret, C.; Briley, M. The Importance of Norepinephrine in Depression. *Neuropsychiatr. Dis. Treat.* **2011**, *7* (Suppl 1), 9–13.
(88) Khurana, I. ENDOCRINAL SYSTEM. In *Essentials of Medical Physiology*; Pathak, R., Nasim, S., Eds.; Elsevier India, 2008; p 460.
(89) Goldstein, D. S. Adrenal Responses to Stress. *Cell. Mol. Neurobiol.* **2010**, *30* (8), 1433–1440.
(90) Callaway, C. W. Epinephrine for Cardiac Arrest. *Curr. Opin. Cardiol.* **2013**, *28* (1), 36–42.
(91) Kemp, S. F.; Lockey, R. F.; Simons, F. E. R. Epinephrine: The Drug of Choice for Anaphylaxis. A Statement of the World Allergy Organization. *Allergy* **2008**, *63* (8), 1061–1070.
(92) Smith, D.; Riel, J.; Tilles, I.; Kino, R.; Lis, J.; Hoffman, J. R. Intravenous Epinephrine in Life-Threatening Asthma. *Ann. Emerg. Med.* **2003**, *41* (5), 706–711.
(93) Eglen, R. M. Muscarinic Receptor Subtypes in Neuronal and Non-Neuronal Cholinergic Function. *Auton. Autacoid Pharmacol.* **2006**, *26* (3), 219–233.
(94) Hurst, R.; Rollema, H.; Bertrand, D. Nicotinic Acetylcholine Receptors: From Basic Science to Therapeutics. *Pharmacol. Ther.* **2013**, *137* (1), 22–54.
(95) Kuo, I. Y.; Ehrlich, B. E. Signaling in Muscle Contraction. *Cold Spring Harb. Perspect.*

*Biol.* **2015**, *7* (2), a006023.
(96) Tiwari, P.; Dwivedi, S.; Singh, M. P.; Mishra, R.; Chandy, A. Basic and Modern Concepts on Cholinergic Receptor: A Review. *Asian Pacific J. Trop. Dis.* **2013**, *3* (5), 413–420.
(97) Hasselmo, M. E. The Role of Acetylcholine in Learning and Memory. *Curr. Opin. Neurobiol.* **2006**, *16* (6), 710–715.
(98) Dingledine, R.; McBain, C. J. Glutamate and Aspartate Are the Major Excitatory Transmitters in the Brain. In *Basic Neurochemistry: Molecular, Cellular and Medical Aspects*; Siegel, G. J., Agranoff, B. W., Albers, R. W., Fisher, S. K., Uhler, M. D., Eds.; Lippincott-Raven: Philadelphia, 1999.
(99) Meldrum, B. S. Glutamate as a Neurotransmitter in the Brain: Review of Physiology and Pathology. *J. Nutr.* **2000**, *130* (4), 1007S-1015S.
(100) McEntee, W. J.; Crook, T. H. Glutamate: Its Role in Learning, Memory, and the Aging Brain. *Psychopharmacology (Berl).* **1993**, *111* (4), 391–401.
(101) Daikhin, Y.; Yudkoff, M. Compartmentation of Brain Glutamate Metabolism in Neurons and Glia. *J. Nutr.* **2000**, *130* (4), 1026S-1031S.
(102) Weltin, A.; Kieninger, J.; Urban, G. A. Microfabricated, Amperometric, Enzyme-Based Biosensors for in Vivo Applications. *Anal. Bioanal. Chem.* **2016**, *408* (17), 4503–4521.
(103) Shigeri, Y.; Seal, R. P.; Shimamoto, K. Molecular Pharmacology of Glutamate Transporters, EAATs and VGLUTs. *Brain Res. Rev.* **2004**, *45* (3), 250–265.
(104) HYND, M. Glutamate-Mediated Excitotoxicity and Neurodegeneration in Alzheimer's Disease. *Neurochem. Int.* **2004**, *45* (5), 583–595.
(105) Shinohe, A.; Hashimoto, K.; Nakamura, K.; Tsujii, M.; Iwata, Y.; Tsuchiya, K. J.; Sekine, Y.; Suda, S.; Suzuki, K.; Sugihara, G.; et al. Increased Serum Levels of Glutamate in Adult Patients with Autism. *Prog. Neuro-Psychopharmacology Biol. Psychiatry* **2006**, *30* (8), 1472–1477.
(106) ROBERTS, E.; FRANKEL, S. Gamma-Aminobutyric Acid in Brain: Its Formation from Glutamic Acid. *J. Biol. Chem.* **1950**, *187* (1), 55–63.
(107) Udenfriend, S. IDENTIFICATION OF γ-AMINOBUTYRIC ACID IN BRAIN BY THE ISOTOPE DERIVATIVE METHOD. *J. Biol. Chem.* **1950**, No. 187, 65–69.
(108) Nuss, P. Anxiety Disorders and GABA Neurotransmission: A Disturbance of Modulation. *Neuropsychiatr. Dis. Treat.* **2015**, *11*, 165–175.
(109) Mathews, G. C. The Dual Roles of GABA in Seizures and Epilepsy Generate More Excitement. *Epilepsy Curr.* **2007**, *7* (1), 28–30.
(110) Snodgrass, S. R. GABA and Epilepsy: Their Complex Relationship and the Evolution of Our Understanding. *J. Child Neurol.* **1992**, *7* (1), 77–86.
(111) Ben-Ari, Y.; Gaiarsa, J.-L.; Tyzio, R.; Khazipov, R. GABA: A Pioneer Transmitter That Excites Immature Neurons and Generates Primitive Oscillations. *Physiol. Rev.* **2007**, *87* (4), 1215–1284.
(112) Attwell, D.; Laughlin, S. B. An Energy Budget for Signaling in the Grey Matter of the Brain. *J. Cereb. Blood Flow Metab.* **2001**, *21* (10), 1133–1145.
(113) Mergenthaler, P.; Lindauer, U.; Dienel, G. A.; Meisel, A. Sugar for the Brain: The Role of Glucose in Physiological and Pathological Brain Function. *Trends Neurosci.* **2013**, *36* (10), 587–597.
(114) McKenna, M. C.; Gruetter, R.; Sonnewald, U.; Waagepetersen, H. S.; Schousboe, A. Energy Metabolism of the Brain. In *Basic Neurochemistry MOLECULAR, CELLULAR AND MEDICAL ASPECTS*; Siegel, G. J., Albers, R. W., Brady, S. T., Price, D. L., Eds.; Elsevier Academic Press: San Diego, 2006; pp 531–557.

(115) Rosing, J.; Slater, E. C. The Value of ΔG° for the Hydrolysis of ATP. *Biochim. Biophys. Acta - Bioenerg.* **1972**, *267* (2), 275–290.
(116) Harvey, L.; Arnold, B.; S, L. Z.; Paul, M.; David, B.; James, D. *Molecular Cell Biology*, 4th ed.; W. H. Freeman: New York, 2000.
(117) Couteaux, R.; Pécot-Dechavassine, M. Synaptic Vesicles and Pouches at the Level of "Active Zones" of the Neuromuscular Junction. *C. R. Acad. Sci. Hebd. Seances Acad. Sci. D.* **1970**, *271* (25), 2346–2349.
(118) Heuser, J. E.; Reese, T. S.; Dennis, M. J.; Jan, Y.; Jan, L.; Evans, L. Synaptic Vesicle Exocytosis Captured by Quick Freezing and Correlated with Quantal Transmitter Release. *J. Cell Biol.* **1979**, *81* (2), 275–300.
(119) Heuser, J. E. Structural Changes after Transmitter Release at the Frog Neuromuscular Junction. *J. Cell Biol.* **1981**, *88* (3), 564–580.
(120) Suzuki, E. High-Resolution Scanning Electron Microscopy of Immunogold-Labelled Cells by the Use of Thin Plasma Coating of Osmium. *J. Microsc.* **2002**, *208* (3), 153–157.
(121) Hitachi High-Tech Launches the SU8000: a New Type of Scanning Electron Microscope https://www.hitachi-hightech.com/global/about/news/2008/nr20080723.html.
(122) Erni, R.; Rossell, M. D.; Kisielowski, C.; Dahmen, U. Atomic-Resolution Imaging with a Sub-50-Pm Electron Probe. *Phys. Rev. Lett.* **2009**, *102* (9), 096101.
(123) Betz, W.; Mao, F.; Bewick, G. Activity-Dependent Fluorescent Staining and Destaining of Living Vertebrate Motor Nerve Terminals. *J. Neurosci.* **1992**, *12* (2), 363–375.
(124) Betz, W.; Bewick, G. Optical Analysis of Synaptic Vesicle Recycling at the Frog Neuromuscular Junction. *Science (80-. ).* **1992**, *255* (5041), 200–203.
(125) Ryan, T. A.; Smith, S. J.; Reuter, H. The Timing of Synaptic Vesicle Endocytosis. *Proc. Natl. Acad. Sci.* **1996**, *93* (11), 5567–5571.
(126) Klingauf, J.; Kavalali, E. T.; Tsien, R. W. Kinetics and Regulation of Fast Endocytosis at Hippocampal Synapses. *Nature* **1998**, *394* (6693), 581–585.
(127) Gaffield, M. A.; Betz, W. J. Imaging Synaptic Vesicle Exocytosis and Endocytosis with FM Dyes. *Nat. Protoc.* **2006**, *1* (6), 2916–2921.
(128) Stevens, C. F.; Williams, J. H. "Kiss and Run" Exocytosis at Hippocampal Synapses. *Proc. Natl. Acad. Sci.* **2000**, *97* (23), 12828–12833.
(129) Fernández-Alfonso, T.; Ryan, T. A. The Kinetics of Synaptic Vesicle Pool Depletion at CNS Synaptic Terminals. *Neuron* **2004**, *41* (6), 943–953.
(130) Newton, J.; Murthy, V. Measuring Exocytosis in Neurons Using FM Labeling. *J. Vis. Exp.* **2006**, No. 1, 117.
(131) Shimomura, O.; Johnson, F. H.; Saiga, Y. Extraction, Purification and Properties of Aequorin, a Bioluminescent Protein from the Luminous Hydromedusan,Aequorea. *J. Cell. Comp. Physiol.* **1962**, *59* (3), 223–239.
(132) Anderson, R. G. W. A View of Acidic Intracellular Compartments. *J. Cell Biol.* **1988**, *106* (3), 539–543.
(133) Miesenböck, G.; De Angelis, D. A.; Rothman, J. E. Visualizing Secretion and Synaptic Transmission with PH-Sensitive Green Fluorescent Proteins. *Nature* **1998**, *394* (6689), 192–195.
(134) Granseth, B.; Odermatt, B.; Royle, S. J.; Lagnado, L. Clathrin-Mediated Endocytosis Is the Dominant Mechanism of Vesicle Retrieval at Hippocampal Synapses. *Neuron* **2006**, *51* (6), 773–786.
(135) Marvin, J. S.; Borghuis, B. G.; Tian, L.; Cichon, J.; Harnett, M. T.; Akerboom, J.; Gordus, A.; Renninger, S. L.; Chen, T.-W.; Bargmann, C. I.; et al. An Optimized Fluorescent

Probe for Visualizing Glutamate Neurotransmission. *Nat. Methods* **2013**, *10* (2), 162–170.
(136) Helassa, N.; Dürst, C. D.; Coates, C.; Kerruth, S.; Arif, U.; Schulze, C.; Wiegert, J. S.; Geeves, M.; Oertner, T. G.; Török, K. Ultrafast Glutamate Sensors Resolve High-Frequency Release at Schaffer Collateral Synapses. *Proc. Natl. Acad. Sci.* **2018**, *115* (21), 5594–5599.
(137) Zhang, Q.; Cao, Y.-Q.; Tsien, R. W. Quantum Dots Provide an Optical Signal Specific to Full Collapse Fusion of Synaptic Vesicles. *Proc. Natl. Acad. Sci.* **2007**, *104* (45), 17843–17848.
(138) Koenig, J. H. Synaptic Vesicles Have Two Distinct Recycling Pathways. *J. Cell Biol.* **1996**, *135* (3), 797–808.
(139) Jackson, M. B.; Chapman, E. R. FUSION PORES AND FUSION MACHINES IN CA 2+ - TRIGGERED EXOCYTOSIS. *Annu. Rev. Biophys. Biomol. Struct.* **2006**, *35* (1), 135–160.
(140) Budzinski, K. L.; Sgro, A. E.; Fujimoto, B. S.; Gadd, J. C.; Shuart, N. G.; Gonen, T.; Bajjaleih, S. M.; Chiu, D. T. Synaptosomes as a Platform for Loading Nanoparticles into Synaptic Vesicles. *ACS Chem. Neurosci.* **2011**, *2* (5), 236–241.
(141) Gubernator, N. G.; Zhang, H.; Staal, R. G. W.; Mosharov, E. V.; Pereira, D. B.; Yue, M.; Balsanek, V.; Vadola, P. A.; Mukherjee, B.; Edwards, R. H.; et al. Fluorescent False Neurotransmitters Visualize Dopamine Release from Individual Presynaptic Terminals. *Science (80-. ).* **2009**, *324* (5933), 1441–1444.
(142) Lee, M.; Gubernator, N. G.; Sulzer, D.; Sames, D. Development of PH-Responsive Fluorescent False Neurotransmitters. *J. Am. Chem. Soc.* **2010**, *132* (26), 8828–8830.
(143) Axelrod, D. Cell-Substrate Contacts Illuminated by Total Internal Reflection Fluorescence. *J. Cell Biol.* **1981**, *89* (1), 141–145.
(144) Steyer, J. A.; Horstmann, H.; Almers, W. Transport, Docking and Exocytosis of Single Secretory Granules in Live Chromaffin Cells. *Nature* **1997**, *388* (6641), 474–478.
(145) Oheim, M.; Loerke, D.; Stühmer, W.; Chow, R. H. The Last Few Milliseconds in the Life of a Secretory Granule. *Eur. Biophys. J.* **1998**, *27* (2), 83–98.
(146) Aoki, R.; Kitaguchi, T.; Oya, M.; Yanagihara, Y.; Sato, M.; Miyawaki, A.; Tsuboi, T. Duration of Fusion Pore Opening and the Amount of Hormone Released Are Regulated by Myosin II during Kiss-and-Run Exocytosis. *Biochem. J.* **2010**, *429* (3), 497–504.
(147) Mutch, S. A.; Kensel-Hammes, P.; Gadd, J. C.; Fujimoto, B. S.; Allen, R. W.; Schiro, P. G.; Lorenz, R. M.; Kuyper, C. L.; Kuo, J. S.; Bajjalieh, S. M.; et al. Protein Quantification at the Single Vesicle Level Reveals That a Subset of Synaptic Vesicle Proteins Are Trafficked with High Precision. *J. Neurosci.* **2011**, *31* (4), 1461–1470.
(148) NEHER, E.; SAKMANN, B. Single-Channel Currents Recorded from Membrane of Denervated Frog Muscle Fibres. *Nature* **1976**, *260* (5554), 799–802.
(149) Neher, E.; Sakmann, B.; Steinbach, J. H. The Extracellular Patch Clamp: A Method for Resolving Currents through Individual Open Channels in Biological Membranes. *Pflügers Arch. Eur. J. Physiol.* **1978**, *375* (2), 219–228.
(150) Neher, E.; Marty, A. Discrete Changes of Cell Membrane Capacitance Observed under Conditions of Enhanced Secretion in Bovine Adrenal Chromaffin Cells. *Proc. Natl. Acad. Sci.* **1982**, *79* (21), 6712–6716.
(151) Vandenbeuch, A.; Zorec, R.; Kinnamon, S. C. Capacitance Measurements of Regulated Exocytosis in Mouse Taste Cells. *J. Neurosci.* **2010**, *30* (44), 14695–14701.
(152) Heien, M. L. A. V.; Johnson, M. A.; Wightman, R. M. Resolving Neurotransmitters

Detected by Fast-Scan Cyclic Voltammetry. *Anal. Chem.* **2004**, *76* (19), 5697–5704.
(153) Petrovic, J.; Walsh, P. L.; Thornley, K. T.; Miller, C. E.; Wightman, R. M. Real-Time Monitoring of Chemical Transmission in Slices of the Murine Adrenal Gland. *Endocrinology* **2010**, *151* (4), 1773–1783.
(154) Engstrom, R. C.; Wightman, R. M.; Kristensen, E. W. Diffusional Distortion in the Monitoring of Dynamic Events. *Anal. Chem.* **1988**, *60* (7), 652–656.
(155) Wightman, R. M.; Jankowski, J. A.; Kennedy, R. T.; Kawagoe, K. T.; Schroeder, T. J.; Leszczyszyn, D. J.; Near, J. A.; Diliberto, E. J.; Viveros, O. H. Temporally Resolved Catecholamine Spikes Correspond to Single Vesicle Release from Individual Chromaffin Cells. *Proc. Natl. Acad. Sci.* **1991**, *88* (23), 10754–10758.
(156) Zhou, Z.; Misler, S.; Chow, R. H. Rapid Fluctuations in Transmitter Release from Single Vesicles in Bovine Adrenal Chromaffin Cells. *Biophys. J.* **1996**, *70* (3), 1543–1552.
(157) Mellander, L. J.; Trouillon, R.; Svensson, M. I.; Ewing, A. G. Amperometric Post Spike Feet Reveal Most Exocytosis Is via Extended Kiss-and-Run Fusion. *Sci. Rep.* **2012**, *2* (1), 907.
(158) Bergman, J. Development of Electrochemical Biosensors for Neurochemical Applications, University of Gothenburg, 2018.
(159) Hochstetler, S.; Wightman, R. Detection of Secretion with Electrochemical Methods. *On-Line Biophys. Textb.* **1998**, *1472* (919).
(160) Albillos, A.; Dernick, G.; Horstmann, H.; Almers, W.; Alvarez de Toledo, G.; Lindau, M. The Exocytotic Event in Chromaffin Cells Revealed by Patch Amperometry. *Nature* **1997**, *389* (6650), 509–512.
(161) Seeber, R.; Zanardi, C.; Inzelt, G. Links between Electrochemical Thermodynamics and Kinetics. *ChemTexts* **2015**, *1* (4), 18.
(162) Bard, A.; Faulkner, L. *Electrochemical Methods: Fundamentals and Applications*, 2nd ed.; Harris, D., Swain, E., Robey, C., Aiello, E., Eds.; John Wiley & Sons, Inc.: U.S.A., 2000.
(163) Shoup, D.; Szabo, A. Chronoamperometric Current at Finite Disk Electrodes. *J. Electroanal. Chem. Interfacial Electrochem.* **1982**, *140* (2), 237–245.
(164) Dzyadevych, S. V.; Arkhypova, V. N.; Soldatkin, A. P.; El'skaya, A. V.; Martelet, C.; Jaffrezic-Renault, N. Amperometric Enzyme Biosensors: Past, Present and Future. *IRBM* **2008**, *29* (2–3), 171–180.
(165) Prodromidis, M. I.; Karayannis, M. I. Enzyme Based Amperometric Biosensors for Food Analysis. *Electroanalysis* **2002**, *14* (4), 241–261.
(166) Clark, L. C.; Lyons, C. ELECTRODE SYSTEMS FOR CONTINUOUS MONITORING IN CARDIOVASCULAR SURGERY. *Ann. N. Y. Acad. Sci.* **1962**, *102* (1), 29–45.
(167) Verma, N.; Bhardwaj, A. Biosensor Technology for Pesticides—A Review. *Appl. Biochem. Biotechnol.* **2015**, *175* (6), 3093–3119.
(168) Tischer, W.; Wedekind, F. Immobilized Enzymes: Methods and Applications; 1999; pp 95–126.
(169) Wang, J. Electrochemical Glucose Biosensors. In *Electrochemical Sensors, Biosensors and their Biomedical Applications*; Zhang, X., Ju, H., Wang, J., Eds.; Academic Press, 2008; pp 57–69.
(170) Zhang, Y.; Hu, Y.; Wilson, G. S.; Moatti-Sirat, D.; Poitout, V.; Reach, G. Elimination of the Acetaminophen Interference in an Implantable Glucose Sensor. *Anal. Chem.* **1994**, *66* (7), 1183–1188.
(171) Nguyen, H. H.; Lee, S. H.; Lee, U. J.; Fermin, C. D.; Kim, M. Immobilized Enzymes in

Biosensor Applications. *Materials (Basel).* **2019**, *12* (1), 121.
(172) Khan, G. F.; Ohwa, M.; Wernet, W. Design of a Stable Charge Transfer Complex Electrode for a Third-Generation Amperometric Glucose Sensor. *Anal. Chem.* **1996**, *68* (17), 2939–2945.
(173) ZHANG, W.; LI, G. Third-Generation Biosensors Based on the Direct Electron Transfer of Proteins. *Anal. Sci.* **2004**, *20* (4), 603–609.
(174) Azevedo, A. M.; Martins, V. C.; Prazeres, D. M. F.; Vojinović, V.; Cabral, J. M. S.; Fonseca, L. P. Horseradish Peroxidase: A Valuable Tool in Biotechnology. In *Biotechnology Annual Review*; 2003; pp 199–247.
(175) Radzicka, A.; Wolfenden, R. A Proficient Enzyme. *Science (80-. ).* **1995**, *267* (5194), 90–93.
(176) Callahan, B. P.; Miller, B. G. OMP Decarboxylase—An Enigma Persists. *Bioorg. Chem.* **2007**, *35* (6), 465–469.
(177) Enzymes Are Powerful and Highly Specific Catalysts. In *Biochemistry*; Berg, J., John, T., Lubert, S., Eds.; W H Freeman: New York, 2002.
(178) Colovic, M. B.; Krstic, D. Z.; Lazarevic-Pasti, T. D.; Bondzic, A. M.; Vasic, V. M. Acetylcholinesterase Inhibitors: Pharmacology and Toxicology. *Curr. Neuropharmacol.* **2013**, *11* (3), 315–335.
(179) Quinn, D. M. Acetylcholinesterase: Enzyme Structure, Reaction Dynamics, and Virtual Transition States. *Chem. Rev.* **1987**, *87* (5), 955–979.
(180) Johnson, K. A.; Goody, R. S. The Original Michaelis Constant: Translation of the 1913 Michaelis–Menten Paper. *Biochemistry* **2011**, *50* (39), 8264–8269.
(181) Kim, J.; Grate, J. W.; Wang, P. Nanostructures for Enzyme Stabilization. *Chem. Eng. Sci.* **2006**, *61* (3), 1017–1026.
(182) Sassolas, A.; Blum, L. J.; Leca-Bouvier, B. D. Immobilization Strategies to Develop Enzymatic Biosensors. *Biotechnol. Adv.* **2012**, *30* (3), 489–511.
(183) Lin, J.; Brown, C. W. Sol-Gel Glass as a Matrix for Chemical and Biochemical Sensing. *TrAC Trends Anal. Chem.* **1997**, *16* (4), 200–211.
(184) Ichimura, K.; Watanabe, S. Preparation and Characteristics of Photocross-Linkable Poly(Vinyl Alcohol). *J. Polym. Sci. Polym. Chem. Ed.* **1982**, *20* (6), 1419–1432.
(185) Ichimura, K. A Convenient Photochemical Method to Immobilize Enzymes. *J. Polym. Sci. Polym. Chem. Ed.* **1984**, *22* (11), 2817–2828.
(186) Bruns, N.; Tiller, J. C. Amphiphilic Network as Nanoreactor for Enzymes in Organic Solvents. *Nano Lett.* **2005**, *5* (1), 45–48.
(187) Hanko, M.; Bruns, N.; Tiller, J. C.; Heinze, J. Optical Biochemical Sensor for Determining Hydroperoxides in Nonpolar Organic Liquids as Archetype for Sensors Consisting of Amphiphilic Conetworks as Immobilisation Matrices. *Anal. Bioanal. Chem.* **2006**, *386* (5), 1273–1283.
(188) Hernandez, K.; Fernandez-Lafuente, R. Control of Protein Immobilization: Coupling Immobilization and Site-Directed Mutagenesis to Improve Biocatalyst or Biosensor Performance. *Enzyme Microb. Technol.* **2011**, *48* (2), 107–122.
(189) D'Souza, S. F. Immobilized Enzymes in Bioprocess. *Curr. Sci.* **1999**, *77* (1), 69–79.
(190) Fu, J.; Reinhold, J.; Woodbury, N. W. Peptide-Modified Surfaces for Enzyme Immobilization. *PLoS One* **2011**, *6* (4), e18692.
(191) Zucca, P.; Sanjust, E. Inorganic Materials as Supports for Covalent Enzyme Immobilization: Methods and Mechanisms. *Molecules* **2014**, *19* (9), 14139–14194.
(192) Husain, Q. Nanomaterials as Novel Supports for the Immobilization of Amylolytic

Enzymes and Their Applications: A Review. *Biocatalysis* **2017**, *3* (1), 37–53.
(193) Lin, Z.; Ji, L.; Zhang, X. Electrodeposition of Platinum Nanoparticles onto Carbon Nanofibers for Electrocatalytic Oxidation of Methanol. *Mater. Lett.* **2009**, *63* (24–25), 2115–2118.
(194) Zhao, Z.; Gong, R.; Zheng, L.; Wang, J. In Vivo Neural Recording and Electrochemical Performance of Microelectrode Arrays Modified by Rough-Surfaced AuPt Alloy Nanoparticles with Nanoporosity. *Sensors* **2016**, *16* (11), 1851.
(195) Jain, R.; Sharma, S. Glassy Carbon Electrode Modified with Multi-Walled Carbon Nanotubes Sensor for the Quantification of Antihistamine Drug Pheniramine in Solubilized Systems. *J. Pharm. Anal.* **2012**, *2* (1), 56–61.
(196) Sardar, M.; Ahmad, R. Enzyme Immobilization: An Overview on Nanoparticles as Immobilization Matrix. *Biochem. Anal. Biochem.* **2015**, *04* (02), 178.
(197) Page Faulk, W.; Malcolm Taylor, G. Communication to the Editors: An Immunocolloid Method for the Electron Microscope. *Immunochemistry* **1971**, *8* (11), 1081–1083.
(198) Neagu, C.; van der Werf, K. O.; Putman, C. A. J.; Kraan, Y. M.; de Grooth, B. G.; van Hulst, N. F.; Greve, J. Analysis of Immunolabeled Cells by Atomic Force Microscopy, Optical Microscopy, and Flow Cytometry. *J. Struct. Biol.* **1994**, *112* (1), 32–40.
(199) Bailes, J.; Gazi, S.; Ivanova, R.; Soloviev, M. Effect of Gold Nanoparticle Conjugation on the Activity and Stability of Functional Proteins. In *Nanoparticles in Biology and Medicine*; Humana Press: Totowa, NJ, 2012; pp 89–99.
(200) Lv, M.; Zhu, E.; Su, Y.; Li, Q.; Li, W.; Zhao, Y.; Huang, Q. Trypsin-Gold Nanoparticle Conjugates: Binding, Enzymatic Activity, and Stability. *Prep. Biochem. Biotechnol.* **2009**, *39* (4), 429–438.
(201) Huang, Y.-F.; Huang, C.-C.; Chang, H.-T. Exploring the Activity and Specificity of Gold Nanoparticle-Bound Trypsin by Capillary Electrophoresis with Laser-Induced Fluorescence Detection. *Langmuir* **2003**, *19* (18), 7498–7502.
(202) Sun, J.; Xu, B.; Shi, Y.; Yang, L.; Ma, H. Activity and Stability of Trypsin Immobilized onto Chitosan Magnetic Nanoparticles. *Adv. Mater. Sci. Eng.* **2017**, *2017*, 1–10.
(203) Vertegel, A. A.; Siegel, R. W.; Dordick, J. S. Silica Nanoparticle Size Influences the Structure and Enzymatic Activity of Adsorbed Lysozyme. *Langmuir* **2004**, *20* (16), 6800–6807.
(204) Keighron, J. D.; Åkesson, S.; Cans, A.-S. Coimmobilization of Acetylcholinesterase and Choline Oxidase on Gold Nanoparticles: Stoichiometry, Activity, and Reaction Efficiency. *Langmuir* **2014**, *30* (38), 11348–11355.
(205) Kiricsi, I.; Fudala, Á.; Kónya, Z.; Hernádi, K.; Lentz, P.; Nagy, J. B. The Advantages of Ozone Treatment in the Preparation of Tubular Silica Structures. *Appl. Catal. A Gen.* **2000**, *203* (1), L1–L4.
(206) Mogilevsky, G.; Chen, Q.; Kleinhammes, A.; Wu, Y. The Structure of Multilayered Titania Nanotubes Based on Delaminated Anatase. *Chem. Phys. Lett.* **2008**, *460* (4–6), 517–520.
(207) Feldkamp, U.; Niemeyer, C. M. Rational Design of DNA Nanoarchitectures. *Angew. Chemie Int. Ed.* **2006**, *45* (12), 1856–1876.
(208) Anwar, M. Z.; Kim, D. J.; Kumar, A.; Patel, S. K. S.; Otari, S.; Mardina, P.; Jeong, J.-H.; Sohn, J.-H.; Kim, J. H.; Park, J. T.; et al. SnO2 Hollow Nanotubes: A Novel and Efficient Support Matrix for Enzyme Immobilization. *Sci. Rep.* **2017**, *7* (1), 15333.
(209) Hirsch, A. Funktionalisierung von Einwandigen Kohlenstoffnanoröhren. *Angew. Chemie* **2002**, *114* (11), 1933.

(210) Iijima, S. Carbon Nanotubes: Past, Present, and Future. *Phys. B Condens. Matter* **2002**, *323* (1–4), 1–5.
(211) Asuri, P.; Bale, S. S.; Karajanagi, S. S.; Kane, R. S. The Protein–Nanomaterial Interface. *Curr. Opin. Biotechnol.* **2006**, *17* (6), 562–568.
(212) Naghshbandi, M. P.; Moghimi, H.; Latif, B. Covalent Immobilization of Phytase on the Multi-Walled Carbon Nanotubes via Diimide-Activated Amidation: Structural and Stability Study. *Artif. Cells, Nanomedicine, Biotechnol.* **2018**, *46* (sup1), 763–772.
(213) LU, J.; ZHANG, X.; ZHAO, X. ELECTRONIC PROPERTIES OF HETEROFULLERENES C 59 X (X=Si, O AND Be). *Mod. Phys. Lett. B* **2000**, *14* (01), 23–29.
(214) Cohen, M. L. Nanotubes, Nanoscience, and Nanotechnology. *Mater. Sci. Eng. C* **2001**, *15* (1–2), 1–11.
(215) Baughman, R. H. Carbon Nanotubes--the Route Toward Applications. *Science (80-. ).* **2002**, *297* (5582), 787–792.
(216) Vashist, S. K.; Zheng, D.; Al-Rubeaan, K.; Luong, J. H. T.; Sheu, F.-S. Advances in Carbon Nanotube Based Electrochemical Sensors for Bioanalytical Applications. *Biotechnol. Adv.* **2011**, *29* (2), 169–188.
(217) Balasubramanian, K.; Burghard, M. Biosensors Based on Carbon Nanotubes. *Anal. Bioanal. Chem.* **2006**, *385* (3), 452–468.
(218) Britto, P. J.; Santhanam, K. S. V.; Ajayan, P. M. Carbon Nanotube Electrode for Oxidation of Dopamine. *Bioelectrochemistry Bioenerg.* **1996**, *41* (1), 121–125.
(219) Rubianes, M.; Rivas, G. Enzymatic Biosensors Based on Carbon Nanotubes Paste Electrodes. *Electroanalysis* **2005**, *17* (1), 73–78.
(220) Day, T. M.; Unwin, P. R.; Wilson, N. R.; Macpherson, J. V. Electrochemical Templating of Metal Nanoparticles and Nanowires on Single-Walled Carbon Nanotube Networks. *J. Am. Chem. Soc.* **2005**, *127* (30), 10639–10647.
(221) Liu, J.; Chou, A.; Rahmat, W.; Paddon-Row, M.; Gooding, J. ?Justi. Achieving Direct Electrical Connection to Glucose Oxidase Using Aligned Single Walled Carbon Nanotube Arrays. *Electroanalysis* **2005**, *17* (1), 38–46.
(222) Deng, W.; Bodart, P.; Pruski, M.; Shanks, B. H. Characterization of Mesoporous Alumina Molecular Sieves Synthesized by Nonionic Templating. *Microporous Mesoporous Mater.* **2002**, *52* (3), 169–177.
(223) Antonelli, D. M.; Ying, J. Y. Synthesis of Hexagonally Packed Mesoporous TiO2 by a Modified Sol–Gel Method. *Angew. Chemie Int. Ed. English* **1995**, *34* (18), 2014–2017.
(224) Hudson, S. P.; White, S.; Goradia, D.; Essa, H.; Liu, B.; Qiao, L.; Liu, Y.; Cooney, J. C.; Hodnett, B. K.; Magner, E. Proteins in Mesoporous Silicates. In *ACS Symposium Series*; 2008; pp 49–60.
(225) Ispas, C.; Sokolov, I.; Andreescu, S. Enzyme-Functionalized Mesoporous Silica for Bioanalytical Applications. *Anal. Bioanal. Chem.* **2009**, *393* (2), 543–554.
(226) Nabavi Zadeh, P. S.; Mallak, K. A.; Carlsson, N.; Åkerman, B. A Fluorescence Spectroscopy Assay for Real-Time Monitoring of Enzyme Immobilization into Mesoporous Silica Particles. *Anal. Biochem.* **2015**, *476*, 51–58.
(227) Nabavi Zadeh, P. S.; Åkerman, B. Immobilization of Enzymes in Mesoporous Silica Particles: Protein Concentration and Rotational Mobility in the Pores. *J. Phys. Chem. B* **2017**, *121* (12), 2575–2583.
(228) Nabavi Zadeh, P. S.; Zezzi do Valle Gomes, M.; Åkerman, B.; Palmqvist, A. E. C. Förster Resonance Energy Transfer Study of the Improved Biocatalytic Conversion of CO 2 to Formaldehyde by Coimmobilization of Enzymes in Siliceous Mesostructured Cellular

Foams. *ACS Catal.* **2018**, *8* (8), 7251–7260.
(229) Dai, Z.; Xu, X.; Wu, L.; Ju, H. Detection of Trace Phenol Based on Mesoporous Silica Derived Tyrosinase-Peroxidase Biosensor. *Electroanalysis* **2005**, *17* (17), 1571–1577.
(230) Talebi, M.; Vaezifar, S.; Jafary, F.; Fazilati, M.; Motamedi, S. Stability Improvement of Immobilized A-Amylase Using Nano Pore Zeolite. *Iran. J. Biotechnol.* **2016**, *14* (1), 33–38.
(231) Gross, J.; Sayle, S.; Karow, A. R.; Bakowsky, U.; Garidel, P. Nanoparticle Tracking Analysis of Particle Size and Concentration Detection in Suspensions of Polymer and Protein Samples: Influence of Experimental and Data Evaluation Parameters. *Eur. J. Pharm. Biopharm.* **2016**, *104*, 30–41.
(232) Filipe, V.; Hawe, A.; Jiskoot, W. Critical Evaluation of Nanoparticle Tracking Analysis (NTA) by NanoSight for the Measurement of Nanoparticles and Protein Aggregates. *Pharm. Res.* **2010**, *27* (5), 796–810.